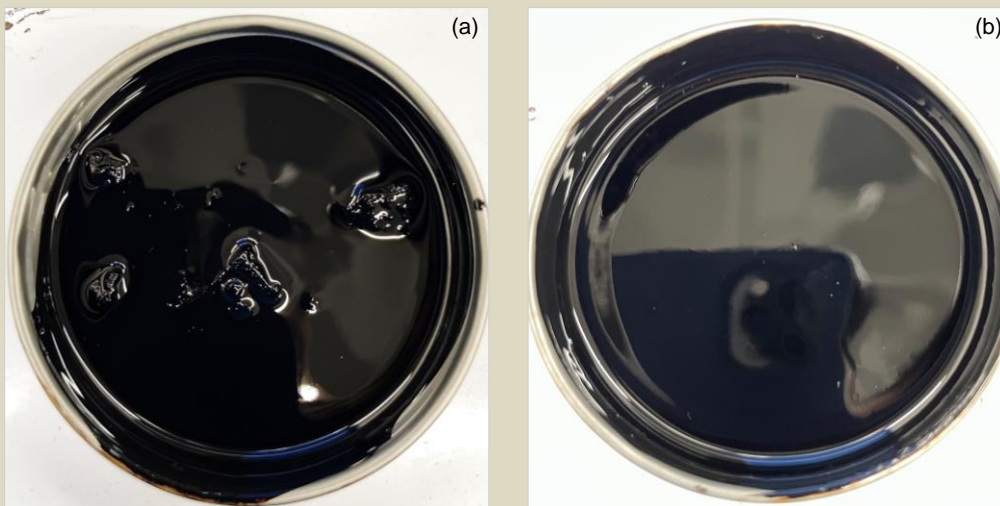




RESEARCH & DEVELOPMENT

Screening of Asphalt Extenders and Recycling Agents



(a) RAS lumps visible after blending in original state (b) No RAS lumps visible after RTFO aging

Cassie Castorena, Ph.D.

Andrew Fried

Jaime Preciado

Saqib Gulzar

Maria Carolina Aparicio Alvis

Lei Gabriel Xue

Department of Civil, Construction, and Environmental Engineering

North Carolina State University

NCDOT Project 2020-16

May 2023

Technical Documentation Page

1. Report No. FHWA/NC/2020-16	2. Government Accession No.	3. Recipient's Catalog No.	
4. Title and Subtitle Screening of Asphalt Extenders and Recycling Agents		5. Report Date June 2023	
		6. Performing Organization Code	
7. Author(s) Cassie Castorena, Ph.D., Andrew Fried, Jaime Preciado, Saqib Gulzar, Maria Carolina Aparicio Alvis, and Lei Gabriel Xue		8. Performing Organization Report No.	
9. Performing Organization Name and Address Civil, Construction, and Environmental Engineering, North Carolina State University 915 Partners Way Raleigh NC 27606		10. Work Unit No. (TRAIS)	
		11. Contract or Grant No.	
12. Sponsoring Agency Name and Address North Carolina Department of Transportation Research and Development Unit 104 Fayetteville Street Raleigh, North Carolina 27601		13. Type of Report and Period Covered Final Report August 1, 2019 –Feb 28, 2023	
		14. Sponsoring Agency Code NCDOT RP2020-16	
Supplementary Notes:			
16. Abstract The objectives of this project are to: 1) develop recommendations for extender and recycling agent product approval and dosage selection; and 2) identify appropriate aging procedure(s) to simulate long-term oxidative aging coupled with test methods and parameters to characterize the cracking resistance of asphalt binders. Three NCDOT approved surface asphalt mixtures were evaluated in this study, including a reclaimed asphalt pavement (RAP) mixture, recycled asphalt shingle (RAS) mixture, and RAP/RAS mixture. Three extenders and two recycling agents (RAs) were evaluated. The extenders were blended with PG 58-28 virgin binder whereas the RAs were blended with PG 64-22 virgin binder. Blends of recycled binder, virgin binder, and a RA or extender were prepared that achieved similar high-temperature AASHTO M 320 performance-graded properties to virgin PG 64-22 binders in North Carolina. These blends exhibit distinct but also potentially superior low- and intermediate-temperature characteristics compared to PG 64-22 virgin binders on the basis of performance-grade properties and several other rheological measures of durability. In contrast, NCDOT's current practice to use a PG 58-28 virgin binder in high recycled binder replacement mixtures resulted in similar intermediate- and low-temperature performance-graded properties to PG 64-22 virgin binders in North Carolina for the materials evaluated. However, the current practice resulted in high-temperature performance-graded properties that were distinct from PG 64-22 virgin binders. The collective results highlight that neither the current practice to use a PG 58-28 virgin binder in high recycled binder replacement mixtures or the use of an extender or RA can fully restore rheological properties of recycled binder blends to those of PG 64-22 virgin binders. The inability of additives to fully restore rheological properties was also identified in some cases through inferior measures of the balance between stiffness and relaxation characteristics, including ΔT_c and R values. Long-term aged asphalt mixtures prepared according to the current practice and with the additives displayed similar dynamic modulus and fatigue cracking resistance, which may have been a consequence of the harsh laboratory-induced age level. Short-term aged mixtures prepared according to the current practice and with the additives met recommended Hamburg Wheel Track Test rutting limits. The additives were found to be ineffective at increasing recycled binder contribution in asphalt mixtures. Based on the collective results and findings, an additive dosage selection and product approval process was proposed. In addition, the results of this study suggest that the consideration of alternative rheological measures of binder durability that are readily obtained from standard Performance Graded (PG) test results may aid in screening of asphalt binders for cracking resistance.			
17. Key Words Asphalt, recycling, reclaimed asphalt pavement, recycled asphalt shingles, recycling agents, extenders		18. Distribution Statement	
19. Security Classif. (of this report) Unclassified	20. Security Classif. (of this page) Unclassified	21. No. of Pages 148	22. Price

Disclaimer

The contents of this report reflect the views of the author who is responsible for the facts and the accuracy of the data presented herein. The contents of the report do not reflect the official views or policies of the North Carolina Department of Transportation. This report does not constitute a standard, specification or regulation.

Acknowledgments

The research team would like to express their gratitude and appreciation to the North Carolina Department of Transportation (NCDOT) for the provided funding needed to conclude this research study. The input of Dr. Shane Underwood through technical discussions are greatly appreciated. The researchers also thank Associated Asphalt, Barnhill Contracting Company, BP, Fred Smith Company, Poet, Safety Kleen, and Sripath Technologies for graciously donating materials for the project.

TABLE OF CONTENTS

Table of Contents	i
List of Figures	iii
List of Tables	vi
Executive Summary	1
1. Introduction.....	3
1.1. Overview	3
1.2. Summary of the Literature	4
1.3. Organization of the Report.....	10
2. Methodology.....	12
2.1. Materials	12
2.2. Selection of Additive Dosages to Restore the Intended High-Temperature Grade	13
2.3. Evaluation of the Effects of Additives on Recycled Binder Contribution.....	17
2.4. Measurement of Asphalt Mixture Rutting Resistance at the Selected Dosages	19
2.5. Benchmarking Binder Blends using Performance-Graded Properties.....	19
2.6. Evaluation of the Durability of Binder Blends using Alternative Parameters and Age Levels	20
2.7. Effects of Additives on the Saturates, Aromatics, Resins, and Asphaltenes Composition of Asphalt Binders.....	23
2.8. Prediction of Binder Blend Properties Using Virgin Blends and Recycled Binder Properties	23
2.9. Evaluation of the Effects of Additives on the Cracking Performance of Long-Term Aged Asphalt Mixtures.....	23
3. Results.....	25
3.1. Evaluation of Dosage Selection Procedures to Restore the Intended High-temperature Climatic Grade	25
3.2. Evaluation of the Impacts of Additives on Recycled Binder Contribution in Asphalt Mixtures	34
3.3. Hamburg Wheel Track Test Results of Blends with Dosage Selected to Restore the Intended High-Temperature Grade	35
3.4. Benchmarking the Binder Blends against North Carolina Virgin Binders using Performance-Graded Properties.....	36
3.5. Effects of Recycling Agents and Extenders on Binder Durability	44
3.6. Effects of Recycling Agents and Extenders on the Dynamic Modulus and Cracking Performance of Long-term Aged Asphalt Mixtures	57
4. Conclusions and Recommendations	63

4.1. Conclusions.....	63
4.2. Recommendations.....	64
5. Implementation and Technology Transfer Plan.....	66
6. Cited References	67
Appendix A: Detailed Literature Review	70
Appendix B: Development of Practical Algorithms to Construct Asphalt Binder Master Curves and Calculate Christensen Anderson (CA) Model Parameters	86
Appendix C: Saturates, Aromatics, Resins, and Asphaltene (SARA) Analysis of the Impacts of Additives	109
Appendix D: Prediction of Binder Blend Properties Using Virgin Blends and Recycled Binder Properties	114
Appendix E: Supplementary Statistical Analysis Results	127

LIST OF FIGURES

Figure 1. Overview of the research methodology.....	12
Figure 2. (a) RAS lumps visible after blending in original state (b) No RAS lumps visible after RTFO aging	15
Figure 3. Dosage selection results for blends according to Method 1: (a) 64.RAP.R1, (b) 64.RAP.E1, (c) 58.RAP.E1, (d) 58.RAP.E2, (e) 58.RAP.E3, (f) 64.RAS.R1, (g) 58.RAS.R1, (h) 64.RAS.R2	27
Figure 4 Comparison of dosage selection according to Methods 1 and 2 for (a) 58.RAP.E1, (b) 58.RAP.E2, (c) 58.RAP.E3, and (d) 58.RAS.R1	28
Figure 5. Relationships between high-temperature grade change and additive content for (a) all blends containing R1 and (b) all blends containing E1	29
Figure 6. Slope of the continuous high-temperature grade change versus additive content based on the different methods evaluated	30
Figure 7. Selected doses according to the different methods evaluated	31
Figure 8. Continuous AASHTO M 320 high-temperature performance grades predicted based on the different dosage selection methods evaluated and measured via verification testing at the dosages selected according to Method 1.....	32
Figure 9. Confidence interval (CI) for Method 3 results of blends prepared using R1	33
Figure 10. Recycled binder contribution results for the RAP mixture	34
Figure 11. Recycled binder contribution results for the RAP/RAS mixture	35
Figure 12. Hamburg Wheel-track test results	36
Figure 13. T_H values	37
Figure 14. T_I values.....	39
Figure 15. T_L values.....	39
Figure 16. ΔT_c values.....	40
Figure 17. Distribution of the Superpave binder properties for North Carolina’s PG 64-22 binders and recycled binder blends: (a) $ G^* /\sin(\delta)$ @64°C (kPa) – Original, (b) $ G^* /\sin(\delta)$ @64°C (kPa) – RTFO, (c) $S(60)$ @-12°C (MPa) – PAV. (d) $m(60)$ @-12°C (MPa) – PAV, (e) $ G^* /\sin(\delta)$ @25°C (kPa) – PAV	42
Figure 18. Bivariate distribution of high- and low-temperature rheological properties: (a) AASHTO M 320 high-temperature rheological space, and (b) AASHTO M 320 low-temperature rheological space.....	43
Figure 19. Linear viscoelastic DSR-based parameters	46
Figure 20. Linear viscoelastic BBR-based parameters	47

Figure 21. Linear amplitude sweep-based parameters.....	47
Figure 22. Relationship between $ G^* $ and δ at 25°C, 10 rad/s at P20 and P40 age levels	53
Figure 23. Dynamic modulus master curves for the RAP mixtures	58
Figure 24. Dynamic modulus master curves for the MRAS mixtures.....	58
Figure 25. Damage characteristic curves for the RAP mixtures.....	59
Figure 26. Damage characteristic curves for the MRAS mixtures	59
Figure 27. Failure criteria (error bars reflect the maximum and minimum individual specimen result)	60
Figure 28. S_{app} results (error bars reflect the maximum and minimum individual specimen result)	60
Figure 29. Comparison of PAV40 and extracted and recovered LTA binder master curves for the RAP binder blends: (a) dynamic shear modulus and (b) phase angle	62
Figure 30. Comparison of PAV40 and extracted and recovered LTA binder master curves for the RAP binder blends: (a) dynamic shear modulus and (b) phase angle	62
Figure 31. AFT analysis (Chandio et al. 2015).....	72
Figure 32. National survey results of laboratory tests used in practice to characterize the properties of asphalt binders modified by recycling agents (Epps Martin et al. 2019).	74
Figure 33. Relationship between RAP/RAS replacement and ΔT_c (Asphalt Institute 2019)	78
Figure 34. Rejuvenator dosage for aromatic extract (Epps-Martin et al. 2019)	81
Figure 35. Recycling agent dosages combined for tail oils, vegetable oils, and reacted bio-based oils (Epps-Martin et al. 2019)	82
Figure 36. Example of the effects of data screening for binder 4 O	89
Figure 37. Example of relationship used to determine ω_c for binder 4 O.....	92
Figure 38. Example relationship used to determine R in the LR method.....	93
Figure 39. Examples of trends of R values calculated according to Equation (6) with respect to $ G^* $	94
Figure 40. Comparison of $\log a_T$ values determined using the Gordon and Shaw (1994) and pairwise interpolation methods	96
Figure 41. R values	97
Figure 42 Master curves for binder 4 P40: (a) $ G^* $ and (b) δ	98
Figure 43. Master curves for binder 8 P20: (a) $ G^* $ and (b) δ	98
Figure 44. Comparison of the measured and predicted (a) $ G^* $ values for the Group A binders, (b) $ G^* $ values for the Group B binders, (c) δ for the Group A binders, and (d) δ for the Group B binders.....	100

Figure 45. Glover-Rowe values calculated at 15°C and 0.005 rad/s using the shift factor and CA models	106
Figure 46. SARA results	111
Figure 47. Micromechanical model predictions for the norm of complex shear modulus at 58°C	118
Figure 48. Mixing model predictions for the norm of complex shear modulus at 58°C	119
Figure 49. Arrhenius model predictions for the norm of complex shear modulus at 58°C	120
Figure 50. Arrhenius model predictions for the norm of complex shear modulus at 64°C	120
Figure 51. Comparison of model predictions for $ G^* $ at 64°C	121
Figure 52. Comparison of model predictions for original $ G^* $ at 64°C ($d=0.35$).....	122
Figure 53. Comparison of model predictions for RTFO $ G^* $ at 64°C ($d=0.35$).....	123
Figure 54. Comparison of model predictions for PAV $ G^* $ at 25°C ($d=0.5$)	123
Figure 55 Comparison of model predictions for original $ G^* /\text{Sin}\delta$ at 64°C ($d=0.35$)	124
Figure 56 Comparison of model predictions for RTFO $ G^* /\text{Sin}\delta$ at 64°C ($d=0.35$).....	124
Figure 57 Comparison of model predictions for PAV $ G^* /\text{Sin}\delta$ at 25°C ($d=0.5$).....	125
Figure 61 Model predicts for 64-MRAS-R2 blends for (a) RTFO and (b) PAV aging conditions ($d=1$).....	125

LIST OF TABLES

Table 1. Types of Rejuvenators (NCAT 2014).....	5
Table 2. Summary of the Mixtures Evaluated	12
Table 3. Summary of the Additives Evaluated	13
Table 4. Blends Evaluated	14
Table 5. Mixtures Used for Recycled Binder Contribution Measurements.....	18
Table 6. Blends Benchmarked using Performance-Graded Properties.....	20
Table 7. Summary of Alternative Indicators of Binder Durability Evaluated	22
Table 8. Virgin and Recycled Binder AASHTO M 320 Continuous High-temperature Grades .	25
Table 9. Slopes and Selected Additive Dosages	26
Table 10. Comparison between High-Temperature Grades Predicted by Methods 1 through 4 at the Dosages Selected According to Method 1 and Those Measured in Verification Testing	32
Table 11. Summary of Continuous AASHTO M 320 Performance Grades.....	37
Table 12. Summary of the Superpave Properties of the Blends and NC PG 64-22 Binders	41
Table 13. Summary of the Durability-Related Binder Parameters Evaluated	44
Table 14. Comparisons between the Rheological Properties of the Modified Blends in Comparison to the Reference (58.RAP or 58.MRAS) at the P20 Age Level	49
Table 15. Comparisons between the Rheological Properties of the Modified Blends in Comparison to the Reference (58.RAP or 58.MRAS) at the P40 Age Level	50
Table 16. Comparisons between the Rheological Properties of the Blends in Comparison to the Target PG 64-22 Virgin Binder at the P20 Age Level.....	51
Table 17. Comparisons between the Rheological Properties of the Blends in Comparison to the Target PG 64-22 Virgin Binder at the P40 Age Level.....	52
Table 18. Spearman’s Rank Correlation Coefficient Values at the P20 Age Level	54
Table 19. Spearman’s Rank Correlation Coefficient Values at the P40 Age Level	54
Table 20. Correlation Coefficients between P20 and P40 Age Levels.....	55
Table 21. Number of Statistically Distinct Groups for Each Durability-Related Parameter	56
Table 22. Comparison of Virgin Binder to Recycled Materials (Epps-Martin et al. 2019)	71
Table 23. Types of Rejuvenators (NCAT 2014).....	73
Table 24. Agencies and their Selected Parameter.....	78
Table 25. Summary of Binder Cracking Indicators	80
Table 26. Summary of the Asphalt Binders and Test Procedures	88

Table 27. Summary of the CA Model Parameters	97
Table 28. $ G^* $ Model Fit Statistics Including All Data.....	102
Table 29. $ G^* $ Model Fit Statistics Excluding $ G^* $ values Below 10^5 Pa.....	103
Table 30. δ Model Fit Statistics Including All Data	104
Table 31. δ Model Fit Statistics Excluding Data Corresponding to $ G^* $ values Below 10^5 Pa..	105
Table 32. SARA Results	110
Table 33. Comparison of Estimate and Measurement of SARA Fractions for 58.RAP.....	110
Table 34. Change with Respect to Reference 58.RAP	112
Table 35. Change with Respect to Reference 64.RAP	112
Table 37. Summary of Blends Evaluated	115
Table 38. Model Parameters for Arrhenius Model	119
Table 39. Assumed Value of Interaction Parameter for Grunberg and Nissan Model	121
Table 40. Tukey HSD Results for $ G^* \times \sin \delta$ @25°C, 10 rad/s (kPa) at the P20 Age Level ...	127
Table 41. Tukey HSD Results for $ G^* \times \sin \delta$ @25°C, 10 rad/s (kPa) at the P40 Age Level ...	127
Table 42. Tukey HSD Results for G-R @ 25°C, 10 rad/s (kPa) at the P20 Age Level	128
Table 43. Tukey HSD Results for G-R @ 25°C, 10 rad/s (kPa) at the P40 Age Level	128
Table 44. Tukey HSD Results for G-R @ 15°C, 0.005 rad/s (kPa) at the P20 Age Level	129
Table 45. Tukey HSD Results for G-R @ 15°C, 0.005 rad/s (kPa) at the P40 Age Level	129
Table 46. Tukey HSD Results for ω_c (Hz) at the P20 Age Level.....	130
Table 47. Tukey HSD Results for ω_c (Hz) at the P40 Age Level.....	130
Table 48. Tukey HSD Results for T_c (°C) at the P20 Age Level	131
Table 49. Tukey HSD Results for T_c (°C) at the P40 Age Level	131
Table 50. Tukey HSD Results for Master Curve R at the P20 Age Level	132
Table 51. Tukey HSD Results for Master Curve R at the P40 Age Level	132
Table 52. Tukey HSD Results for NCHRP 09-59 R at the P20 Age Level.....	133
Table 53. Tukey HSD Results for NCHRP 09-59 R at the P40 Age Level.....	133
Table 54. Tukey HSD Results for S(60) @ -18°C (MPa) at the P20 Age Level	134
Table 55. Tukey HSD Results for S(60) @ -18°C (MPa) at the P40 Age Level	134
Table 56. Tukey HSD Results for m(60) @ -18°C at the P20 Age Level	135
Table 57. Tukey HSD Results for m(60) @ -18°C at the P40 Age Level	135
Table 58. Tukey HSD Results for ΔT_c (°C) at the P20 Age Level.....	136

Table 59. Tukey HSD Results for ΔT_c ($^{\circ}\text{C}$) at the P40 Age Level.....	136
Table 60. Pearson's Correlation Coefficients at the P20 Age Level	137
Table 61. Pearson's Correlation Coefficients at the P40 Age Level	137

EXECUTIVE SUMMARY

High recycled content mixtures can be prone to cracking without the use of soft virgin binders, often achieved through the incorporation of extenders, or the addition of recycling agents (RAs). RAs include a wide-range of both softening agents and rejuvenators. Nationally, specifications pertaining to RAs and extenders are limited. Consequently, research is needed to identify methods to characterize asphalt binders and blends of recycled binders, virgin binders, and additives to enable the screening of extender and RA modified asphalt binder. The objectives of this project are to: (1) develop recommendations for extender and recycling agent product approval and dosage selection; and (2) identify appropriate aging procedure(s) to simulate long-term oxidative aging coupled with test methods and parameters to characterize the cracking resistance of asphalt binders that uses Superpave binder equipment.

Three North Carolina Department of Transportation (NCDOT) approved surface asphalt mixtures were evaluated in this study, including a RAP mixture, RAS mixture, and RAP/RAS mixture. All study mixtures specified a PG 58-28 virgin binder. The RAP-only and RAS-only mixtures were used for additive dosage selection and to evaluate the effects of additives on performance at both the asphalt binder and mixture scales. The RAP/RAS mixture and RAP only mixtures were used to evaluate the effects of additives on recycled binder contribution in asphalt mixtures. Three extenders and two RAs were evaluated. The extenders were blended with PG 58-28 virgin binder whereas the RAs were blended with PG 64-22 virgin binder.

Various dosage selection procedures to achieve an AASHTO M 320 high-temperature grade of 64°C in the blend of virgin binder, recycled binder, and additive were evaluated on the basis of the recommendations of the NCHRP Project 09-58. The results show that different RA and extender products can yield different rates of change in the asphalt binder continuous AASHTO M 320 high-temperature grade with additive content. However, the rate of change in asphalt binder continuous AASHTO M 320 high-temperature grade with additive content for a given additive was similar for different recycled binder and virgin binder combinations. The AASHTO M 320 high-temperature grading results of verification blends prepared at selected dosages yielded considerable discrepancies with those predicted from dosage selection testing in some cases; these results suggest uncertainty in the dosage selection results of around 3°C that should be incorporated into the dosage selection procedure. Recycled binder contribution measurements for the two mixtures evaluated suggest complete recycled binder contribution does not exist in asphalt mixtures and that additives are ineffective at increasing recycled binder contribution. However, all Hamburg Wheel-Track tests conducted on asphalt mixtures prepared at dosages intended to achieve a continuous AASHTO M 320 grade of 64°C passed the minimum rutting criteria proposed in NCHRP Project 09-58 for the North Carolina climate conditions.

The AASHTO M 320 performance-graded properties and alternative rheological indicators of binder durability of the study binder systems at the selected dosages were evaluated. The results show that the NCDOT's current practice to use a PG 58-28 virgin binder in high recycled binder replacement mixtures resulted in similar intermediate- and low-temperature performance-graded properties to PG 64-22 virgin binders in North Carolina (i.e., the intended condition) for the RAP and RAS cases evaluated. However, the current practice resulted in high-temperature performance-graded properties that were distinct from PG 64-22 virgin binders. In contrast, the blends of virgin binder, recycled binder, and an extender or RA at a dosage selected to restore the intended high-temperature grade of 64°C display high-temperature performance-graded properties similar to

virgin PG 64-22 binders. However, these systems exhibit distinct but and potentially superior low- and intermediate-temperature characteristics compared to PG 64-22 virgin binders on the basis of performance-grade properties and several alternative rheological measures of durability. The collective results highlight that neither the current practice to use a PG 58-28 virgin binder in high recycled binder replacement mixtures or the use of extenders or RAs can fully restore rheological properties of recycled binder blends to those of PG 64-22 virgin binders. While properties in either the high or low temperature regime can be restored, the consequence will be notably different properties for the opposite temperature regime. The inability of additives of fully restore rheological properties was also identified in some cases through inferior ΔT_c and/or R values.

The majority the rheological parameters evaluated indicate that the blends containing the vacuum gas oil extender and the RAs have superior durability compared to the respective reference blends of PG 58-28 virgin binder and recycled binder and equal or superior durability compared to the PG 64-22 virgin binder evaluated. These blends also generally passed recommended durability parameter criteria in specifications and the literature. The blends containing the extenders that contain Re-refined engine oil bottoms (REOB) failed recommended criteria for rheological parameters in several cases at the RTFO plus 40-hour PAV age level and also exhibited parameters deemed inferior to the PG 64-22 virgin binder. Most notably, these blends failed to meet the recommended minimum ΔT_c limit of -5°C at the 40-hour PAV age level, suggesting potential performance concerns. This potentially inferior performance was not identified at the standard, 20-hour PAV age level. Also noteworthy, the Glover-Rowe parameter, obtained from standard intermediate-temperature performance-graded test results, better discriminated among the performance of the study binders and blends compared to the current intermediate-temperature specification parameter.

Long-term aged, laboratory-mixed asphalt mixture samples of a subset of the study binder blends were prepared and subjected to dynamic modulus and cyclic fatigue testing to further evaluate the effect of RAs and extenders on durability. The dynamic modulus and fatigue cracking performance of long-term aged asphalt mixtures containing extenders and recycling agents all performed similarly to their corresponding reference mixture containing PG 58-28 virgin binder. However, the long-term aged mixture condition was found to be much harsher than the binder aging procedures and thus, may have been overly harsh. The harsh long-term age level could have limited the sensitivity of the mixture performance results to the binder variables evaluated.

Based on the collective project findings, it is recommended that extender and RA additive dosages be selected to restore the AASHTO M 320 high-temperature grade of the blend of recycled binder, virgin binder, and additive to 67°C . It is further suggested that the blend with the additive at the selected dosage must meet specified AASHTO M 320 intermediate- and low-temperature properties for PG 64-22 binders and does not yield a ΔT_c that falls below -5°C at the RTFO plus 40-hour PAV age level for product approval. It is also recommended that the NCDOT consider adding a minimum ΔT_c requirement to its low-temperature performance-graded specifications for asphalt binders and consider adopting the RTFO plus 40-hour PAV long-term aging procedure. It is also recommended that the NCDOT consider adopting the Glover-Rowe parameter at 25°C as an alternative to the current intermediate-temperature performance-graded specification parameter and further investigates the need for controlling and best measure of the R value. However, the above recommendations to binder specifications should be evaluated using additional asphalt binders prior to adoption.

1. INTRODUCTION

1.1. Overview

1.1.1. Introduction

The use of asphalt mixtures containing high amounts of Reclaimed Asphalt Pavement (RAP) and Reclaimed Asphalt Shingles (RAS) is becoming increasingly common. Reclaimed and recycled asphalt materials reduce the use of virgin aggregate and binder required in the production of asphalt mixtures, resulting in significant economic and environmental benefits. However, RAP binders are generally oxidized from time in service and thus, more susceptible to cracking than virgin binders. RAS binders are intentionally air blown and thus, more stiff and brittle than typical paving asphalts. Consequently, high recycled content mixtures are expected to be prone to cracking without the addition of soft virgin binders and/or recycling agents.

Recycling agents (RAs) include a wide-range of both softening agents and rejuvenators that are intended to restore the physical and chemical properties of aged asphalt binders. Nationally, specifications pertaining to RAs are limited. Crude oil refiners have improved the efficiency of extracting gasoline and other light distillates, which has impacted the yield and properties of asphalt binders produced. The need to produce soft virgin binder grades combined with these recent changes has led to increased use of asphalt extenders. Some petroleum-based extender products have been in existence for a long time. For example, Re-refined Engine Oil Bottoms (REOB) has been used as an extender to soften asphalt since the 1980s. Recent evidence suggests that REOB degrades pavement durability, prompting heightened interest. In addition, new types of extenders have been introduced. The uncertainty of liquid asphalt supply and spike in price that occurred approximately 15 years ago prompted specific interest in non-petroleum based extenders. Accordingly, bio-based extenders have been introduced that differ from asphalt in terms of both origin and composition.

The increasing use of recycled materials in asphalt mixtures has prompted heightened interest in RAs and necessitated the use of asphalt extenders to produce softer virgin binder grades. Consequently, improved methods are needed to characterize asphalt binder to enable the screening of extender and RA modified asphalt binder.

1.1.2. Research Need Definition

The AASHTO M 320 Performance-Graded (PG) specification was developed primarily on the basis of unmodified asphalts. Consequently, it has been demonstrated that the specification parameters and aging procedures often fail to discriminate the performance of modified asphalt binders. This shortcoming has been overcome with respect to rutting resistance and with the introduction of AASHTO M 332 and the associated Multiple Stress Creep and Recovery (MSCR) test. However, the ability of the current PG specification to discriminate binder performance with respect to cracking has not been addressed. The characterization of binder cracking resistance requires an appropriate aging procedure to simulate long-term oxidative aging coupled with a test method to capture cracking resistance. The Pressure Aging Vessel (PAV) long-term aging procedure used in the Superpave PG system was calibrated using conventional, unmodified asphalt binders. Recent research suggests that the standard PAV does not simulate prolonged field aging for many modern binders, which can preclude the detection of binders susceptible to oxidation induced embrittlement. In addition, the intermediate- and low-temperature PG test methods and associated criteria may not adequately capture the cracking resistance of modified asphalt binders.

The intent of RAs and many extenders is to restore the cracking resistance of recycled materials without compromising rutting. Consequently, the ability to capture the cracking susceptibility of binders is critically important to the successful use of RAs and extenders. Several alternative parameters to better reflect asphalt binder cracking resistance have gained attention recently that merit consideration when evaluating RA and extender modified binder systems.

An in-depth study is needed to evaluate RA and extender effectiveness and correspondingly establish a framework to qualify RA and extender products and establish their dosage requirements using both conventional and emerging characterization metrics. The study should rely on the use of relatively simple experiments that make use of standard binder laboratory equipment to ensure that the research results are implementable.

1.1.3. Research Objectives

The objectives of this project are to:

- (1) Develop recommendations for extender and recycling agent product approval and dosage selection; and
- (2) Identify appropriate aging procedure(s) to simulate long-term oxidative aging coupled with test methods and parameters to characterize the cracking resistance of asphalt binders and blends that uses Superpave binder aging and testing equipment.

1.2. Summary of the Literature

A comprehensive review of the literature pertaining to this project is presented in Appendix A. A summary of most relevant components of this review is presented below.

1.2.1. Recycling Agents and Extender Products

Recycling Agents (RAs)

RAs are a class of materials used to improve the cracking resistance and in some cases, workability of RAP and RAS mixtures without adversely affecting rutting resistance (Epps Martin et al. 2020). Recycling agents are typically blended with the virgin binder prior to combining with reclaimed materials and aggregate (Kaseer et al. 2019). RAs are often separated into two classes of materials: softening agents and rejuvenators. Softening agents are soft asphalt binders or other additives that lower the viscosity of the RAP binder. Alternatively, rejuvenators are additives that are intended to restore physical and chemical properties of the unaged binder (Daly 2017). The composition of RAs are largely proprietary (Daly 2017) and various strategies have been proposed for rejuvenation. Nahar et al. (2013) suggested addition of volatile and light constituents lost during aging whereas Roberts et al. (2009) suggest oils comprised of aromatics and resins are best. Table 1 lists common classes of rejuvenators used in practice (NCAT 2014). ASTM D4552 provides a classification system for petroleum-based RAs on the basis of viscosity.

Table 1. Types of Rejuvenators (NCAT 2014)

Category	Description
Paraffinic Oils	Refined used lubricating oils
Aromatic Extracts	Refined crude oil products with polar aromatic components
Napthenic Oils	Engineered hydrocarbons
Triglycerides and Fatty Acids	Derived from vegetable oils
Tall Oils	Paper industry by-products, same chemical family as liquid antistrip agents and emulsifiers

Extenders

Asphalt extenders are products substituted for a portion of the asphalt binder, in many cases to soften the asphalt. One type of extender that has been given significant attention recently is REOB, also known as Vacuum Tower Asphalt Extender (VTAE), which is defined as “the non-distillable residuum from a vacuum tower in a used oil re-refinery” (Asphalt Institute 2019). Asphalt binder producers have used REOB as an extender to soften asphalt since the 1980s, with typical dosage rates falling between 4 and 8 percent (Asphalt Institute 2019). Other vacuum gas oils (VGOs) are also used as extenders to soften asphalt and improve economy. The increasing use of softer virgin asphalt binders to meet grade requirements in RAP and RAS mixtures has prompted increased use of REOB in recent years (Asphalt Institute 2019). Research demonstrates that REOB can exacerbate oxidation induced embrittlement, which led 10 states to ban its use as of 2016 (Asphalt Institute 2019).

In response to the heightened use and concern regarding REOB, the Asphalt Institute prepared a state of the knowledge report on the use of REOB/VTAE (Asphalt Institute 2019). Their review highlights that the oxidation induced embrittlement caused by REOB may not be adequately captured using conventional Rolling Thin Film Oven (RTFO) plus 20-hour PAV aging coupled with standard Dynamic Shear Rheometer (DSR) and Bending Beam Rheometer (BBR) test parameters. Rather, it was found that the detrimental effects of REOB were only captured after prolonged PAV aging coupled with the characterization of properties that more directly relate to ductility. The presence of REOB can be inferred within asphalt binder by the detection of metals. X-ray fluorescence (XRF) can be used to determine the REOB content of an asphalt binder (ASTM D6481-14), which has been employed by the NCDOT. The simultaneous detection of calcium, zinc, copper, and molybdenum are used to detect REOB and infer its concentration (Asphalt Institute 2019).

The uncertainty of liquid asphalt supply and spike in price that occurred in 2008 prompted increased interest in non-petroleum based extenders. Bio-based materials constitute the majority of non-petroleum based extenders (Daly 2017). While bio-based materials have been primarily proposed for use as extenders, it should be noted that bio-binder have also been proposed for use as RAs (Oldham et al. 2016). The literature on the characterization of asphalt modified by bio-based materials has primarily focused on rheological characterization with little relatively little attention given to long-term oxidative aging and performance within asphalt mixtures (Daly 2017). While the literature suggests promising performance benefits from the use of bio-based extenders, their composition can differ significantly from asphalt, which suggests that the metrics used within the current PG system may be insufficient to adequately capture performance concerns. For

example, Fini et al. (2011) found that bio-binders derived from swine manure have very low molecular weight and relatively high oxygen content compared to asphalt binder.

1.2.2. Dosage Selection Procedures

Dosage selection is important for effective use of RAs and extenders in asphalt pavements. Low dosages may yield poor asphalt mixture cracking resistance whereas excessively high dosages may yield asphalt mixtures that are susceptible to rutting (Epps Martin et al. 2020). A standardized protocol for extender and RA dosage selection does not presently exist. Therefore, most state agencies currently follow the additive manufacturer's recommendations for dosage selection (Kaseer et al. 2019).

The NCHRP Project 09-58 sought to establish a dosage selection procedure for RAs (Epps Martin et al. 2020). They considered three methods:

- Method 1 - restore low-temperature PG, verify high-temperature PG,
- Method 2 - achieve $\Delta T_c = -5.0$ after 20 hours of PAV aging, and
- Method 3 - restore high-temperature grade.

Method 1 was found to yield the lowest RA dosages while Method 2 resulted in the highest RA dosages. Method 2 also produced dosages that resulted in high-temperature grades that were too low and could indicate rutting issues. Method 3 produced the intermediate dosage and resulted in the highest possible amount of RA without compromising rutting resistance. Method 3 was found to restore the climatic low-temperature PG of the blend to the target or achieve a lower grade. Consequently, a dosage selection procedure was established on the basis of Method 3. The authors suggested that blends could be prepared with no additive and at two additive dosage levels to determine the expected change in high-temperature PG per percent of additive added to the blend and correspondingly use Equation (1) to calculate the required additive dosage for a given blend. In an effort to establish a simplified procedure, the authors further proposed that Equations (1) and (2) be used to calculate the additive dose with the average slope (X) values observed in the NCHRP Project 09-58 study for aromatic extract and other additive types, which consisted of the combination of tall oils, vegetable oils, and reacted bio-based oils.

$$\text{Additive (\%)} = \frac{PGH_{\text{Blend}} - PGH_{\text{Target}}}{X} \quad (1)$$

$$PGH_{\text{Blend}} = RAP_{BR} \times PGH_{RAP} + RAS_{BR} \times PGH_{RAS} + B_{BR} \times PGH_{\text{Virgin}} \quad (2)$$

where: Additive (%) = additive content by total weight of asphalt binder; X = slope (equal to 1.38 for aromatic extracts and 1.82 for all other products based on NCHRP 09-58 results); PGH_{Blend} = continuous high-temperature PG of the blend of recycled and virgin binder ($^{\circ}\text{C}$); PGH_{Target} = target high-temperature PG for the blend ($^{\circ}\text{C}$); RAP_{BR} = RAP binder recycled binder ratio, equal to the weight of RAP binder in the mix divided by total binder weight in the mix; RAS_{BR} = RAS binder recycled binder ratio, equal to the weight of RAS binder in the mix divided by total binder weight in the mix; $B_{BR} = 1 - RAP_{BR} - RAS_{BR}$; and PGH_{Virgin} = virgin binder high-temperature continuous grade ($^{\circ}\text{C}$).

While the NCHRP Project 09-58 sought to evaluate a diverse set of RAs and corresponding binder blends, the universality of the X values given in Equation (1) to all RAs and other types of softening additives remains unknown. NCHRP Project 09-58 did not focus on extenders and therefore, the slope values for extenders merits investigation. Furthermore, Equation (2) assumes that the

recycled binder completely mobilizes and blends with the virgin binder and the RA. However, there is general consensus that complete recycled binder availability is not achieved in practice (McDaniel and Anderson 2001, Epps Martin et al. 2020, Castorena et al. 2022). The erroneous assumption of complete recycled binder availability may yield additive dosages that are too high and consequently yield asphalt mixtures with poor rutting performance.

1.2.3. Alternative Measures of Asphalt Binder Durability

Bahia et al. (2001) found that modified and unmodified binders often demonstrate similar properties according to the AASHTO M 320 performance-graded specification but exhibit drastically different cracking performance. The needs for an improved procedure to mimic field aging coupled with a test method to capture binder cracking resistance are also highlighted by the three recent NCHRP projects; NCHRP 09-60: *Addressing Impacts of Changes in Asphalt Binder Formulation and Manufacture on Pavement Performance through Changes in Asphalt Binder Specifications*, NCHRP 09-59: *Relating Asphalt Binder Fatigue Properties to Asphalt Mixture Fatigue Performance*, and NCHRP 09-61: *Short- and Long-Term Binder Aging Methods to Accurately Reflect Aging in Asphalt Mixtures*.

The *delta T critical* (ΔT_c), which is equal to the difference between the low-temperature critical PG specification temperatures for creep stiffness ($S(60)$) and m-value ($m(60)$), has been given considerable attention in recent years for capturing the effects of embrittlement on pavement cracking potential. The parameter was first introduced by Anderson et al. (2011) who observed a strong correlation between ΔT_c and pavement block cracking; correspondingly, the authors postulated that ΔT_c is a good indicator of asphalt binder ductility at low temperature. They found that the value of ΔT_c decreases with oxidative aging, indicating an imbalance in stiffness and relaxation characteristics with a poor ability to relax thermal stresses. Correspondingly, the authors suggested that evaluating ΔT_c at a long-term age condition may be helpful to identify binders susceptible to oxidative embrittlement. Subsequently, researchers have found that the parameter can be used to identify problems associated with REOB (Asphalt Institute 2019). ΔT_c has been adopted into specifications by at least 10 state agencies (Asphalt Institute 2019). Most agencies have adopted a minimum limit for ΔT_c of -5.0°C . Some agencies apply the limit to the 20-hour PAV age level whereas others apply it to the 20-hour PAV age level (Asphalt Institute 2019). The parameter is implemented into practice relatively easily because it can be calculated using the results of standard BBR testing used for PG determination.

The NCHRP Project 09-60 evaluated trends in ΔT_c with aging and asphalt modifier dosage for a diverse set of asphalts (Elwardany et al. 2020). The authors found that ΔT_c decreases as polymer content in an asphalt increases, which is counterintuitive to the expected performance trend. Consequently, the NCHRP Project 09-60 team suggested that failure properties must be integrated into specifications to capture the benefits of polymer modification. They proposed the use of the Asphalt Binder Cracking Device (ABCD) in combination with the BBR to comprehensively address low-temperature cracking performance (Elwardany et al. 2022). The ABCD subjects a constrained asphalt binder sample to cooling until fracture. The test result is reported as the critical cracking temperature. The authors proposed that at the 20-hour PAV level, binders should be accepted without ABCD testing if ΔT_c exceeds -2°C (Elwardany et al. 2022). If the binder has a ΔT_c between -2°C and -6°C , ABCD is recommended and the binder is allowed to pass if the difference between the continuous low temperature grade based on stiffness and the ABCD test result exceeds a critical limit whereas the binder is considering failing if the limit is not met. They recommended that binders with ΔT_c lower than -6°C should be deemed failing, irrespective of the

ABCD test result. If the 40-hour PAV level is used, the authors suggested that the limits of -2°C and -6°C be changed to -3°C and -7°C.

Researchers have also demonstrated that several alternative rheological parameters related to brittleness can be derived from the DSR (Anderson et al. 1994, Glover et al. 2005, Anderson et al. 2011, Christensen and Tran 2022). Glover et al. (2005) first proposed a rheological parameter as an indicator of ductility that could be determined using DSR testing rather than the more cumbersome force-ductility testing. For non-polymer-modified asphalt binders, the Glover parameter is highly correlated with force-ductility tests conducted at 15°C and a loading rate of 1 cm/min when evaluated at 15°C and 0.005 rad/s, with a higher G-R value indicative of lower ductility. Rowe (2011) subsequently simplified the Glover parameter to yield the so-called Glover-Rowe (G-R) parameter, equal to $|G^*| \cdot (\cos \delta)^2 / \sin \delta$. Anderson et al. (2011) demonstrated that the G-R parameter correlates with pavement block cracking when evaluated at 15°C and 0.005 rad/s. The authors observed maximum limits of 180 kPa and 450 kPa correspond to the onset of block cracking and occurrence of significant block cracking, respectively. Directly measuring the G-R parameter at 0.005 rad/s is not practical or feasible given the slow loading rate. Therefore, Glover et al. (2005) proposed evaluating the parameter at 44.7°C and 10 rad/s, which yielded approximately equivalent results as those based on 15°C and 0.005 rad/s based on time-temperature equivalencies. However, Anderson et al. (2011) demonstrated that a single time-temperature equivalency is not valid for all binders and therefore, that the G-R parameters obtained from a master curve are more highly correlated with force-ductility results. Therefore, the authors proposed the use of temperature-frequency sweep testing coupled with a master curve model to obtain the G-R parameter. The NCHRP Project 09-59 recently proposed that the G-R parameter be measured at an intermediate temperature, selected based on the low-temperature climatic grade, and 10 rad/s in place, which negates the need for a master curve (Christensen and Tran 2022). The authors suggested replacing the current $|G^*| \times \sin \delta$ specification with the G-R measured at 10 rad/s to screen binder fatigue cracking resistance. The NCHRP 09-59 Project suggested corresponding maximum limits for G-R of 5,000 kPa and 8,000 kPa at the 20-hour PAV and 40-hour PAV age levels, respectively (Christensen and Tran 2022).

Master curves are used to describe the time and temperature dependence of the rheological behavior of asphalt binders. The Strategic Highway Research Program (SHRP) considered the use of master curves as the basis for providing rational specification parameters (Anderson et al. 1994). The effort yielded the Christensen-Anderson (CA) model (Christensen 1992), which persists as the most widely applied asphalt binder master curve model today. The CA model is a phenomenological model applied to describe the reduced frequency (ω_R) dependence of asphalt binder dynamic shear modulus ($|G^*|$) and phase angle (δ) and is given in Equations (3) and (4).

$$|G^*|(\omega) = G_g \left[1 + \left(\frac{\omega_c}{\omega_R} \right)^{(\log 2/R)} \right]^{-R/\log 2} \quad (3)$$

$$\delta(\omega) = \frac{90}{\left[1 + \left(\frac{\omega_R}{\omega_c} \right)^{\log 2/R} \right]} \quad (4)$$

where G_g = glassy modulus, often assumed to equal 1 GPa, which is supported by experimental evidence from asphalt binders (Christensen 1992); ω_c = crossover frequency, equal to the reduced

frequency where the phase angle equals 45° ; and R = rheological index, equal to the logarithmic distance between G_g and $|G^*|$ at ω_c .

The CA model parameters themselves have been proposed as potential measures to evaluate asphalt binder cracking resistance (Christensen 1992). The ω_c defines the point where the storage and loss moduli are equal and thus, constitutes a transition point from elastic- to viscous-dominated behavior. As asphalt binders undergo oxidative aging, the ω_c decreases and the R value increases (Anderson et al. 1994). Thus, a higher ω_c is considered and lower R is generally considered desirable. While single-point measurements were ultimately adopted for asphalt binder specification during SHRP, recent studies suggest master curve-based parameters may better capture the cracking resistance of asphalt binders than the current specification parameters. Studies suggest that the R value in the CA model is an indicator of asphalt binder cracking potential (Rowe and Sharrock 2011, Christensen and Tran 2022). Furthermore, through the NCHRP Project 09-59, Christensen and Tran (2022) recently proposed that the R value of an asphalt binder is an indicator of its fatigue strain capacity. The authors stated that for thin pavements that experience high strains, high R values can result in poor fatigue performance at low temperature. Correspondingly, the authors proposed maximum R value limits of 2.50 and 3.20 at the 20-hour PAV and 40-hour PAV age levels, respectively. The also indicated there was also some evidence that very low R values can be problematic for thick pavements but caution that the evidence was weaker evidence for this scenario than the thin pavement scenario. The authors proposed an alternative means to calculate the R value using standard BBR test results and also stated it is closely related to ΔT_c , suggesting that either could be adopted into specifications to better address cracking resistance. Cucalon et al. (2017) introduced another master curve-based parameter closely related to ω_c , termed the cross over temperature (T_c), equal to the temperature where $\delta = 45^\circ$. The authors proposed the crossover temperature as both a parameter for tracking asphalt binder aging and a measure of rheological balance in terms of rutting and age-induced embrittlement when combined with a binder's high-temperature grade.

While master curve-based parameters have shown promise, a standard for conducting temperature-frequency sweep testing of asphalt binders and constructing corresponding master curves does not presently exist. However, researchers have questioned the ability of these alternative rheological parameters to discriminate the performance of modified and unmodified binders because they do not quantify failure properties (Elwardany et al. 2020).

Several test methods to quantify the failure properties of asphalt binder exist. One, discussed above, is the ABCD test. An alternative, the Linear Amplitude Sweep (LAS) test, can be conducted in the DSR using the standard 8-mm parallel plate geometry. Changes in loading resistance with respect to number of loading cycles are used to evaluate damage resistance and determine fatigue failure (Safaei et al. 2016). The test has shown promising relationships to asphalt mixture fatigue performance (Safaei et al. 2016). However, counterintuitive trends in fatigue life with respect to age level have been reported (Yang et al. 2022).

Recent studies show that the current 20-hour PAV procedure (AASHTO R 28) provides insufficient oxidation to mimic the effects of prolonged field aging (Glover et al. 2005, Wright et al. 2011, Kim et al. 2017, Bonaquist et al. 2021). Studies also suggest that standard PAV aging is insufficient to capture the negative effects of additives. For example, much recent attention has been given to binders that contain re-refined engine oil bottoms (REOB) because they contribute to the premature cracking of pavements as a result of embrittlement (Asphalt Institute 2016). NCHRP Project 09-61 recently sought to improve short- and long-term asphalt binder aging

methods (Bonaquist et al. 2021). The NCHRP Project 09-61 proposed that either the standard Rolling Thin Film Oven (RTFO) or static thin film conditioning of 12.5 g of binder in a standard PAV pan placed in an oven for 85 minutes at a temperature of 163°C can be used to simulate short-term aging (i.e., from production to placement). Furthermore, the project suggested conditioning 12.5 g samples placed in standard PAV pans for 20 hours at a pressure of 2.1 MPa and temperature falling between 85°C and 115°C, selected on the basis of climatic conditions, simulates approximately 10 years of in-service aging near the pavement surface. The authors indicated that roughly equivalent aging to the 20 hours of conditioning using 12.5 g per PAV pan is achieved using 40 hours of PAV conditioning with the standard 50 g per PAV pan, suggesting that the current procedure may not simulate extensive in-service aging. The use of 12.5 g samples necessitates more stringent leveling requirements for PAV pans and requires casting of the thin film samples under nitrogen gas.

1.2.4. Summary of Knowledge Gaps and Applications

The literature indicates that a wide-range of RA and extender products are currently available, with the potential to enable the production of good-performing high recycled content mixtures. However, the accurate characterization of the cracking resistance of asphalt binders modified by extenders and RAs is necessary to ensure that the products in use achieve the desired performance outcomes. Past studies demonstrate that the current Superpave PG laboratory aging and test methods fail to adequately capture the performance of modified asphalt binders. However, the literature suggests that prolonged or thin-film PAV aging combined with several alternative parameters related to brittleness that can be measured using standard BBR and DSR testing equipment can provide practical indicators of modified binder cracking resistance. Consequently, there is promise for extending the state-of-the art knowledge within the proposed scope of work to meet the objectives of this study. The viability of RA and extender products should be evaluated using both standard and emerging binder parameters to understand their potential impacts on durability.

Dosage selection is an important aspect to the use of RA and extender products. While the NCHRP Project 09-58 established a dosage selection procedure, the universality of their proposed dosage selection procedure to materials local to NC merits dedicated evaluation. NCHRP Project 09-58 did not focus on extenders and therefore, extension of the procedure to extender products also merits investigation. Furthermore, the NCHRP Project 09-58 dosage selection procedure assumes that the recycled binder completely mobilizes and blends with the virgin binder and the recycling agent. However, there is general consensus that complete recycled binder availability is not achieved in practice. The erroneous assumption of complete recycled binder availability may yield additive dosages that are too high and consequently yield asphalt mixtures with poor rutting performance. Consequently, there are research needs to evaluate the universality of the blended system high-temperature grade versus additive content slope values proposed in the NCHRP Project 09-58 and evaluate the rutting resistance of asphalt mixtures with additive dosages selected to restore the intended AASHTO M 320 high-temperature grade.

1.3. Organization of the Report

This report is composed of six primary sections and five appendices. Section 1 presents the needs, objectives, and summarizes the most relevant literature. Section 2 describes the research methodology, including the materials evaluated and experimental methods. Section 3 presents the results and findings of the experiments. Section 4 summarizes the conclusions and

recommendations drawn from the results. Section 5 provides a suggested implementation and technology transfer plan. Appendix A provides the detailed literature review. Appendix B summarizes the development of practical methods to construct asphalt binder master curves used within the experimental plan. Appendix C details chemical compositional analysis of the asphalt binders and recycled binder blends with additives evaluated. Appendix D discusses efforts to evaluate the ability to predict the properties of recycled binder blends with an additive from known recycled binder properties and the properties of a blend containing virgin binder and the additive. Appendix E provides detailed statistical analysis results of the binder durability parameters evaluated.

2. METHODOLOGY

Figure 1 presents an overview of the research methodology undertaken to achieve the study objectives. The details of each step outlined in Figure 1 are detailed below.

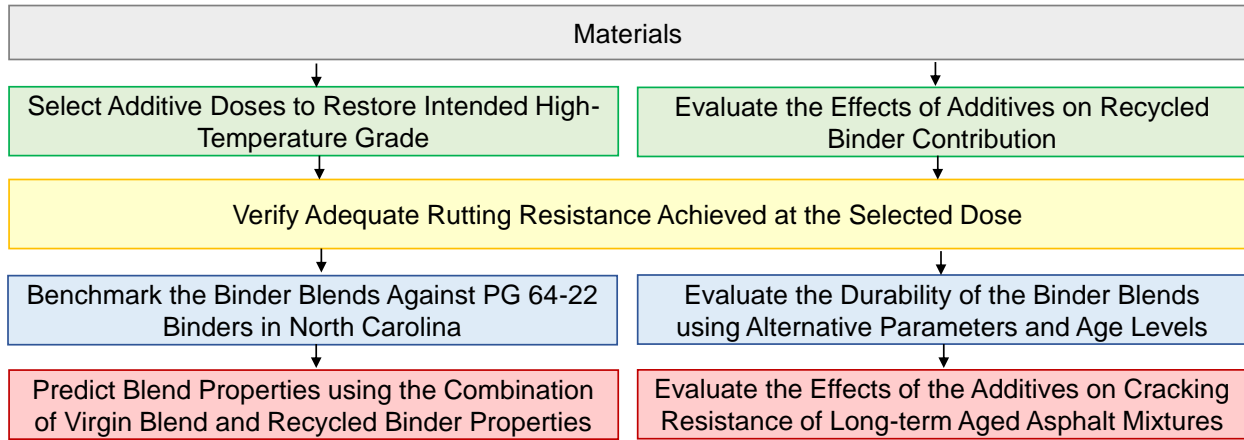


Figure 1. Overview of the research methodology

2.1. Materials

Table 2 details the three North Carolina Department of Transportation (NCDOT) approved asphalt mixtures evaluated in this study. Each mixture had a Nominal Maximum Aggregate Size (NMAS) of 9.5-mm. Each mixture was sourced from a different supplier. As per NCDOT standards, these mixtures specified a PG 58-28 virgin binder. The specified AASHTO M 320 PG for virgin binders in North Carolina is PG 64-22 in the absence of recycled materials or the requirement for polymer modification. A single PG 58-28 virgin binder and PG 64-22 binder were used in this study. The RAP only and RAS only mixtures were used for additive dosage selection and performance evaluation of the effects of additives at both the asphalt binder and mixture level. The RAP/RAS mixture and RAP only mixtures were used to evaluate the effects of additives on recycled binder contribution in asphalt mixtures.

Table 2. Summary of the Mixtures Evaluated

M	RAP/RAS	RAP	RAS
NCDOT Designation	RS9.5C	RS9.5B	RS9.5B
RAP (%)	25	40	0
RAS (%)	4	0	5
RBR (%)	29	36	14.5
Virgin PG	58-28	58-28	58-28
VMA	17.9	17.4	18.1
VFA	78.8	77.2	78.0
Dosage and Performance Evaluation		✓	✓
Recycled Binder Contribution Measurements	✓	✓	

Table 3 details the additives evaluated, codified to preserve the anonymity of the suppliers. The additives included three extenders and two recycling agents. To preserve the anonymity of the

suppliers, the recycling agents are designated R1 and R2 and extenders are designated as E1, E2, and E3.

Table 3. Summary of the Additives Evaluated

Additive ID	Description
R1	Recycling agent derived from triglycerides and fatty acids in a vegetable oil
R2	Recycling agent derived from triglycerides and fatty acids in a vegetable oil
E1	REOB
E2	Extender containing REOB
E3	Vacuum gas oil extender

2.2. Selection of Additive Dosages to Restore the Intended High-Temperature Grade

The dosage selection study undertaken sought to evaluate the universality of the blended system high-temperature grade versus additive content slope values proposed in the NCHRP Project 09-58 (Epps Martin et al. 2020).

2.2.1. Binder Blends

Eleven binder blends detailed in Table 4 containing different additives, recycled binder sources, and virgin binder were evaluated using the RAP and RAS binders from the RAP and RAS mixtures detailed in Table 2. The blends were prepared to match the RBR indicated in Table 2 for the respective mixture. Within Table 4, 58 indicates the blend contains a PG 58-28 virgin binder whereas 64 indicates the blend contains a PG 64-22 virgin binder. Asphalt binder was extracted and recovered from the RAP and RAS materials in accordance with ASTM D2172 Test Method A and ASTM D5404 for characterization and use in the preparation of the blends for this and subsequent tasks.

Preliminary blends of the PG 58-28 binder, extenders, and RAS indicated that dosage required to restore the blended binder high-temperature grade to 64°C would exceed the maximum limit for dosage proposed in the NCHRP Project 09-58 of 10 percent (Epps Martin et al. 2020); therefore, extenders were only evaluated in combination with the RAP binder. Select blends were prepared at a selected dosage to evaluate agreement between the measured and intended high-temperature grade.

Hamburg Wheel-track (HWT) testing was conducted on mixtures prepared using a subset of the blends at a selected dosage to restore the intended high-temperature AASHTO M 320 PG to evaluate rutting performance. In addition, the PG 58-28 binder was also blended with the recycled materials and no RA to serve as a control case representing the current practice in North Carolina. An additional RAP mixture, mix ID 11 in Table 4, was prepared and tested that was expected to fail the rutting criteria to ensure this was captured by the HWT test; this mix included a PG 58-28 virgin binder and R1, using the dosage established using the PG 64-22 virgin binder. Asphalt Mixture Performance Tester (AMPT) dynamic modulus and cyclic fatigue tests were also performed on long-term aged mixtures prepared based on a subset of the blends using additive dosages selected to restore the intended high-temperature PG.

Within the results, the blends are identified based on the virgin binder (58 for the PG 58-28 binder versus 64 for the PG 64-22 binder), recycled binder (RAP versus RAS) and additive type as shown in Table 4.

Table 4. Blends Evaluated

Blend ID	Blend Designation	Additive	Dosage Selection	Blend Verification	Hamburg Testing	AMPT Testing
1	58.RAP	None			✓	✓
2	58.RAS	None			✓	✓
3	64.RAP.R1	R1	✓	✓	✓	✓
4	64.RAP.E1	E1	✓			
5	58.RAP.E1	E1	✓	✓		
6	58.RAP.E2	E2	✓	✓	✓	✓
7	58.RAP.E3	E3	✓	✓		
8	64.RAS.R1	R1	✓	✓	✓	✓
9	58.RAS.R1	R1	✓			
10	64.RAS.R2	R2	✓	✓	✓	✓
11	58.RAP.R1	R1			✓	

2.2.2. Virgin and Recycled Binder Characterization

The high-temperature continuous PGs of the two virgin binders, two recycled binders, and blends of each recycled binder and PG 58-28 at the respective mixture RBR were determined using Dynamic Shear Rheometer (DSR). All testing and analysis was conducted in accordance with AASHTO T 315 and the grading criteria specified in AASHTO M 320.

To prepare blends of virgin and RAP binder, the virgin binder was preheated to 140°C and the RAP was pre-heated to 165°C. The RAP and virgin binders were thoroughly blended using a power drill with a paddle attachment for one minute. This procedure generally adheres to the recommendations given in NCHRP 09-58 (Epps Martin et al. 2020) that suggested preheating the recycled binder to 160°C to 200°C until sufficiently fluid and then mixing with the virgin binder. However, NCHRP 09-58 recommended hand mixing of samples whereas the drill was used herein because the authors felt it produced more repeatable mixing. A temperature of 200°C was insufficient to liquefy the RAS binder. Therefore, the ambient temperature RAS binder was ground using a mortar and pestle and combined with virgin binder pre-heated to 140°C. The combination of RAS and virgin binder was then mixed using a power drill for one minute. Pre-heating the RAS following grinding was found to increase agglomeration when added to the virgin binder and therefore, avoided.

Rolling Thin Film Oven (RTFO) aging was used to prepare short-term aged binder according to AASHTO T 240 for the virgin binders, RAP binder, and blends of virgin and recycled binder. The RAS binder did not achieve sufficiently low viscosity at 163°C to allow for RTFO aging. For the blends of RAS and virgin binder, and also blends of RAS, virgin binder, and recycling agents, clumps of RAS were visually evident in the original binder as shown in Figure 2 (a). However, these clumps were not evident in RTFO-aged samples containing RAS as shown in Figure 2 (b); therefore, testing of all binder blends containing RAS relied on RTFO-aged binder testing only and original binder test results were omitted.

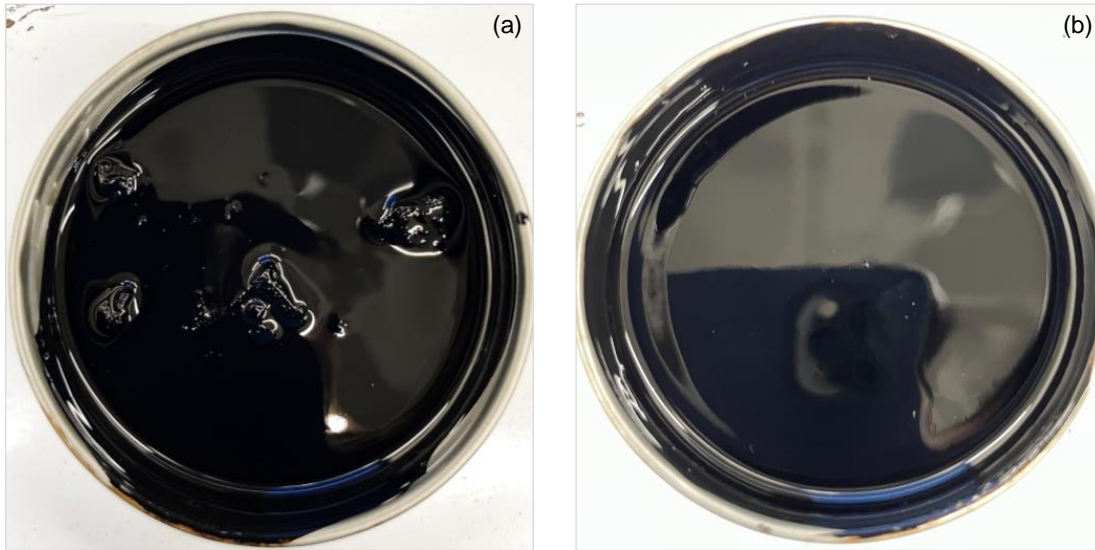


Figure 2. (a) RAS lumps visible after blending in original state (b) No RAS lumps visible after RTFO aging

DSR testing was conducted on original and RTFO aged samples according to AASHTO T 315. The results were analyzed to determine the standard high-temperature grade according to AASHTO M 320 and the continuous high-temperature grade according to ASTM D7463. DSR testing was conducted at a minimum of two temperatures, one passing the AASHTO M 320 high-temperature grading criteria and one failing. The RAS binder was only tested in the original age condition since RTFO testing was not possible; however, the RTFO-aged binder criteria given in AASHTO M 320 was used for high-temperature grade determination under the assumption that the binder would not undergo significant further oxidative age hardening if subjected to short-term aging.

2.2.3. Additive Dosage Selection

Blends 3 to 10 in Table 4 were each prepared at two trial additive dosage levels. For blends containing RAS, dosages of 10 percent and 6 percent by weight of total binder were used for all blends because the dosages estimated using Equations (1) and (2) exceeded the maximum dosage recommended in NCHRP 09-58 of 10 percent when using the PG 64-22 virgin binder and was very close to this limit when using the PG 58-28 virgin binder. For blends containing RAP, one of the two dosages was selected to coincide with the dosage level calculated using Equations (1) and (2) with $X = 1.82$. In this case, the high-temperature continuous grade of the blends of virgin and recycled binders were first calculated at the original ($PGH_{Blend, original}$) and RTFO ($PGH_{Blend, RTFO}$) levels using Equation (2) based on the measured high-temperature PG results of the recycled and virgin binders using the mixture RAP_{BR} of 0.36; the minimum of the two calculated grades was used in Equation (1) as the PGH_{Blend} . For a given blend, once PGH_{Blend} was determined, it was used along with a PGH_{Target} of 64 and X value of 1.82 in Equation (1) to calculate the first dosage level. The second dosage level was set at 2 percent by total weight of binder.

Blends of virgin and recycled binder were prepared in the same way as described under *Virgin and Recycled Binder Characterization*. Following blending of the virgin and recycled binder, the blended system was placed back in an oven set to 165°C for one minute. Then, the binder was removed from the oven, the additive was added, and the system was mixed for an additional minute

using the power drill. After mixing, a portion of each blend was poured into an RTFO bottle and subjected to short-term aging according to AASHTO T 240 and a portion was used directly for DSR testing. Original and RTFO-aged samples of blends containing RAP and RTFO-aged samples of blends containing RAS only were subjected to DSR testing in accordance with AASHTO T 315 and AASHTO M 320 for high-temperature grade determination. DSR testing was conducted at a minimum of two temperatures, one passing the AASHTO M 320 high-temperature grading criteria and one failing. Using the results, continuous high-temperature grades were calculated according to ASTM D7463. The results were used to evaluate four methods of selecting the additive dosages.

Method 1

Linear regression of the continuous high-temperature grade results was applied to determine the X_i values in Equations (5) and (6) using fixed intercepts corresponding to the $PGH_{\text{Blend, original}}$ and $PGH_{\text{Blend, RTFO}}$ values determined from Equation (2). The corresponding additive dosages required to yield the target high-temperature grade of 64°C at the original and RTFO age levels (i.e., Selected Additive_{Original} (%) and Selected Additive_{RTFO} (%)) were calculated using Equations (7) and (8), respectively. The minimum of the calculated Selected Additive contents from the two age levels was reported as the selected dosage and the corresponding X values were tabulated. For the RAS blends, the same procedure was followed using results corresponding to the RTFO age level only.

$$PGH_{\text{Blend+Additive,original}} = PGH_{\text{Blend,original}} - X_{\text{original}} \times \text{Additive}(\%) \quad (5)$$

$$PGH_{\text{Blend+Additive,RTFO}} = PGH_{\text{Blend,RTFO}} - X_{\text{RTFO}} \times \text{Additive}(\%) \quad (6)$$

$$\text{Selected Additive}_{\text{original}} (\%) = \frac{PGH_{\text{Blend, original}} - 64}{X_{\text{original}}} \quad (7)$$

$$\text{Selected Additive}_{\text{RTFO}} (\%) = \frac{PGH_{\text{Blend, RTFO}} - 64}{X_{\text{RTFO}}} \quad (8)$$

Method 2

For the blends containing PG 58-28 virgin binder (i.e., Blends 5, 6, 7, and 9 in Table 4), the required additive dosages were also calculated using an analogous approach as described above, but using the measured PGH_{Blend} values rather than those estimated using Equation (2). This process allowed for assessing the impacts of any errors introduced from estimating the grade of virgin-recycled binder blends using Equation (2) on the selected additive dosage.

Method 3

The collective results of blends containing the same additive were used to evaluate the universality of the slope of the change in the continuous high-temperature PG at the RTFO age level (ΔPGH_{RTFO}) versus additive content (termed X_{Additive}). The results of blends with the same additive (i.e., Blends 3, 8, and 9 that all contain R1 were aggregated, and Blends 4 and 5 were aggregated that both contain E1) and linear regression was used to determine the X_{Additive} in Equation (9), using a fixed intercept of zero. Then, the selected additive contents according to Method 3 (i.e., Selected Additive_{RTFO} (%)) were calculated using Equation (10). Method 3 was only applied to the RTFO age level results because dosages selected using Methods 1 and 2 were found to be driven by the RTFO age level for these blends.

$$\Delta PGH_{RTFO} = PGH_{Blend+Additive,RTFO} - PGH_{Blend,RTFO} = X_{Additive} \times Additive(\%) \quad (9)$$

$$\text{Selected Additive}_{RTFO} (\%) = \frac{PGH_{Blend, RTFO} - 64}{X_{Additive}} \quad (10)$$

Method 4

Equations (1) and (2) were used to calculate the required dosage for each blend using the average X values reported in the NCHRP 09-58 project. The selected dosages corresponding to the X values suggested for both petroleum-based aromatic extracts (Method 4A) and other additive types (Method 4O) were tabulated for the blends containing extenders whereas dosages were only calculated using the X value suggested for all other additive types (Method 4O) for the blends containing recycling agents. The recycling agents evaluated are both vegetable oils. Vegetable oil recycling agents were included as part of the dosage selection procedure in NCHRP Project 09-58 and included in the non-aromatic extract category (Epps Martin et al. 2020). However, the slopes suggested for both classes of materials were evaluated for blends containing extenders because it is not clear if the extenders evaluated are more similar to aromatic extracts or the other product category used in NCHRP Project 09-58. The extenders evaluated herein are derived from petroleum extracts, similar to aromatic extracts. However, they most closely align with the paraffinic oil classification given in NCHRP Project 09-58, but paraffinic oils were not evaluated as part of the dosage selection procedure development in that project (Epps Martin et al. 2020).

2.2.4. Blend Verification at a Selected Dose

Blends 3, 5, 6, 7, 8, and 10 in Table 4 were prepared at the additive dose selected using Method 1. The verification blends were prepared and tested using the same procedures used as part of dosage selection to determine their continuous high-temperature grades. The results were compared to the expected high-temperature PG from dosage selection analysis conducted according to Methods 1 through 4.

2.3. Evaluation of the Effects of Additives on Recycled Binder Contribution

The RAP and RAP/RAS mixtures in Table 2 were used to evaluate the effects of extenders and RAs on recycled binder contribution using the mixture design variations detailed in Table 5. The additive contents used in each mixture are given by the number in parentheses following the mixture ID. In Table 5, the number at the front of the mixture ID indicates the virgin binder used in the mixture (i.e., PG 58-28 or PG 64-22), RAP indicates the mixture design corresponding to the RAP mixture design in Table 2 whereas RAP.RAS indicates the mixtures design corresponding to the RAP/RAS mixture design in Table 2 and then the additive is indicated (if included) followed by the dose in percentage. For a given mixture design, the total binder content was fixed among the mix variations (i.e., 58.RAP, 64.RAP, 64.RAP.R1, and 64.RAP.E1 all had the same total binder content, considering the additive as part of the binder volume). The 64.RAP mixture was included in an effort to isolate the effects of the additives and virgin binder on the recycled binder contribution in the RAP mixture.

Table 5. Mixtures Used for Recycled Binder Contribution Measurements

Mixture ID (additive dose)
58.RAP
64.RAP
64.RAP.R1 (5.5)
64.RAP.E1 (7.0)
58.RAP.RAS
58.RAP.RAS.R1 (5.5)
58.RAP.RAS.R2 (5.5)

Recycled binder contribution was measured using tracer-based microscopy according to the specimen fabrication and analysis procedure proposed by Pape and Castorena (2021) and briefly summarized here. Laboratory-mixed, laboratory-compacted asphalt mixture samples were prepared using a titanium dioxide microparticle tracer with 0.2 micron diameter added to the virgin binder to distinguish it from the recycled binder. The titanium dioxide was added at a dosage of 10 percent by mass of the virgin binder using high shear mixing. For mixtures containing additives, the additive and virgin asphalt were first mixed following the same procedure described in Section 2.2.2 and then the tracer was added. Titanium is not naturally present in asphalt whereas sulfur is present in all binders. Small prism samples were sawn from the gyratory-compacted samples for microscopy analysis. Measurements of titanium and sulfur were used to quantify the concentration of recycled binder within local regions of the virgin binder matrix of asphalt mixtures using Energy Dispersive X-ray Spectroscopy Scanning Electron Microscopy (EDS-SEM). EDS analysis was also performed to measure the sulfur and titanium concentrations of the virgin and extracted recycled binders. EDS analysis was performed in a Hitachi S3200N VPSEM outfitted with an Oxford X-Max silicon drift detector. The ratio of the measured recycled binder concentration to the expected value under the condition of complete availability reflects the recycled binder contribution.

EDS-SEM measurements were made at a minimum of 10 locations within each mixture analyzed. Each measurement was used to calculate the local recycled binder contribution according to Equation (11). The results were averaged and reported as the overall mixture recycled binder contribution. Calculation of the recycled binder contribution using Equation (11) considers the amount of recycled binder present in the image using the Ti:S ratios. These are compared to the theoretical level of the perfect contribution scenario to calculate the recycled binder contribution. It is noted that measurements of recycled binder contribution in RAP/RAS mixtures include contributions from both RAP and RAS together.

$$\text{Local Recycled Binder Contribution (\%)} = \left(\frac{\text{Virgin}_{Ti:S}}{\text{Mix}_{Ti:S}} - 1 \right) \times \frac{AC - RAP_{AC} - RAS_{AC}}{RAP_{AC} + RAS_{AC}} \times \frac{S_V}{S_R} \times 100\% \quad (11)$$

Where: Local Recycled Binder Contribution (%) = ratio of measured recycled binder concentration divided by the recycled binder concentration expected under the condition of complete contribution; $\text{Virgin}_{Ti:S}$ = titanium to sulfur concentration ratio in the virgin binder; $\text{Mix}_{Ti:S}$ = Ti:S concentration ratio of mix sample in area of interest; AC = total asphalt content; RAP_{AC} = RAP binder content; RAS_{AC} = RAS binder content; S_V = sulfur content of the virgin binder; and S_R = sulfur content of the recycled binder.

2.4. Measurement of Asphalt Mixture Rutting Resistance at the Selected Dosages

HWT testing was completed in accordance with AASHTO T 324 for a subset of the study blends at the dosages selected according to Method 1, see Table 4. The purpose of the HWT testing was to evaluate the rutting resistance of asphalt mixtures with additive dosages selected to restore the intended AASHTO M 320 high-temperature grade.

Laboratory-mixed samples were prepared and subjected to short-term aging for two hours at 135°C as recommended in the NCHRP Project 09-52 (Newcomb et al. 2015); this procedure was found to yield approximately the same age level as the asphalt binder RTFO procedure in the NCHRP Project 09-61 (Bonaquist et al. 2021). The HWT test specimens were fabricated with 7 ± 0.5 percent air void content and a height of 62 mm (2.44 in.) and diameter of 150 mm (6 in.) using the gyratory compactor. Throughout the HWT test, specimens were submerged under the water at 50°C in order to induce moisture damage and control the testing temperature. After preconditioning the specimens for 45 minutes, they were subjected to the repeated rolling steel wheel with the constant load of 705 ± 4.5 N (158 ± 1.0 lb) and passing rate of 52 ± 2 passes/min. LVDTs were used to measure the rut depth at 11 uniformly spaced locations in the wheel path. The rut depth was reported as the average of the five measurements closest to the center of the sample. The test results were reported as the number of wheel passes to reach a 12.5-mm rut depth. Tests were terminated at 20,000 cycles if a rut depth of 12.5-mm had not been reached. NCHRP Project 09-58 proposed that mixtures in climates with grades of PG 64-22, such as North Carolina, should exceed 10,000 cycles to a failure rut depth of 12.5-mm to ensure adequate rutting resistance (Epps Martin et al. 2020).

2.5. Benchmarking Binder Blends using Performance-Graded Properties

To complement the AASHTO M 320 high-temperature performance-grading discussed in Section 2.2.4, intermediate- and low-temperature grading was also conducted on blends prepared at the selected dosages and an additional blend was evaluated. The intermediate-temperature characterization was conducted using a DSR according to AASHTO T 315 and the low-temperature characterization was conducted using a bending beam rheometer (BBR) according to AASHTO T 313. Testing was conducted at a minimum of two temperatures, one passing the AASHTO M 320 high-temperature grading criteria and one failing with the exception of the low-temperature grades of the MRAS blends with recycling agents. Satisfactory BBR data was obtained at -18°C for all blends. However, BBR results at the second test temperature failed to meet repeatability requirements of AASHTO T 313 in several MRAS blend cases so the test results were omitted. It is speculated this was due to storage stability issues associated specifically with the MRAS. The blends with problematic repeatability were stored longer than other blends and displayed evidence of agglomerated RAS binder prior to annealing the binder to prepare BBR test specimens. Thus, MRAS blends may have a short shelf life due to storage stability concerns. Continuous PGs were determined in accordance with either AASHTO M 320 and ASTM D7463. The intermediate- and low-temperature characterization of the blends was conducted on RTFO plus the standard 20-hour pressure aging vessel (PAV)-aged (P20) material and on RTFO plus the increasingly common 40-hour PAV-aged (P40) material. Table 6 details the study blends. The RBRs of the blends detailed in Table 6 coincide with those used in Section 2.2 and the dosages coincide with those selected according to Method 1 described in Section 2.2.3.

Table 6. Blends Benchmarked using Performance-Graded Properties

Blend Designation	Additive Dose (%)
58.RAP	--
58.RAS	--
64.RAP.R1	5.5
64.RAP.R2	5.5
58.RAP.E1	7.0
58.RAP.E2	3.6
58.RAP.E3	6.7
64.RAS.R1	6.6
64.RAS.R2	7.4

The AASHTO M 320 performance-graded properties of the blends containing RAs and extenders were compared to those of PG 64-22 virgin binders in the state of North Carolina. PG 64-22 virgin binders were considered a reference condition to benchmark the recycled binder blends against since they represent the binder used in the absence of recycled materials for the majority of asphalt mixtures specified in North Carolina. Quality assurance (QA) data from 2016 to 2021 provided by the NCDOT for PG 64-22 virgin binders were used to establish benchmarks against which to compare the blends with RAs and extenders. A total of 200 PG 64-22 binders were used to constitute a reference binder for North Carolina’s (NC’s) recycled asphalt binder blends.

2.6. Evaluation of the Durability of Binder Blends using Alternative Parameters and Age Levels

A more through analysis of the durability of the study virgin binders and recycled binder blends detailed in Table 6 was conducted using alternative parameters proposed in the literature as better measures of durability. The basis for these parameters is described in Section 1.2.3. The parameters were calculated using intermediate- and low-temperature performance-graded test results, temperature-frequency sweep (TFS) test results, and Linear Amplitude Sweep (LAS) test results. The parameters and test methods used to evaluate binder durability are detailed below. Each parameter was characterized at the P20 and P40 age level.

2.6.1. Parameters from Standard PG Test Methods

The ΔT_c values and R values were calculated from BBR test results in addition to the standard low-temperature PG parameters (i.e., creep stiffness at 60 seconds of loading in the BBR ($S(60)$) and relaxation rate at 60 seconds of loading in the BBR ($m(60)$). The ΔT_c values could not be calculated for the MRAS blends containing R1 and R2 due to the BBR repeatability issues at -12°C noted above. The R values were calculated using the $S(60)$ and $m(60)$ results at -18°C according to Equation (12) in accordance with the recommendations from NCHRP Project 09-59 and denoted the ‘ R_{09-59} ’ herein (Christensen and Tran 2022). Data at -18°C rather than -12°C (i.e., critical test temperature for PG 64-22 climate) was used due to the issues with the -12°C for the MRAS blends noted above.

$$R_{09-59} = \log(2) \times \frac{\log(S(60) / 3,000)}{\log(1 - m(60))} \quad (12)$$

In addition, the intermediate-temperature PG test results were used to calculate the G-R parameter (i.e., $|G^*| \times \cos^2 \delta / \sin \delta$) was determined at 25°C and 10 rad/s in addition to the standard parameter (i.e., $|G^*| \times \sin \delta$) to align with the recommendations of NCHRP Project 09-59 (Christensen and Tran 2022).

2.6.2. Temperature-Frequency Sweep Test and Associated Parameters

As discussed in Section 1.2.3, several durability-related parameters have been proposed that are derived from asphalt binder master curves. Master curves are typically constructed using temperature-frequency sweep (TFS) test results. Standard methods for TFS testing and master curve construction do not presently exist. Herein, temperature-frequency sweep testing was conducted using the 8-mm parallel plate geometry in a DSR at 5°C, 20°C, 35°C, and 50°C using a frequency range of 0.1 to 10 Hz. A strain amplitude of 1.0 percent was applied at 35°C, and 50°C and a lower strain of 0.1 percent was applied at 5°C, 20°C. These strains were verified to yield test results that fell within the linear viscoelastic regime based on strain sweep testing of a subset of the study binders. Testing adhered to AASHTO T 315. A minimum of two replicate tests were conducted for each binder and age level combination. Replicates were run until repeatability was evaluated and verified to meet AASHTO T 315 precision limits. The average test results for a given binder and age level combination were used to construct the master curves. Given the lack of a standardized method to construct an asphalt binder master curve, an initial effort was conducted to establish practical methods to construct asphalt binder master curves and obtain CA model coefficients. This effort is detailed in Appendix B. Within the main body of the report, the results presented coincide with master curves constructed using the pairwise interpolation method detailed in Appendix B. The time-temperature shift factor model and CA model coefficients were subsequently calculated using the linear regression (LR) method detailed in Appendix B. The crossover frequency (ω_c) and R CA model coefficients were evaluated. Crossover frequency was calculated at a reference temperature of 20°C. In principle, the R values calculated from TFS and BBR results should be the same. However, this has not been directly assessed in the literature. Additional master curve-based parameters evaluated include the G-R parameter 15°C and 0.005 rad/s and crossover temperature (T_c) calculated using the resultant time-temperature shift factor and CA model coefficients for the master curves. The T_c was calculated as the temperature where phase angle is equal to 45° and frequency of 10 rad/s based on the recommendations of Cucalon et al. (2017).

2.6.3. Linear Amplitude Sweep Test and Associated Parameters

Linear amplitude sweep (LAS) tests were also conducted as another measure of fatigue damage resistance. LAS tests adhered to the recommendations of Hintz and Bahia (2013) and Safaei and Castorena (2016). The test temperatures were either 16°C or 19°C, depending on the binder modulus. Test temperatures were selected to have linear viscoelastic $|G^*|$ values at the test frequency of 10 Hz that fell within the range of 12 to 60 MPa based on recommendations of Safaei and Castorena (2016) to ensure cohesive cracking failure. In the LAS test, a frequency sweep tests is first used to measure the undamaged binder response using a strain amplitude of 0.1 percent over a frequency range from 0.2 to 30 Hz at the test temperature. After the frequency sweep test has been performed, an amplitude sweep is performed. This test is performed in strain-controlled mode with a frequency of 10 Hz. The loading is increased in a linear manner from 0 to 30 percent over five minutes with phase angle and dynamic shear modulus being recorded every 10 load cycles. A simplified viscoelastic continuum damage-based (S-VECD-based) model is calibrated using the test results and used to predict the fatigue life under constant strain amplitude conditions.

In this study, the results were used to calculate the fatigue life at 5 percent and 15 percent strain levels following the approach employed by Yang et al. (2022).

2.6.4. Analysis of the Durability-related Parameters

Table 7 provides a summary of the collective alternative indicators of binder durability evaluated. Table 7 includes a list of abbreviations for the different parameters used within the results. For each parameter listed in Table 7, Tukey Honest Significant Different (HSD) tests were conducted using the Tukey Kramer method at the P20 and P40 age levels (separately) using a confidence level of 95 percent. The Tukey HSD test is a multiple comparison test that identifies samples with statistically equal versus different mean values. The outcome of the test is the identification of rank order of groups of samples identified as having statistically different means. The Tukey HSD tests were used to evaluate the ability of the different parameters to discriminate differences among the different binders and blends evaluated. The Tukey HSD test outcomes were also used to evaluate cases where a parameter indicated a given blend was better, worse, or equal to the PG 64-22 virgin binder evaluated (and constituting the target binder properties in the absence of recycled binder). Similar comparisons were made between the properties of blends containing additives and the respective ‘reference’ 58.RAP and 58.MRAS blends which reflect the current practice for the mixtures evaluated. In addition, Pearson’s correlation coefficients and Spearman’s rank correlation coefficients were calculated for each possible pair of parameters to identify groups of durability-related parameters that provide similar insight regarding the relative performance of binders. Correlation coefficients were calculated separately for results at the P20 and P40 age levels. Pearson’s correlation coefficients evaluate the strength of linear relationships between variables. Spearman’s rank correlation is a nonparametric measure of rank correlation between two variables. It assesses whether monotonic relationships exist between two variables without the stipulation of a linear relationship. Pearson’s correlation coefficients and Spearman’s rank correlation coefficients were also calculated for each variable at the P20 versus P40 level to evaluate whether or not the two age levels provide similar or distinct insight regarding the relative performance of the binders evaluated.

Table 7. Summary of Alternative Indicators of Binder Durability Evaluated

Parameter	Abbreviation	Test Method
$ G^* \times \sin \delta @ 25^\circ\text{C}, 10 \text{ rad/s}$	$ G^* \times \sin \delta \text{ (kPa)}$	AASHTO T 315
G-R @ 25°C, 10 rad/s	GR _{25°C} (kPa)	AASHTO T 315
G-R @ 15°C, 0.005 rad/s	GR _{15°C} (kPa)	TFS
ω_c	$\omega_c \text{ (Hz)}$	TFS
T_c	$T_c \text{ (}^\circ\text{C)}$	TFS
Master Curve R	R _{MC}	TFS
NCHRP 09-59 R	R ₀₉₋₅₉	AASHTO T 313
$S(60) @ -18^\circ\text{C}$	$S(60) @ -18^\circ\text{C (MPa)}$	AASHTO T 313
$m(60) @ -18^\circ\text{C}$	$S(60) @ -18^\circ\text{C (MPa)}$	AASHTO T 313
ΔT_c	$\Delta T_c \text{ (}^\circ\text{C)}$	AASHTO T 313
$N_f @ 5\%$	$N_f @ 5\%$	LAS
$N_f @ 15\%$	$N_f @ 15\%$	LAS

2.7. Effects of Additives on the Saturates, Aromatics, Resins, and Asphaltenes Composition of Asphalt Binders

To complement the rheological evaluation of the asphalt binders and blends, the effects of the additives on the composition of asphalt binders was evaluated using Saturates, Aromatics, Resins, and Asphaltenes (SARA) analysis of virgin binders, RAP binder, and select blends at the RTFO and RTFO plus 40-hour PAV (P40) age levels. The analysis suggested that E1 and E2 affect colloidal stability negatively whereas R1 and R2 did not. This effort is detailed in Appendix C.

2.8. Prediction of Binder Blend Properties Using Virgin Blends and Recycled Binder Properties

Given that extraction, recovery, and testing of recycled binders or blends containing recycled binder is cumbersome, the ability to screen the performance of binders using testing of the virgin binder blended with additives alone was evaluated. Accordingly, blends of virgin binder and additives were prepared at dosages to reflect their relative proportions in the blends containing virgin binder, additive, and recycled binder detailed in Table 6. The blending process aligned with that described in Section 2.2.1. The AASHTO M 320 performance-graded DSR properties of the virgin blends were determined, consistent with the testing detailed in Section 3.5. Subsequently, the ability to predict the rheological properties of the blends of virgin binder, recycled binder, and additives on the basis of properties of the recycled binder and properties of the blend of virgin binder and additive was assessed using micromechanical and mixing models. Models generally yielded poor prediction results unless a recycled binder/virgin binder blend specific interaction parameter was considered, suggesting screening performance on the basis of a blend of virgin binder and additive is not possible. This effort is detailed in Appendix D.

2.9. Evaluation of the Effects of Additives on the Cracking Performance of Long-Term Aged Asphalt Mixtures

Laboratory-mixed asphalt mixture samples of a subset of the study blends were prepared and subjected to both short- and subsequent long-term aging for cracking performance evaluation to further evaluate the effect of RAs and extenders on durability. A long-term age condition was used for cracking evaluation given that the literature indicates additive effectiveness may diminish over the life of the pavement. The blends used for cracking performance evaluation are identified in Table 4. The corresponding additive dosages used for each blend are given in Table 6. Short-term aging was conducted in accordance with AASHTO R 30 guidance for preparing performance test specimens, consisting of 4 hours of oven conditioning at 135°C. The short-term aged loose mixture was then subjected to long-term aging according to the recommendations of the NCHRP Project 09-54 (Kim et al. 2021). In this method, the long-term oven aging of the loose mixtures is accomplished by separating the mixture into several pans such that each pan had a relatively thin layer of loose mix that was approximately equal to the nominal maximum aggregate size (NMAS) of the aged mix. The pans of loose mixture were conditioned in an oven at 95°C and systematically rotated to minimize any effects of an oven temperature gradient and/or draft on the degree of aging. The aging duration is selected using the so-called climatic aging index (CAI) which prescribes the duration of aging at 95°C required to achieve the same aging level as a given hourly pavement temperature history and depth below the pavement surface of interest. Herein, the oven aging duration was chosen to reflect 12 years of aging in Raleigh at a depth of 20-mm below the pavement service (i.e., the representative age level of a surface layer in North Carolina at the end of its life prior to an overlay). The corresponding oven aging duration identified was 7 days.

The Asphalt Mixture Performance Tester (AMPT) was used to measure the cracking performance of the long-term aged asphalt mixtures. Test specimens for dynamic modulus and cracking characterization were prepared in accordance with AASHTO PP 99. Dynamic modulus testing adhered to AASHTO TP 132 and cyclic fatigue testing was executed in accordance with AASHTO TP 133. Dynamic modulus master curves were constructed and represented by the 2S2P1D model in accordance with AASHTO TP 133. The collective dynamic modulus and cyclic fatigue test results were also analyzed according to AASHTO TP 133 to obtain two key material functions of the simplified viscoelastic continuum damage (S-VECD) model: the damage-characteristic curve (i.e., pseudostiffness (C) versus the internal state parameter representing damage (S)) and the pseudostrain energy-based fatigue failure criterion (D^R). The damage-characteristic curve and failure criteria are independent of the loading mode and loading history. Consequently, they enable prediction of the damage response to any given loading history of interest. AMPT cyclic fatigue test results can also be used to calculate an index parameter to indicate asphalt mixture fatigue resistance, termed the apparent damage capacity (S_{app}). The S_{app} value incorporates the effects of the material's modulus and toughness on its fatigue resistance and measures the amount of fatigue damage the material can tolerate under loading. The temperature for the S_{app} calculation is equal to the average of high- and low-temperature grades at the standard 98-percent reliability level minus 3°C for the climate where the mixture is to be placed. Higher S_{app} values indicate increased fatigue resistance. The S_{app} values were calculated according to AASHTO TP 133. The location for S_{app} calculations herein was taken to be Raleigh, NC. In addition, the asphalt binder blends were extracted and recovered in accordance with ASTM D2172 Test Method A and ASTM D5404 from the long-term aged mixtures and subjected to temperature-frequency sweep testing in accordance with the methods described in Section 2.6.2.

3. RESULTS

3.1. Evaluation of Dosage Selection Procedures to Restore the Intended High-temperature Climatic Grade

3.1.1. Virgin and Recycled Binder AASHTO M 320 High-Temperature Grades

Table 8 shows the continuous high-temperature grades for the virgin binders, recycled binders, and blends of virgin and recycled binders. The numbers in parentheses in Table 8 correspond to high-temperature grades estimated using Equation (2) from the virgin and recycled binder high-temperature grade results. The results show that the virgin binders met specified high-temperature grade. The RAS binder has an extremely high measured grade of 176.6°C. The RAS high-temperature grade is considered an estimate because the test temperatures used were outside of the calibration range of the rheometer so the accuracy of the temperature recording from the DSR is unknown. Nevertheless, the results were used as part of dosage selection according to Methods 1, 2, and 4.

For the binder blends, the results show that both the estimated and measured high-temperature grades exceed the intended grade of 64°C even when a PG 58-28 virgin binder is used. Comparing the results of direct measurements of the blends' high-temperature grades against those estimated using Equation (2) reveal differences ranging from 0.7°C (blend of PG 58-28 virgin binder and RAP at the RTFO age level) to 3.6°C (blend of PG 58-28 virgin binder and RAS binder). The implications of these discrepancies on additive dosage selection were assessed by comparing the results of Methods 1 and 2 for blends prepared with the PG 58-28 virgin binder.

Table 8. Virgin and Recycled Binder AASHTO M 320 Continuous High-temperature Grades

Recycled Binder	Virgin Binder	Original Binder Grade	RTFO Binder Grade
--	PG 58-28	60.7	61.2
--	PG 64-22	67.3	69.0
RAP	--	91.0	90.7
RAS	--		176.6
RAP	PG 58-28	73.4 (71.5)	72.5 (71.7)
RAS	PG 58-28	--	78.4 (82.0)
RAP	PG 64-22	(75.7)	(76.8)
RAS	PG 64-22	--	(88.4)

3.1.2. Dosage Selection

Table 9 shows the compiled slope of the blended systems according to Methods 1 through 4. A maximum dosage of 10 percent was recommended in NCHRP Project 09-58 (Epps Martin et al. 2020); therefore, 10 percent is shown in parentheses in cases where the calculated dose exceeded this maximum limit. A detailed discussion of the results of each method along with comparisons across the methods is provided in the following sections.

Table 9. Slopes and Selected Additive Dosages

Blend	Slope			Selected Additive (%)				
	Method 1	Method 2	Method 3	Method 1	Method 2	Method 3	Method 4	
							A	O
64.RAP.R1	2.33		2.42	5.5		5.3		6.4
64.RAP.E1	1.27		1.17	10.1 (10)		11.0 (10)	11.2 (10)	8.5
58.RAP.E1	1.08	1.23	1.17	7.0	6.9	6.6	5.4	4.1
58.RAP.E2	2.06	2.53		3.6	3.7		5.4	4.1
58.RAP.E3	1.12	1.32		6.7	6.9		5.4	4.1
64.RAS.R1	2.20		2.42	11.0 (10)		10.1 (10)		13.4 (10)
58.RAS.R1	2.69	2.27	2.42	6.6	6.3	7.4		9.8
64.RAS.R2	3.23			7.4				13.4

Method 1

Figure 3 shows the dosage selection results according to Method 1 for Blends 3 to 10. The resultant Equation (5) or (6) used to select the dosage required to restore the continuous high-temperature grade to 64°C is shown for each blend in Figure 3. The legend in this figure indicates whether the original, Equation (5), or RTFO, Equation (6), results dictated the selected dose (i.e., yielded a lower required dose). The selected dose data points correspond to those calculated using the equations shown to yield a high-temperature grade of 64°C. The intercept values shown correspond to the $PGH_{Blend, original}$ and $PGH_{Blend, RTFO}$ estimates using Equation (2). Figure 3 (a) through (d) shows that for three out of the four RAP blends evaluated, the RTFO age level results dictated the selected dose. Overall, Figure 3 shows that the relationship between the blend high-temperature grade and additive content adhere to the linear relationship prescribed by Equations (5) and (6) quite well based on the high R^2 values shown. The first exception is the RTFO aging level for 58.RAP.E2, Figure 3 (d). This blend is one out of two of the only RAP blends where the original age level dictated the selected dose. The second exception is 64.RAS.R2, shown in Figure 3 (h). Blend 64.RAS.R2 was the only blend that contained additive R2. The results in Figure 3 (b), (c), and (f) show that extrapolation was required to predict the dosage that would yield a high-temperature grade of 64°C. Note that higher dosages for these blends were not tried for additive E1, shown in Figure 3 (b) and (c), because this would have led to REOB contents that exceed the NCDOT's maximum limit. A higher dose was also not attempted for blend 64.RAS.R1, shown in Figure 3 (f), because this would have yielded a dose higher than the maximum of 10 percent recommended in NCHRP Project 09-58. Figure 3 shows that the slopes of the blend high-temperature PG versus additive content differ considerably among blends, spanning a range of 1.08 to 3.23. Within a given additive type (i.e., Figure 3 (a), (f), and (g); Figure 3 (b) and (c)), the slopes for blends containing different virgin and recycled binders are generally more similar than across blends containing different additive types.

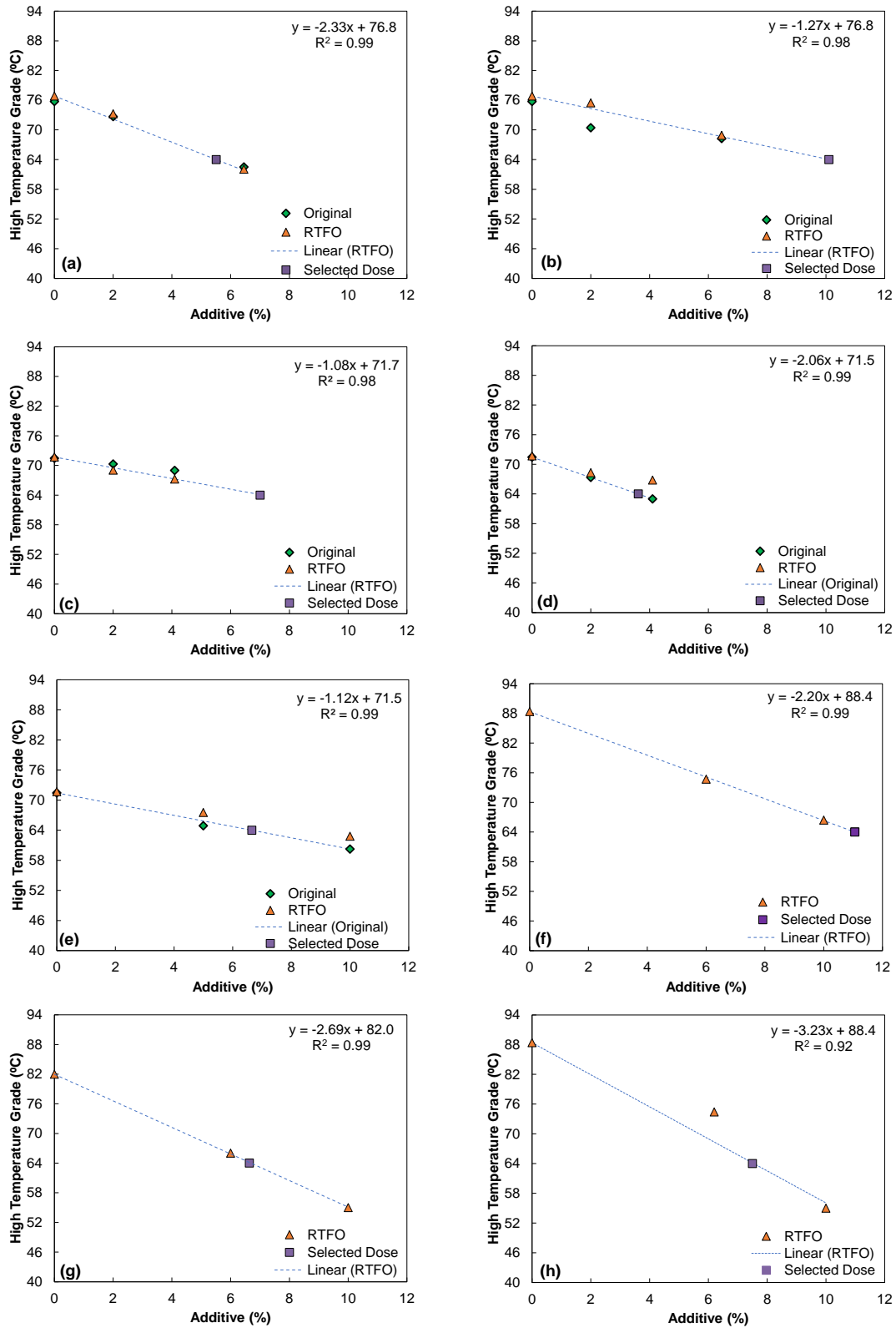


Figure 3. Dosage selection results for blends according to Method 1: (a) 64.RAP.R1, (b) 64.RAP.E1, (c) 58.RAP.E1, (d) 58.RAP.E2, (e) 58.RAP.E3, (f) 64.RAS.R1, (g) 58.RAS.R1, (h) 64.RAS.R2

Method 2

Figure 4 shows the comparison between the dosage selection results according to Method 1 and Method 2 for Blends 5, 6, 7, and 9. Method 2 is the same as Method 1 with the exception that the intercept of the line fit to the relationship between the high-temperature grade and additive content is the measured grade of the blend of the recycled and virgin binder rather than that estimated using Equation (2). Figure 4 includes the results at only the age level that dictated the selected dosage for the given blend (i.e., yielded the minimum selected dosage). The selected dose data points correspond to those calculated using the equations shown to yield a high-temperature grade of 64°C. The results show that the two methods yield somewhat different slopes of high-temperature grade versus additive content due to the difference in intercept values. However, the calculated dosages to restore the high-temperature grade to 64°C from the two methods are very close in all cases with a maximum difference of 0.3 percent.

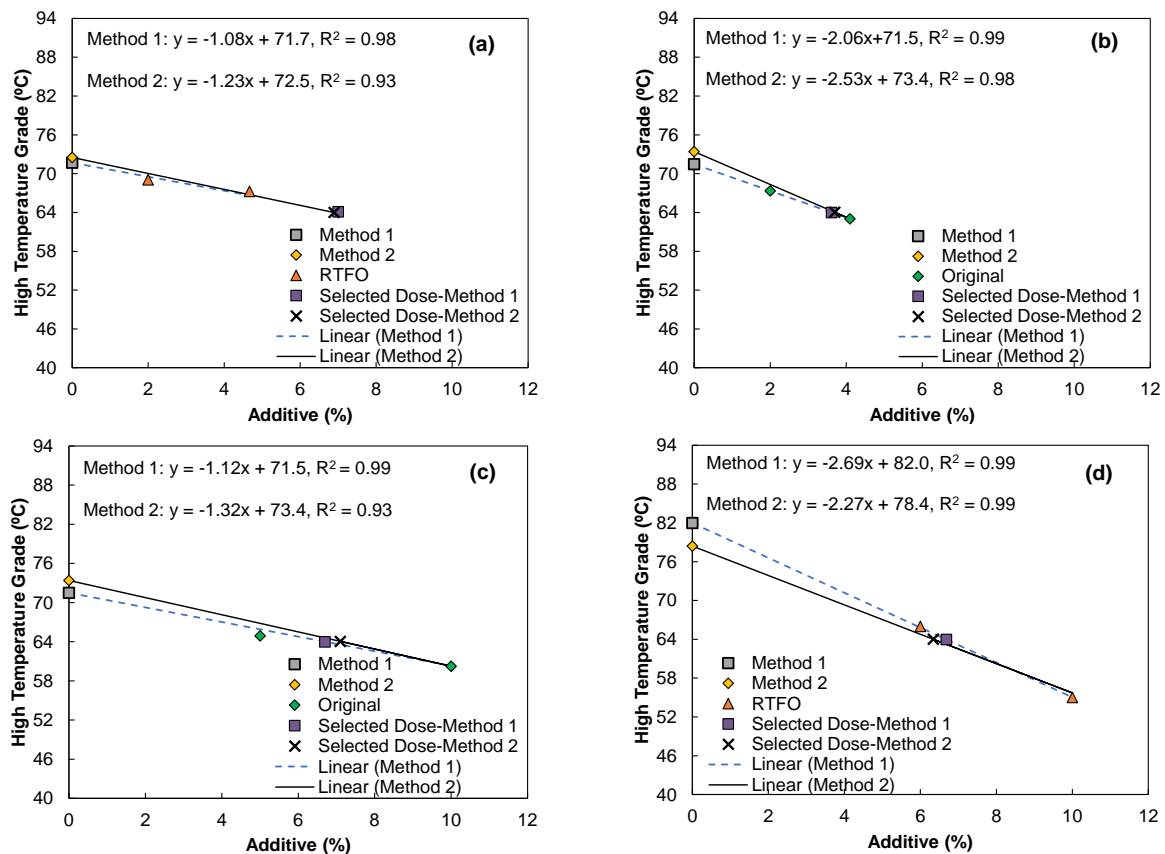


Figure 4 Comparison of dosage selection according to Methods 1 and 2 for (a) 58.RAP.E1, (b) 58.RAP.E2, (c) 58.RAP.E3, and (d) 58.RAS.R1

Method 3

Figure 5 shows the relationship between the change in high-temperature grade versus additive content at the RTFO age level for (a) the collective results of blends containing R1 (Blends 3, 8, and 9) and (b) the collective results of blends containing E1 according to Method 3 (Blends 4 and 5). The change in high-temperature grades were calculated using the estimate of the high-temperature grade of the blend of recycled and virgin binder using Equation (2). Linear regression was used to determine the slope ($X_{additive}$) values for R1 and E1 given in Equation (10) using the

results shown in Figure 5 (a) and (b), respectively. The corresponding X_{additive} values and R^2 values are conveyed by the equations shown in Figure 5. The values calculated when using the measured high-temperature grades to calculate the difference in high-temperature grade due to the additive are also shown for blends 58.RAS.R1 and 58.RAP.E1 as faded data series to visually show the effect of the error introduced by Equation (2) on the calculated high-temperature grade differences. The results suggest good agreement between the Equation (9) results and the measured data, suggesting promise for the use of Method 3 in practice. Method 3 is advantageous in that it would not require testing of blends prepared at trial dosages for each new blend of virgin and recycled binder. Rather, a representative set of virgin binder, recycled binder, and additive blends could be tested and used to calibrate Equation (9), which then could be applied for dosage selection for new virgin-recycled binder blends using the same additive. Some of the scatter in Figure 5 (a) could be due to the uncertainty in the RAS binder high-temperature grade used in Equation (2) as it is evident that the 58.RAS.R1 data better aligns with the PG 64.RAP.R1 data when the measured rather than estimated PGH_{Blend} value is used.

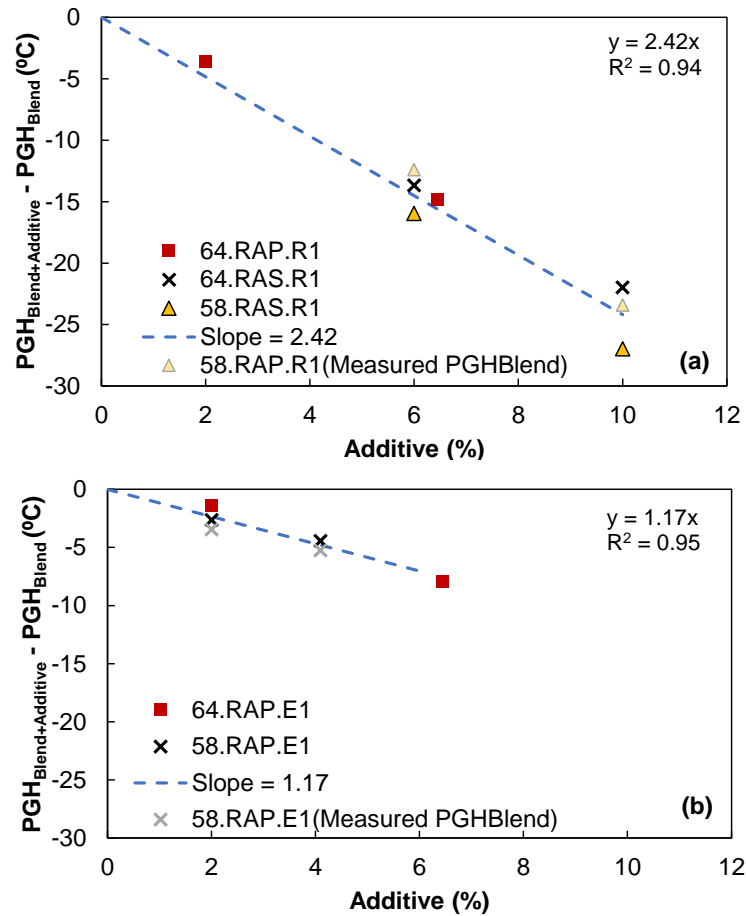


Figure 5. Relationships between high-temperature grade change and additive content for (a) all blends containing R1 and (b) all blends containing E1

Comparison of the Different Methods

Figure 6 shows the comparison of slopes of high-temperature grade versus additive content obtained from Methods 1 through 3 as well as the values used in Method 4 based on the average

values measured for aromatic extracts (A) and other (O) additive types in the NCHRP Project 09-58. The error bars in Figure 6 convey the standard error of the slope values. Figure 7 shows the dosages intended to restore the binder grade to 64°C calculated using the different methods. Figure 6 shows that Methods 1 through 3 generally yield similar slope values and dosages. The maximum difference in selected dosages between Methods 1 and 2 was 0.3 percent and the maximum difference between Methods 1 and 3 was 0.9 percent. The maximum differences between Methods 1 and 3 coincide with calculated dosages that exceed 10 percent, which is the maximum limit recommended in the NCHRP Project 09-58 (Epps Martin et al. 2020) and therefore, both would effectively lead to a selected dose of 10 percent. The slopes of all blends containing recycling agents determined using Methods 1 through 3 exceeded those from Method 4O. Consequently, Method 4O yielded a higher dose than Methods 1 through 3 for all blends containing R1 and R2, suggesting the approach may yield a high-temperature grade that falls below the intended grade. The slope used in Method 4A is close to the results of blends containing E1 and E3 and the slope in Method 4O is relatively close to the results of blends containing E2 results; therefore, the extenders evaluated do not align clearly with either aromatic or other additive type classification proposed in the NCHRP Project 09-58 simplified dosage selection procedure.

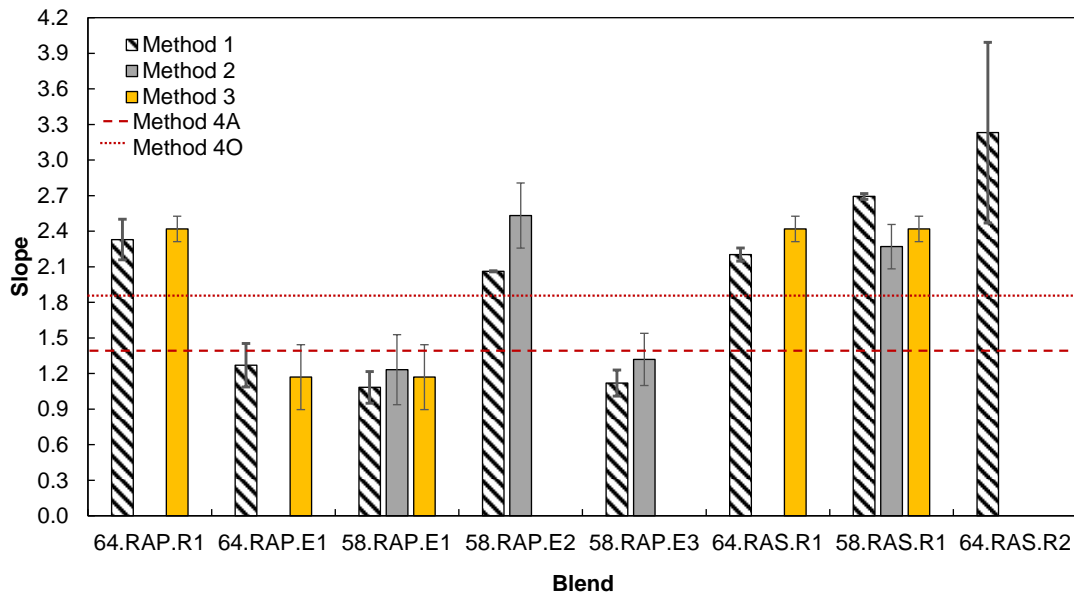


Figure 6. Slope of the continuous high-temperature grade change versus additive content based on the different methods evaluated

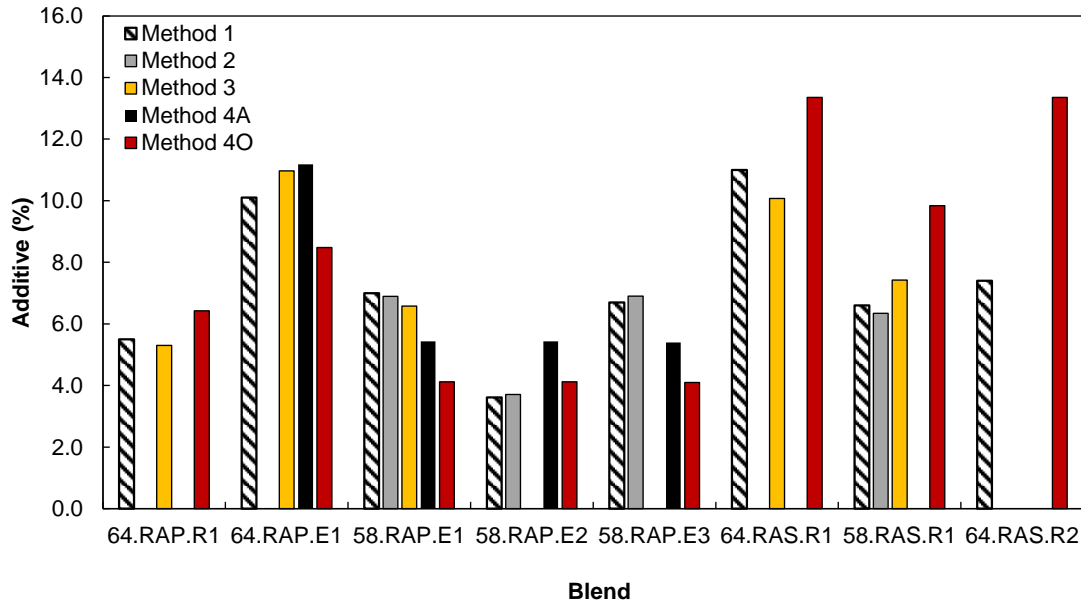


Figure 7. Selected doses according to the different methods evaluated

3.1.3. Verification Testing Results

Table 10 shows the verification testing results of the additional blends prepared at the dosages selected according to Method 1 along with the blends of recycled binder and the PG 58-28 binder in the absence of any additive. In addition, Table 10 shows the AASHTO M 320 continuous high-temperature grades predicted at the selected dosage based on the dosage selection results of Methods 1 through 4. Figure 8 shows the AASHTO M 320 continuous high-temperature grade results graphically. The verification blends all passed high-temperature grading criteria at 64°C according to AASHTO M 320. The results also show that blend 64.RAS.R2 passed grading criteria at 70°C despite the intended grade being 64°C.

The results demonstrate some notable discrepancies between the measured and predicted high-temperature grades. The expected grades according to Method 1 are very close to 64°C since this coincides with the basis for the dosage selection for the verification blends, with the exception of 64.RAS.R1 where the calculated dose exceeded the maximum limit of 10 percent. The expected grades according to Methods 2 through 4 differed from Method 1 somewhat due to differences in the intercept and/or slope values used to predict the relationship between high-temperature grade and additive content. Differences in the continuous high-temperature grades measured using the verification samples compared to those expected from Method 1 range from 0.2°C to 5.8°C. The maximum difference in the continuous grade measured from the two replicate samples of a given verification blend was 0.2°C, indicating that the discrepancy between the measured grades of verification samples and the predicted values is due to variability among the batches of blends prepared with a given set of materials and/or deviation from the assumed linear relationship between the additive content and blend high-temperature grade.

With the exception of blend 64.RAS.R2, the average errors between expected grades and those measured using the verification samples were less than 2.0°C for Methods 1 through 3. Methods 1 through 3 yielded similar accuracy in terms of agreement with the verification testing results. Therefore, Method 3 is most appealing because it would negate the need for virgin binder-recycled

binder blend-specific dosage selection testing after a reliable measure of the grade reduction versus additive content slope is obtained for a given product. Method 4 continuous high-temperature grade results are the most distinct from those measured in verification testing, further suggesting that additive-specific dosage selection calibration is necessary.

Table 10. Comparison between High-Temperature Grades Predicted by Methods 1 through 4 at the Dosages Selected According to Method 1 and Those Measured in Verification Testing

Blend	Additive (%)	AASHTO M 320 Continuous High-Temperature Grade (°C)					Verification Result
		Method 1	Method 2	Method 3	Method 4		
					A	O	
58.RAP	--	--	--	--	--	--	72.5
58.RAS	--	--	--	--	--	--	78.4
64.RAP.R1	5.5	64.0	--	63.5	--	65.7	64.2
58.RAP.E1	7.0	64.2	63.9	63.6	61.8	58.8	67.3
58.RAP.E2	3.6	64.0	67.5	--	66.5	64.9	67.7
58.RAP.E3	6.7	64	64.6	--	66.5	64.9	65.7
64.RAS.R1	10.0	66.3	--	64.2	--	70.2	65.0
64.RAS.R2	7.4	64.5	--	--	--	74.9	70.3

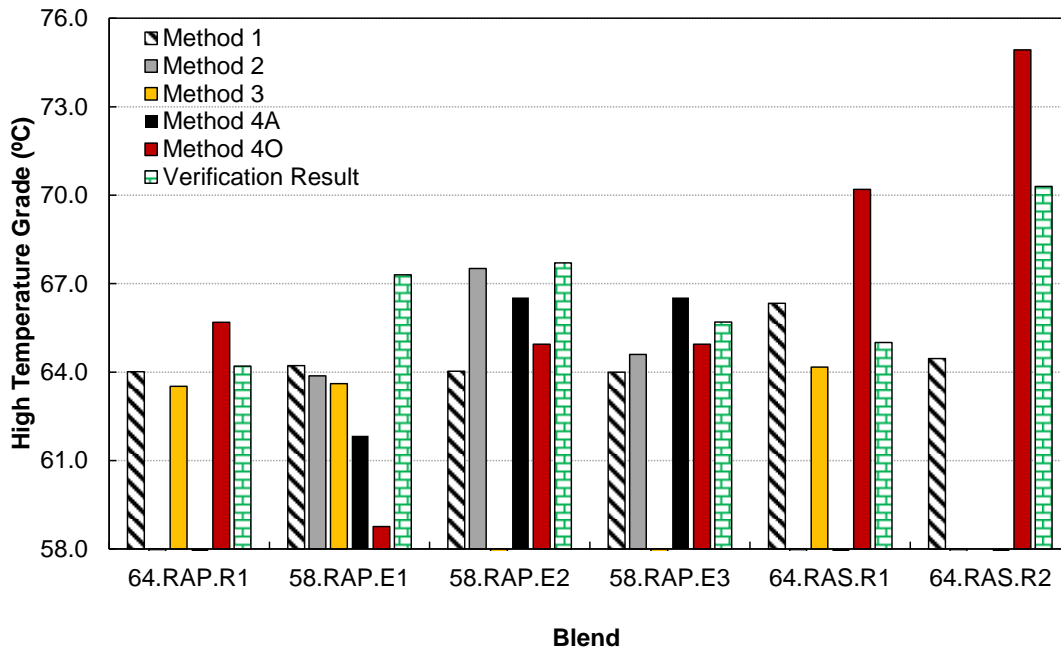


Figure 8. Continuous AASHTO M 320 high-temperature performance grades predicted based on the different dosage selection methods evaluated and measured via verification testing at the dosages selected according to Method 1

The verification testing results highlight inherent uncertainty in additive dosage selection procedure that should be accounted for as part of additive dosage selection. To visually depict the

uncertainty in the dosage selection results herein, a 90 percent confidence interval was constructed for the Method 3, i.e., Equation (9), results of additive R1. The results are shown in Figure 9. The results suggest uncertainty in the high-temperature grade reduction of around 3°C to 4°C at additive contents near six percent, and higher uncertainty at lower and higher dosages. Efforts to reduce uncertainty should be considered as part of the establishment of a robust dosage selection procedure. Potential ways to reduce the span of the confidence interval include incorporating the results of additional blends of the same materials at additional dosages and incorporating additional virgin and recycled binder blends. In addition, it is speculated that using the measured rather than estimated high-temperature grade of the blend of recycled and virgin binder, particularly in the case of RAS binders, may reduce uncertainty. A reduction in variability may also be achieved by establishing more robust sample preparation and blending procedures. Even with these measures, uncertainty will still exist. Therefore, it is suggested that uncertainty quantification be incorporated into the additive dosage selection process either by dosage selection according to the lower bound of a confidence interval or by targeting a higher continuous high-temperature than the minimum accepted based on measured uncertainty.

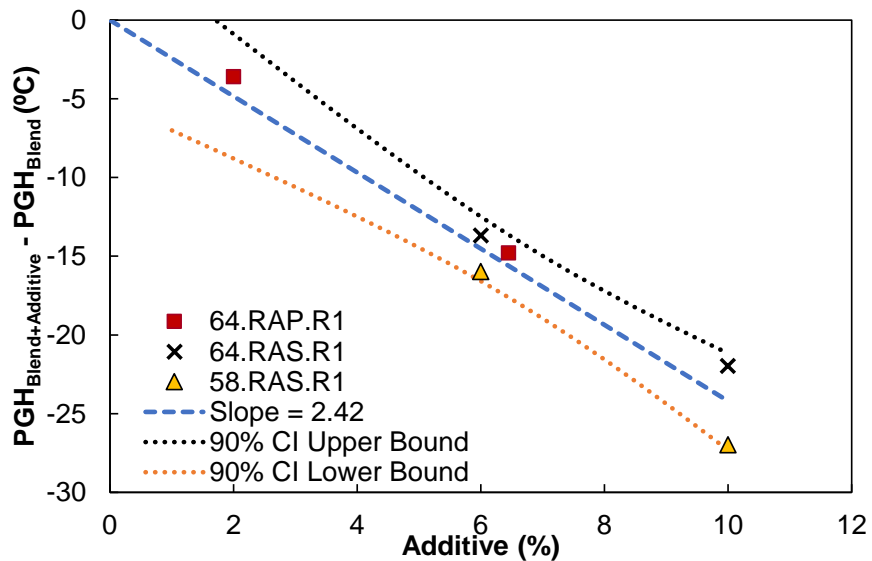


Figure 9. Confidence interval (CI) for Method 3 results of blends prepared using R1

3.1.4. Summary of Findings

Collectively, the dosage selection investigation demonstrated that different recycling agent and extender products can yield different rates of change in the asphalt binder continuous AASHTO M 320 high-temperature grade with additive content. However, the rate of change in asphalt binder continuous AASHTO M 320 high-temperature grade with additive content for a given additive was similar for different recycled binder and virgin binder combinations. Correspondingly, dosage selection can be achieved for a given additive by testing of a limited set of recycled and virgin binder blends (either by a product supplier or the NCDOT) to determine the rate of change in high-temperature grade versus additive content. This rate can then be applied to calculate the required additive dose for alternative recycled-virgin binder blends if the high-temperature grade of the virgin-recycled binder blend in the absence of any additive is known.

The results of the dosage selection investigation also indicate that testing of blends containing RAS at the original age level should be avoided as residual agglomerations of RAS may remain.

It was found that RTFO aging can be used to achieve a homogenous binder blend with RAS. Testing of virgin-recycled binder blends rather than relying on linear blending theory to estimate the high-temperature grade is recommended, especially in the case of RAS binders because conducting high-temperature grading of RAS binders imparts considerable uncertainty.

The AASHTO M 320 high-temperature grading results of verification blends prepared at selected dosages yielded considerable discrepancies with those predicted from dosage selection testing in some cases; these results suggest uncertainty in the dosage selection results should be incorporated into the dosage selection procedure. One way to incorporate this uncertainty is to target a PG 67 rather than PG 64 when selecting the dosage.

3.2. Evaluation of the Impacts of Additives on Recycled Binder Contribution in Asphalt Mixtures

Figure 10 shows the recycled binder contribution results for the RAP mixture evaluated. In all cases, the recycled binder contribution is less than 100 percent, suggesting that the assumption of complete recycled binder contribution commonly used in mixture design procedures is erroneous. The results further show that the PG 64-22 virgin binder yielded a higher recycled binder contribution than the PG 58-28 virgin binder; the cause for the higher recycled binder contribution with the PG 64-22 virgin binder may be due to its better compatibility evident by the colloidal instability index (CII) results from SARA analysis shown in Appendix C. It is speculated that chemical compatibilities between the virgin and recycled binders in the mixture may affect recycled binder contribution but this hypothesis has not been investigated. The results of the RAP mixtures with RA1 and E1 are statistically equivalent to the mixture with the PG 64-22 virgin binder and no additive. Since the RA1 and E1 mixture contained PG 64-22 virgin binder, these results suggest that the additives had no effect on recycled binder contribution.

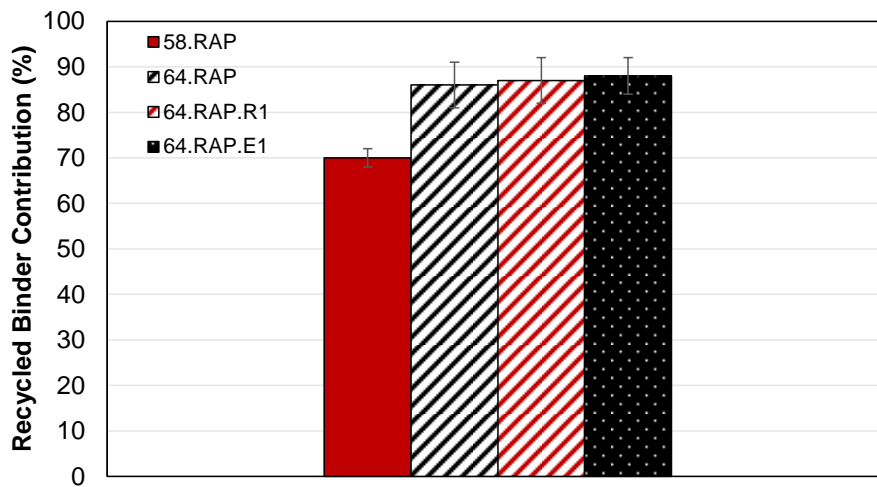


Figure 10. Recycled binder contribution results for the RAP mixture

Figure 11 shows the recycled binder contribution results for the RAP/RAS mixture evaluated. Figure 11 shows that the inclusion of RAS led to a lower recycled binder contribution compared to the RAP only mixture and further suggests that the assumption of complete recycled binder availability is erroneous. The RAP/RAS mixture with RA1 yielded a statistically higher recycled binder contribution than the mixture without any additives (i.e., 58.RAP.RAS). However, the increase in recycled binder contribution in the RA1 and RA2 mixtures could have been caused by

the difference in the virgin binder, since the alternative binder was used for these mixtures, and/or the RA. It is speculated that the higher recycled binder contribution is caused by the virgin binder rather than the RA because the PG 64-22 virgin binder yielded an increase in recycled binder contribution in the RAP only mixture. However, the RAP/RAS mixture was not prepared and evaluated with the PG 64-22 virgin binder and no additive to confirm this hypothesis.

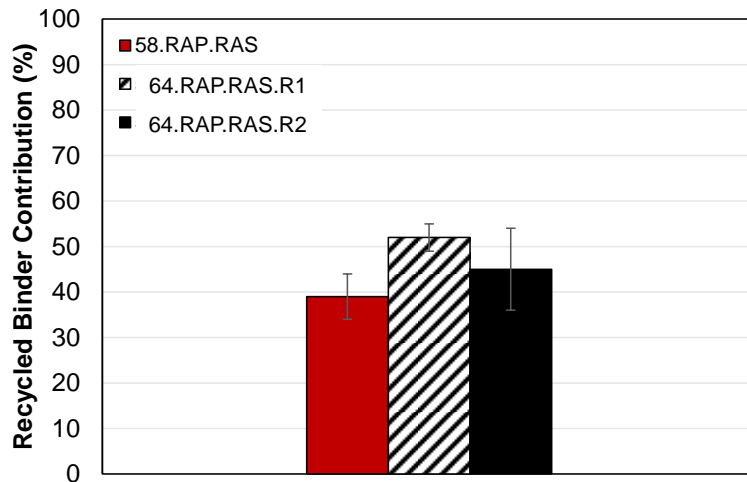
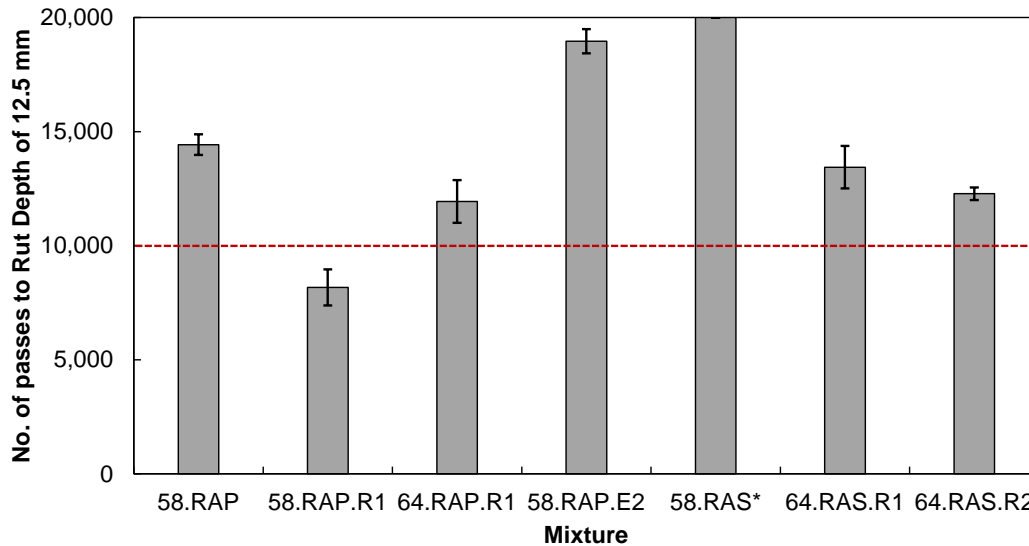


Figure 11. Recycled binder contribution results for the RAP/RAS mixture

3.3. Hamburg Wheel Track Test Results of Blends with Dosage Selected to Restore the Intended High-Temperature Grade

Figure 12 shows the HWT test results of the mixtures prepared at the dosages selected according to Method 1 for select blends along with the results of control mixtures prepared without any additives, which coincide with current mixture practices in North Carolina. Figure 12 also includes the results of a mixture prepared that was expected to fail the HWT rutting criteria (58.RAP.R1); this mix was prepared using the same R1 content as 64.RAP.R1 and thus, expected to have a high-temperature grade below 64°C. The error bars shown in Figure 12 reflect the standard error of the test results. NCHRP Project 09-58 suggested a minimum of 10,000 cycles to failure before a rut depth of 12.5 mm is reached in the HWT for warm climates, such as North Carolina to ensure adequate rutting resistance (Epps Martin et al. 2020). With the exception of the mix intentionally designed with inferior rutting resistance, all mixtures pass this minimum limit, suggesting that dosage selection to restore the high-temperature grade may yield adequate rutting resistance even if only partial recycled binder availability exists in the mixture. However, this finding should be confirmed with testing of additional mixtures. Interestingly, the mixture containing 58.RAP.E2 mixture exhibits superior rutting resistance to the reference 58.RAP mixture based on the HWT results despite including a softening additive. The other mixtures containing an additive show a reduction in rutting resistance compared to the corresponding control mixture without any additive.



*Failure not reached after 20,000 cycles

Figure 12. Hamburg Wheel-track test results

3.4. Benchmarking the Binder Blends against North Carolina Virgin Binders using Performance-Graded Properties

3.4.1. Continuous Performance Grades

The continuous high-temperature (T_H), intermediate-temperature (T_I), and low-temperature (T_L) temperature performance grades of the study virgin binders, blends of the virgin binder and recycled binder, and blends of the virgin, recycled binder, and additives with dosages selected according to Method 1 detailed in Section 3.1.2 were calculated according to the AASHTO M 320 specification criteria and ASTM D7463. The T_I and T_L values were calculated at both the P20 and P40 age levels, applying the same intermediate and low temperature specification criteria from AASHTO M 320 at both age levels despite the potential need for refining the AASHTO M 320 criteria if the P40 age level were adopted for specification. In addition, ΔT_c values were calculated at both the 20-hour PAV (i.e., P20) and 40-hour PAV (i.e., P40) age levels. Note that T_L and ΔT_c results are not included for the blends of 58.MRAS.R1 and 58.MRAS.R2 blends due to BBR testing challenges noted in Section 2. Table 11 details the resultant continuous grades of the virgin binders and blends. Within the results, the PG 58-28 and PG 64-22 virgin binders are denoted as binders 58 and 64, respectively. The PG 64-22 binder is considered a ‘target’ since it constitutes the binder targeted in the absence of recycled binder. The 58.RAP and 58.MRAS are considered the ‘reference blends’ since they reflect the binder blends prepared according to the current practice of the NCDOT.

Table 11. Summary of Continuous AASHTO M 320 Performance Grades

Binder/Blend	T_H (°C)	P20			P40		
		T_I (°C)	T_L (°C)	ΔT_c (°C)	T_I (°C)	T_L (°C)	ΔT_c (°C)
58	60.6	15.1	-30.5	0.3	19.8	-22.0	-8.3
64	67.3	22.5	-25.6	-0.4	23.8	-23.4	-1.8
58.RAP	72.5	21.5	-27.6	-0.3	26.1	-24.8	-1.9
64.RAP.R1	64.2	12.7	-32.1	2.9	17.9	-28.7	-2.0
64.RAP.R2	67.5	16.6	-32.0	-0.2	19.4	-30.0	-1.2
58.RAP.E1	67.3	19.3	-28.9	-3.3	20.6	-26.4	-5.0
58.RAP.E2	67.7	18.2	-29.5	-1.7	19.2	-24.7	-5.1
58.RAP.E3	65.7	19.3	-31.9	0.6	19.4	-30.7	-0.9
58.MRAS	78.4	23.7	-25.1	-2.3	25.6	-22.2	-4.8
64.MRAS.R1	65.0	13.5	-36.9	12.7	16.3	NA	NA
64.MRAS.R2	70.2	17.2	-33.9	6.0	21.8	NA	NA

Figure 13 shows the T_H values graphically, which coincide with those presented in Section 3.1.3 for Method 1 with incorporation of the 58 virgin binder and 58.RAP.R2 blend. The reference 58.RAP and 58.MRAS blends (i.e., coinciding with the current practice) exhibit T_H values of 72.5°C and 78.4°C, respectively, which exceed the intended climatic grade of 64°C to 70°C (i.e., coinciding with the high-temperature grade range of a PG 64-22 binder). All blends containing additives exhibited T_H values within the range of 64°C to 70°C and thus, aligning with the intended climatic grade and matching expectations since the dosages were selected to restore the intended T_H .

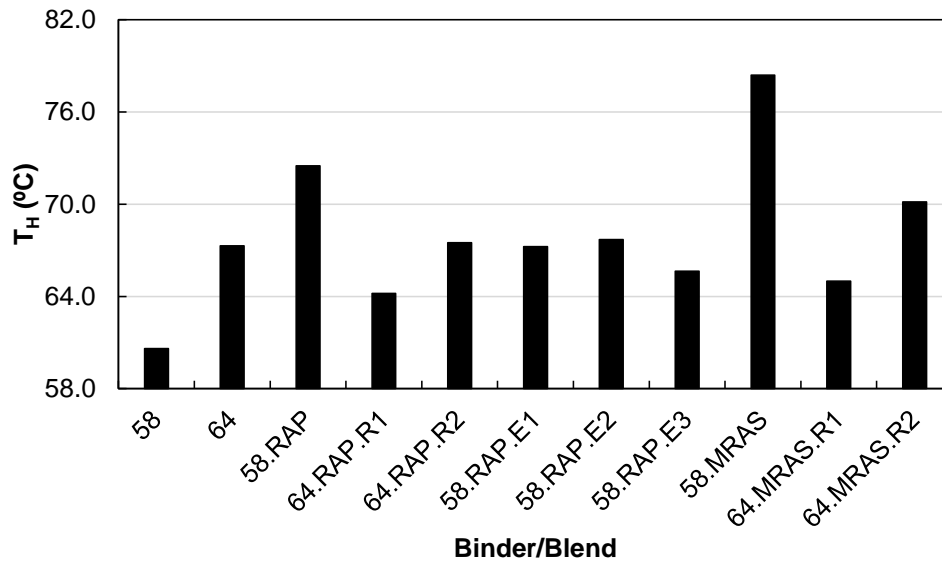


Figure 13. T_H values

Figure 14, Figure 15, and Figure 16 show the T_I , T_L , and ΔT_c results, respectively. Figure 14 shows that all blends and virgin binders have T_I values falling below the critical intermediate temperature of 25°C at the P20 age level for the intended grade of PG 64-22 in NC. Figure 14 reveals that the

T_I values of the 58.RAP and 58.MRAS blends are 21.5°C and 23.7°C, respectively, at the P20 age level, which are very close to that of the 64 virgin binder. In contrast, the blends containing extenders and RAs exhibit notably lower T_I values at the P20 age level spanning from 12.7°C to 19.3°C. The blends containing R1 notably had T_I values lower than the 58°C virgin binder at the P20 age level. Similarly, Figure 15 shows that the 58.RAP and 58.MRAS blends exhibit T_L values that are close to the 64 virgin binder. In contrast, the T_L values of the blends containing RAs and extenders span from -28.9°C to -32.1 °C at the P20 age level, and thus, yield lower, low-temperature grades than the -22°C required in NC. Figure 16 shows that the ΔT_c values at the P20 age level all exceed the -5.0°C threshold adopted by many state agencies, indicating an acceptable balance in stiffness and relaxation characteristics at low-temperature. However, differences among the binders and blends are noted. The 58.RAP blend exhibits a ΔT_c value close to the 64 virgin binder whereas the 58.MRAS blends exhibits a poorer (i.e., more negative) ΔT_c value. It is also noted that the E1 and E2 extenders lowered the ΔT_c value in comparison to the 58.RAP, suggesting a potential negative impact on thermal cracking resistance. The 64.RAP.R2 and 58.RAP.E3 blends exhibit comparable ΔT_c values to the 58.RAP blend. In contrast, the 64.RAP.R1 displays a notably higher ΔT_c values compared to the reference 58.RAP and 58.MRAS blends.

Figure 15 shows that at P40 age level, the 64 virgin binder and 58.RAP, 58.MRAS, 58.RAP.E1, and 58.RAP.E2 blends exhibit T_L values falling between -22.0°C and -28.0°C, indicating they still meet the specified low-temperature grading criteria even after the extended aging. Blends 64.RAP.R1, 64.RAP.R2, and 58.RAP.E3 have T_L values falling between -28.0°C and -34.0°C, indicating potentially better low-temperature performance at the P40 age level than the other blends. However, Figure 16 shows the ΔT_c values of the 58.RAP.E1 and 58.RAP.E2 fall below the recommended maximum limit of -5.0°C, indicating potentially high susceptibility to thermal cracking at the P40 age level. Also noteworthy, the decrease in T_L and ΔT_c values from the P20 to P40 age level are highest for the 64.RAP.R1 and 58.RAP.E2 blends compared to the other blends and virgin binders evaluated. These blends exhibited decreases in both T_L and ΔT_c of 3.4°C or more due to the increase in age level from the P20 to the P40 condition, indicating relatively high aging susceptibility compared to the other blends and virgin binders evaluated. Similarly, Figure 14 shows that these cases tended to result in the biggest changes in T_I from the P20 to P40 age level compared to other blends. The reference 58.RAP blend also exhibits a large increase in T_I from the P20 to P40 age level.

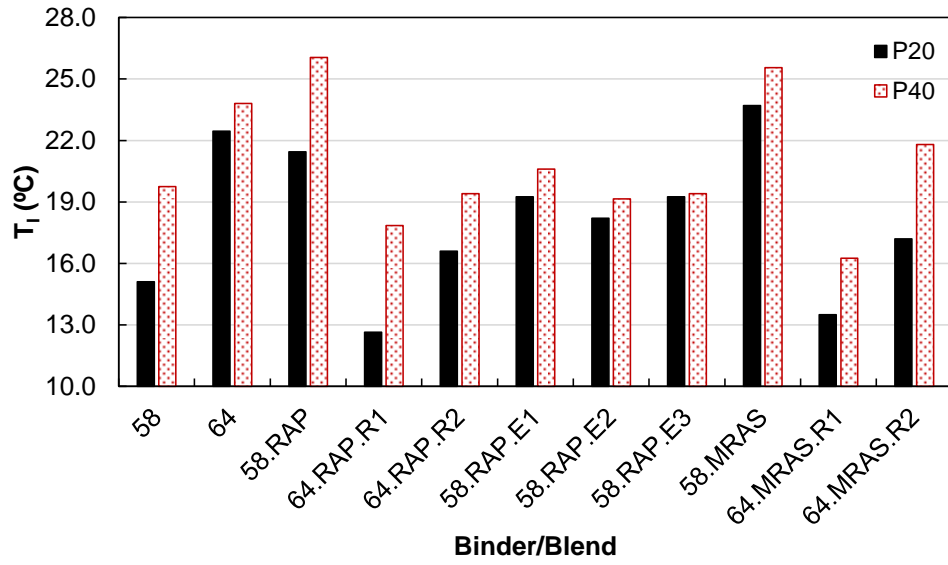


Figure 14. T₁ values

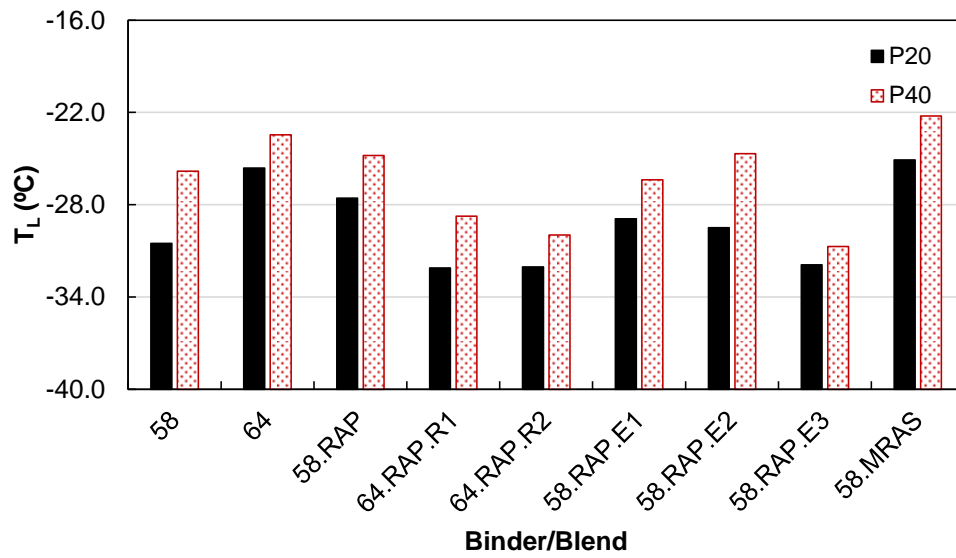


Figure 15. T_L values

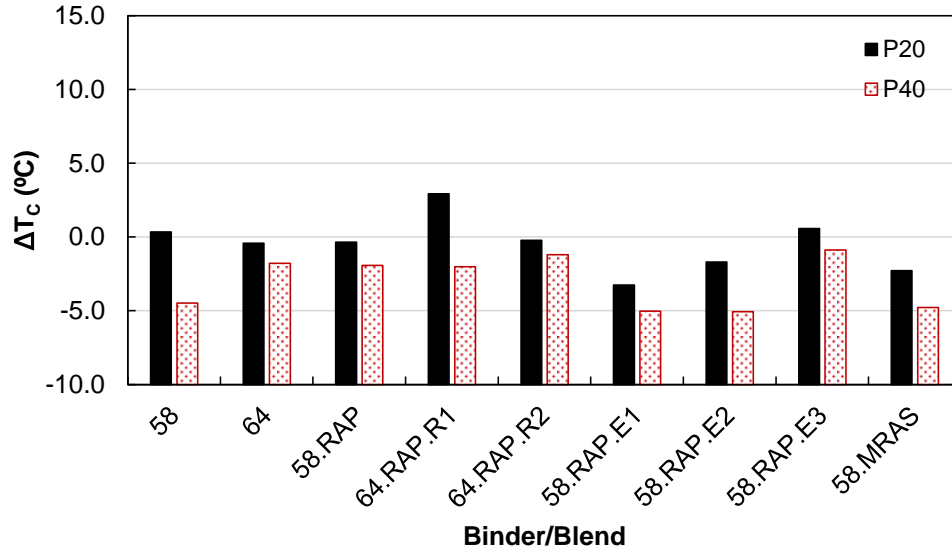


Figure 16. ΔT_c values

3.4.2. Benchmarking Against PG 64-22 Virgin Binder Properties

The performance-graded properties of the blends were benchmarked against QA data for PG 64-22 virgin binders in NC to further evaluate their ability to restore rheological properties to the target condition in the absence of recycled materials. A summary of the study virgin binders and blends relative to the QA database of PG 64-22 virgin binders is presented in Table 12. The percentile where each blend falls within the distribution of NC's PG 64-22 binders is shown in parentheses. The results revealed that the blends evaluated have similar high-temperature performance grade properties to PG 64-22 binders, which matches expectations and previously reported results since the dosages were established to yield a high-temperature grade of 64. However, the intermediate- and low-temperature performance grade properties are distinct from PG 64-22 binders as evident by the very low percentiles listed for $|G^*| \times \sin \delta$ and creep stiffness at 60 seconds of loading ($S(60)$) and very high percentiles for $m(60)$, suggesting superior thermal cracking resistance.

Table 12. Summary of the Superpave Properties of the Blends and NC PG 64-22 Binders

Recycled binder blend	$ G^* /\sin \delta^1$, kPa	$ G^* /\sin \delta^2$, kPa	$ G^* \times\sin \delta^3$, kPa	$m(60)^4$	$S(60)^4$, MPa
64.RAP.R1	1.02 (0.00)	3.07 (0.10)	1405 (0.00)	0.369 (0.99)	80 (0.00)
64.RAP.R2	1.50 (0.75)	3.38 (0.38)	1636 (0.00)	0.408 (1.00)	79 (0.00)
58.RAP.E1	1.47 (0.70)	3.74 (0.17)	2486 (0.00)	0.345 (0.85)	95 (0.00)
58.RAP.E2	1.55 (0.87)	3.75 (0.71)	2902 (0.06)	0.375 (1.00)	103 (0.00)
64.MRAS.R1	NA	2.45 (0.00)	1273 (0.00)	NA	NA
64.MRAS.R2	NA	4.58 (0.97)	1986 (0.00)	NA	NA
58.RAP	3.25 (1.00)	6.35 (1.00)	3043 (0.10)	0.359 (0.98)	133 (0.02)
58.MRAS	-	11.26 (1.00)	4432 (0.96)	0.324 (0.22)	159 (0.24)
58.RAP.E3	1.38 (0.47)	2.72 (0.01)	1976 (0.00)	0.391 (1.00)	84 (0.00)
<i>Statistics of NC's PG 64-22</i>					
Min.	1.12	2.54	2550	0.300	126
Max.	1.74	4.86	4930	0.371	244
Mean	1.40	3.57	3585	0.332	175
Standard deviation	0.13	0.44	447	0.012	23

¹ Value measured at 64°C in original condition

² Value measured at 64°C in RTFO-aged condition

³ Value estimated at 25°C in PAV-aged condition

⁴ Value estimated at -12°C in PAV-aged condition

Figure 17 (a) and Figure 17 (b) show the probability distributions of $|G^*|/\sin \delta$ @64°C for NC's PG 64-22 binders and the blends in the unaged (Original) and short-term-aged (RTFO) conditions. As previously noted, the characterization of the recycled blends containing MRAS was avoided in the Original condition, as a non-uniform distribution of the MRAS was observed in this state. Figure 17 (a) and Figure 17 (b) show that the 58.RAP and 58.MRAS blends exhibit higher $|G^*|/\sin \delta$ @64°C values than virgin PG 64-22 binders in the state. In contrast, Figure 17 (a) and Figure 17 (b) show that the blends containing extenders and RAs generally fall within the range of $|G^*|/\sin \delta$ @64°C values of virgin PG 64-22 binders in the state with the exception of the 64.RAP.R1 blend at the original age level. Furthermore, Figure 17 shows that PG 64-22 binders from NC generally have a continuous high-temperature grade of 67°C rather than 64°C. Therefore, if the intention is to replicate the common or typical binder grade of NC's virgin binders, one should select the dosage level based on 67°C.

Figure 17 (d) shows the distribution of $m(60)$ @-12°C; Figure 17 (c) shows the distribution of $S(60)$ @-12°C. Here, the 58.RAP and 58.MRAS blends fall within the range of typical PG 64-22 binder values whereas the the blends with RAs and extenders fall outside the distribution of PG 64-22 virgin binder $S(60)$ and $m(60)$ values. The blends with additives exhibit an $m(60)$ higher than 98% to 100% of the PG 64-22 binders in NC. Regarding $S(60)$, all blends containing additives present a stiffness lower than 100% of the virgin binders used as a reference.

Figure 17 (e) shows the distribution of $|G^*|\times\sin \delta$ @25°C. As with $S(60)$ and $m(60)$, the 58.RAP and 58.MRAS blends fall within the range of PG 64-22 values whereas the blends with additives generally fall outside to the left of the distribution of reference binders except for 58.RAP.E2,

indicating that the selected dosages yield systems softer at intermediate temperature than typical PG 64-22 from NC.

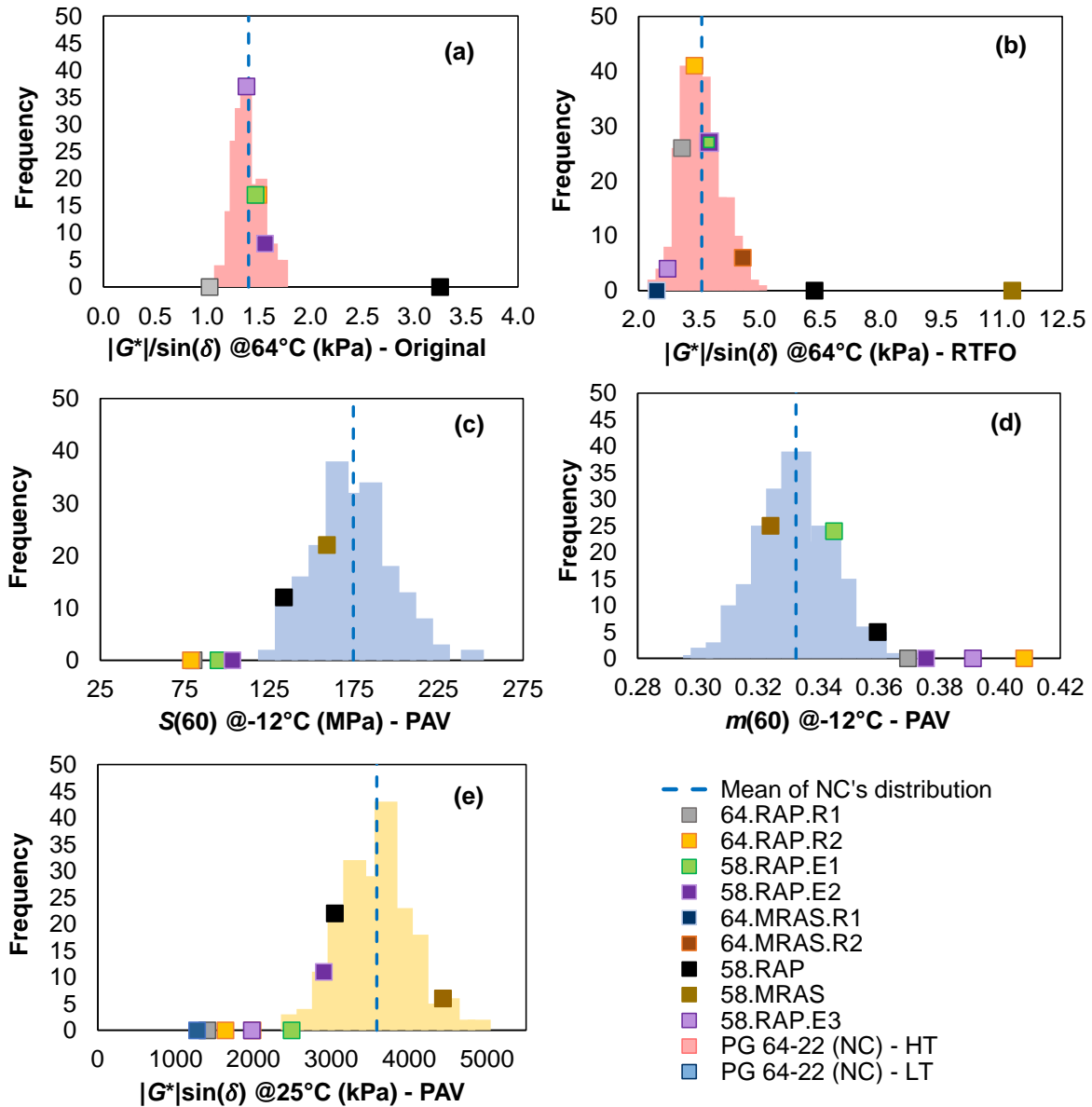


Figure 17. Distribution of the Superpave binder properties for North Carolina’s PG 64-22 binders and recycled binder blends: (a) $|G^*|/\sin(\delta)$ @64°C (kPa) – Original, (b) $|G^*|/\sin(\delta)$ @64°C (kPa) – RTFO, (c) $S(60)$ @-12°C (MPa) – PAV. (d) $m(60)$ @-12°C (MPa) – PAV, (e) $|G^*|\sin(\delta)$ @25°C (kPa) – PAV

To further compare the properties of the recycled binder blends to PG 64-22 binders in NC, the high- and low-temperature performance-graded properties are presented as bivariate distributions of different rheological properties in Figure 18. Only the blends containing RAP are shown in Figure 18 (a) since the blends containing MRAS were not characterized at the original age level. Figure 18 (a) shows that the blends containing additives fall within the bivariate distribution of PG

64-22 high-temperature properties with the exception of 64.RAP.R1 whereas the 58.RAP blend falls outside of the distribution of PG 64-22 binders. Only the blends containing RAP are shown in Figure 18 (b) with the exception of the 58.MRAS blend due to the testing issues encountered at -12°C for the RA modified MRAS blends noted earlier. Figure 18 (b) indicates that the 58.RAP and 58.MRAS blends have similar low-temperature properties to PG 64-22 virgin binders whereas the blends with additives have distinct low-temperature rheological properties.

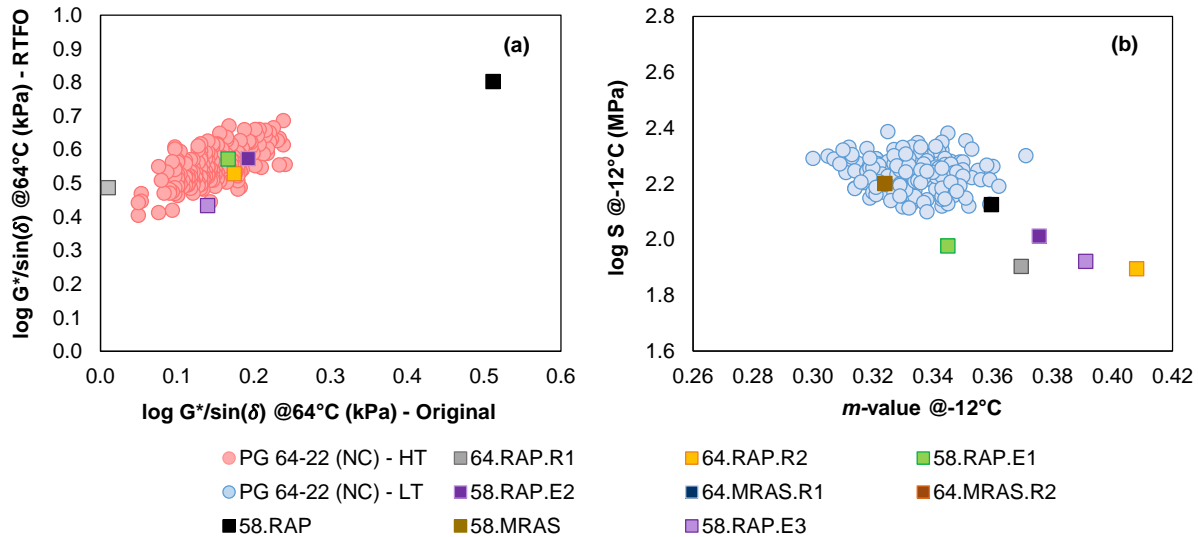


Figure 18. Bivariate distribution of high- and low-temperature rheological properties: (a) AASHTO M 320 high-temperature rheological space, and (b) AASHTO M 320 low-temperature rheological space

3.4.3. Summary of Findings

The current practice to use a PG 58-28 virgin binder in high RBR mixtures resulted in similar intermediate- and low-temperature performance-graded properties to PG 64-22 virgin binders (i.e., the intended condition) for the RAP and MRAS cases evaluated. However, the current practice resulted in high-temperature performance-graded properties that were distinct from PG 64-22 virgin binders. The blends of PG 58-28 virgin binder and recycled binders evaluated resulted in higher $|G^*| \times \sin \delta$ values than those of PG 64-22 binders in the state. The blends of virgin binder, recycled binder, and an extender or RA at a dosage selected to restore the intended high-temperature grade of 64°C display high-temperature performance-graded properties similar to virgin PG 64-22 binders. However, these systems exhibit distinct low- and intermediate-temperature performance-graded characteristics from PG 64-22 virgin binders. The results also suggest that, in some cases, additives can increase long-term aging susceptibility of recycled binder blends when evaluated at the 40-hour PAV conditions on the basis of ΔT_c values, indicating the benefits of some additives on cracking resistance may diminish with time. The collective results highlight that neither the current practice to use a PG 58-28 virgin binder in high RBR mixtures or the use of extenders or RAs can fully restore rheological properties of recycled binder blends to those of PG 64-22 virgin binders. While properties in either the high or low temperature regime can be restored, the consequence will be notably different properties at the opposite temperature regime.

3.5. Effects of Recycling Agents and Extenders on Binder Durability

3.5.1. Benchmarking Against Established Limits

Table 13 provides a summary of the durability-related asphalt binder parameters evaluated along with suggested limits (if available in the literature and/or specifications) and whether a higher or lower value is generally desired. It is noted that some of the suggested limits are given for a specific age level whereas other limits were not given in the context of a specific age level.

Table 13. Summary of the Durability-Related Binder Parameters Evaluated

Parameter	Suggested Limit(s)	Higher or Lower Desired?	Reference
$ G^* \times \sin \delta$ (kPa)	Max 6,000 kPa ⁺ @ P20	Lower	AASHTO M 320-21
GR _{25°C} (kPa)	Max 5,000 kPa @ P20 Max 8,000 kPa @ P40	Lower	Christensen and Tran 2022
GR _{15°C} (kPa)	Max 180 kPa for crack onset Max 450 kPa for sig. cracking	Lower	Anderson et al. 2011
ω_c (Hz)	NA	Higher	Anderson et al. 1994
T _c (°C)	Warning 32°C Max 45°C	Lower	Cucalon et al. 2017
R _{MC}	NA	Lower	Christensen and Tran 2022
R ₀₉₋₅₉	Max 2.50 @ P20 Max 3.20 @ P40	Lower	Christensen and Tran 2022
S(60) @ -18°C (MPa)	*Max 300 MPa @ P20	Lower	AASHTO M 320-21
m(60) @ -18°C (MPa)	*Min 0.300 @ P20	Higher	AASHTO M 320-21
ΔT_c (°C)	Min -5°C	Higher	Asphalt Institute 2019
N _f @ 5%	NA	Higher	Yang et al. 2022
N _f @ 15%	NA	Higher	Yang et al. 2022

⁺ Also must satisfy a min δ of 42° if $|G^*| \times \sin \delta$ exceeds 5,000 kPa @ P20.

*Limit should be applied at -12°C for NC climate so limit not directly applicable.

Figure 19, Figure 20, and Figure 21 show the durability-related parameters obtained from linear viscoelastic DSR testing, linear viscoelastic BBR testing, and LAS testing, respectively. Where applicable, the limits in Table 13 are conveyed in the graphs. Limits are not shown if all binders met the limit and thus, the limit falls outside of the measurement range of the results. Results are shown at the P20 and P40 age levels for the 58 and 64 virgin binders and the recycled binder blends. Consistent with Section 3.4, the 64 virgin binder results are considered a target result since PG 64-22 virgin binders are used in the absence of recycled binder. Similarly, the 58.RAP and 58.MRAS blend results are considered reference results for blends containing additives and RAP and RAS, respectively since they constitute the current practice. The 58 virgin binder meets all identified durability-related criteria. The 64 virgin binder meets most of the identified criteria. The 64 virgin binder fails the onset of cracking limit for GR_{15°C} at P40, warning limit for T_c at P40. The target 64 virgin binder also fails the S(60) and m(60) criteria at -18°C at the P20 age level, which is expected since its low-temperature grade is -22°C. The reference 58.RAP blend fails the same criteria as the 64 virgin binder. The reference 58.MRAS also fails these criteria as well as additional criteria, including the GR_{25°C} limit at both the P20 and P40 age levels, the onset of cracking limit for GR_{15°C} at the P20 age level, the significant cracking limit for GR_{15°C} at the P40

age level, the warning T_c limit at the P20 age level, and the maximum T_c limit at the P40 age level. Given that the 58.MRAS reference blend fails many of the identified durability-related criteria, it is inferred this binder system may have relatively poor durability. All blends evaluated fail to meet the warning limit for T_c at the P40 age level suggesting this criterion may be overly harsh. Aside from T_c , the RA modified blends and 58.RAP.E3 blend meet all identified criteria. The 58.RAP.E1 and 58.RAP.E2 blends fail certain criteria, indicating potentially inferior durability. Both 58.RAP.E1 and 58.RAP.E2 have ΔT_c values just below the -5°C limit at the P40 age level, as previously discussed. This was somewhat expected given that both E1 and E2 contain REOB, which is known to negatively impact ΔT_c (Asphalt Institute 2019). It is noted that the 58 virgin binder was also close to this limit at the P40 age level but the 58.RAP had a notably higher ΔT_c and thus, it does appear that E1 and E2 negatively affected ΔT_c . The 58.RAP.E2 blend also fails to meet the cracking onset limit for $\text{GR}_{15^\circ\text{C}}$ at the P40 age level. The 58.RAP.E1 has a notably higher R_{MC} than all other binders, which could further suggest inferior performance.

In most cases, the durability-related parameters suggest inferior performance at the P40 versus P20 age level based on the indications of whether a higher or lower value is desired given in Table 13. The exception is the fatigue life (i.e., N_f) results from the LAS test shown in Figure 21 and the R_{09-59} of the 64.MRAS.R1 blend only. The reason for the outlier behavior of the 64.MRAS.R1 is unknown. In many cases, the N_f at a given strain level is higher at the P40 compared to P20 age level, which implies better fatigue resistance at the higher age level. This is counterintuitive and therefore, further research is needed to better understand the reasons for the results and possibly revise the interpretation of fatigue resistance from the test.

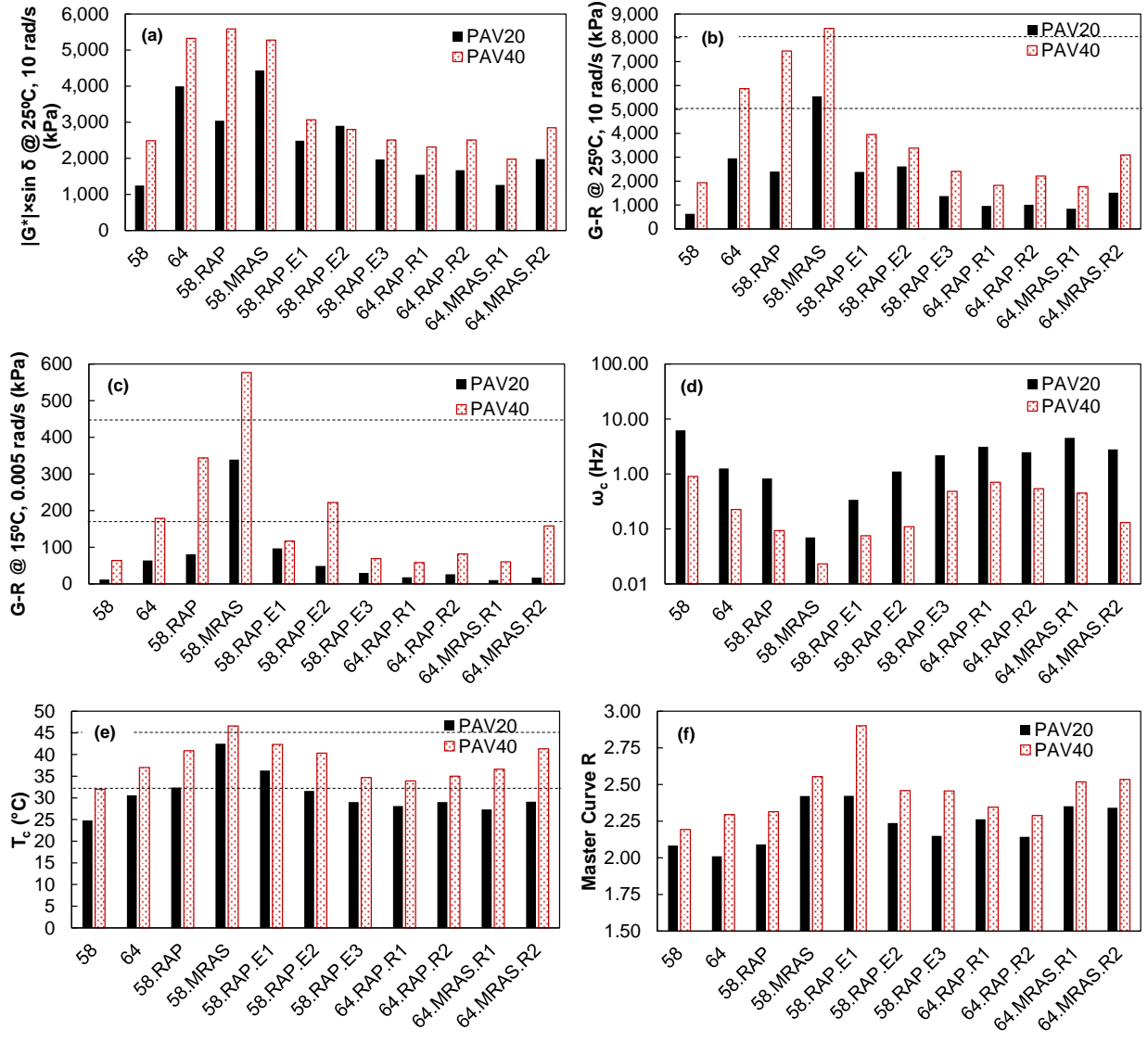


Figure 19. Linear viscoelastic DSR-based parameters

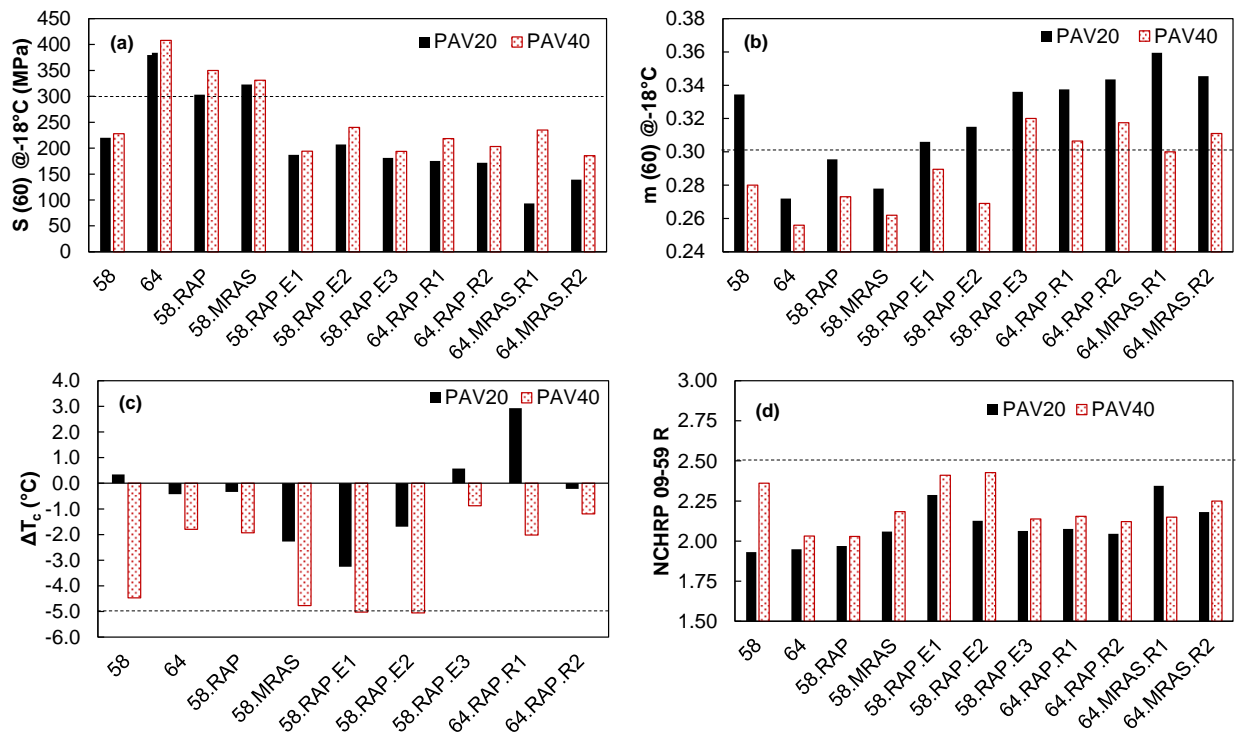


Figure 20. Linear viscoelastic BBR-based parameters

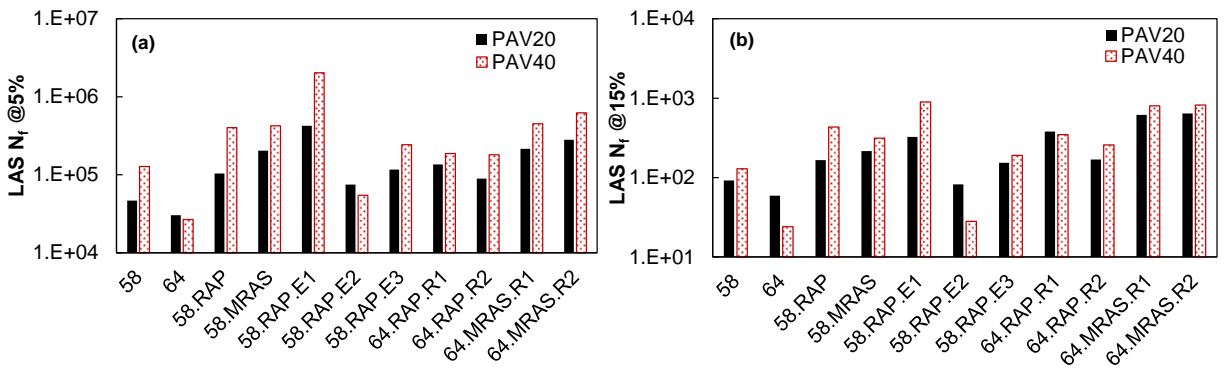


Figure 21. Linear amplitude sweep-based parameters

3.5.2. Benchmarking Against the Reference Blends and the Target Binder

To complement the results shown in Figure 19, Figure 20, and Figure 21, Tukey HSD tests were conducted using a 95 percent confidence level for each parameter at the P20 and P40 age levels separately. Tukey HSD tests group binders and blends into groups with statistically equal means and assigns the groups rank orders. Detailed Tukey HSD test results are provided in Appendix E. The LAS results were omitted from the Tukey HSD analysis given their counterintuitive trends with respect to age level. Table 14 and Table 15 summarizes whether a given blend containing an additive was deemed worse, equal, or better than the respective reference (58.RAP or 58.MRAS) at the P20 and P40 age levels, respectively, based on the Tukey HSD analysis and interpretation of whether a higher or lower value is desirable according to Table 13. The blends with additives are deemed equal or better than the respective reference at both the P20 and P40 age levels in all cases for the parameters $|G^*| \times \sin \delta$, $GR_{25^\circ C}$, $S(60)$, $m(60)$. In the majority of these cases, the blends containing the additives are deemed better than the respective reference. The blends are also deemed equal or better than the respective reference on the basis of $GR_{15^\circ C}$ and T_c with the exception of the 58.RAP.E1 blend. Most blends have equal ΔT_c values compared to the respective reference at the P20 and P40 age levels with the exception of the 58.RAP.E1 blend at both age levels and 58.RAP.E2 blends at the P40 age level where inferior values are observed. Also, the 64.RAP.R1 blend at the P20 age level has a better ΔT_c value than the 58.RAP. In the majority of cases, the results suggest that the R_{MC} and R_{09-59} of the blends with additives are worse than the respective reference at the P20 age level and equal or worse at the P40 age level, which is distinct from the other parameters evaluated. However, all R_{09-59} meet recommended criteria by the NCHRP 09-59 project (Christensen and Tran 2022). The 64.MRAS.R1 and 64.MRAS.R2 blends also have inferior ω_c values compared to the 58.MRAS at the P40 age level.

Table 14. Comparisons between the Rheological Properties of the Modified Blends in Comparison to the Reference (58.RAP or 58.MRAS) at the P20 Age Level

Blend	Comparison to Reference		
	Worse	Equal	Better
64.RAP.R1	R _{MC} , R ₀₉₋₅₉	--	G* ×sin δ, GR _{25°C} , GR _{15°C} , ω _c , T _c , S(60), m(60), ΔT _c
64.RAP.R2	R _{MC}	R ₀₉₋₅₉ , ΔT _c	G* ×sin δ, GR _{25°C} , GR _{15°C} , ω _c , T _c , S(60), m(60)
58.RAP.E1	GR _{15°C} , R ₀₉₋₅₉ , R _{MC} , T _c , ΔT _c	G* ×sin δ, GR _{25°C} , ω _c ,	S(60), m(60)
58.RAP.E2	R _{MC} , R ₀₉₋₅₉	G* ×sin δ, GR _{25°C} , ω _c , ΔT _c	GR _{15°C} , T _c , S(60), m(60)
58.RAP.E3	R _{MC} , R ₀₉₋₅₉	ΔT _c	G* ×sin δ, GR _{25°C} , GR _{15°C} , ω _c , T _c , S(60), m(60)
64.MRAS.R1	R ₀₉₋₅₉	--	G* ×sin δ, GR _{25°C} , GR _{15°C} , R _{MC} , ω _c , T _c , S(60), m(60)
64.MRAS.R2	R ₀₉₋₅₉	--	G* ×sin δ, GR _{25°C} , GR _{15°C} , R _{MC} , ω _c , T _c , S(60), m(60)

Table 15. Comparisons between the Rheological Properties of the Modified Blends in Comparison to the Reference (58.RAP or 58.MRAS) at the P40 Age Level

Blend	Comparison to Reference		
	Worse	Equal	Better
64.RAP.R1	--	R_{09-59} , R_{MC} , ΔT_c	$ G^* \times \sin \delta$, $GR_{25^\circ C}$, $GR_{15^\circ C}$, ω_c , T_c , $S(60)$, $m(60)$
64.RAP.R2	--	R_{09-59} , R_{MC} , ΔT_c	$ G^* \times \sin \delta$, $GR_{25^\circ C}$, $GR_{15^\circ C}$, ω_c , T_c , $S(60)$, $m(60)$
58.RAP.E1	R_{09-59} , R_{MC} , T_c , ΔT_c	ω_c , $m(60)$	$ G^* \times \sin \delta$, $GR_{25^\circ C}$, $GR_{15^\circ C}$, $S(60)$
58.RAP.E2	R_{09-59} , R_{MC} , ΔT_c	ω_c , T_c , $m(60)$	$ G^* \times \sin \delta$, $GR_{25^\circ C}$, $GR_{15^\circ C}$, $S(60)$
58.RAP.E3	R_{MC}	R_{09-59} , ΔT_c	$ G^* \times \sin \delta$, $GR_{25^\circ C}$, $GR_{15^\circ C}$, ω_c , T_c , $S(60)$, $m(60)$
64.MRAS.R1	ω_c	R_{09-59} , R_{MC}	$ G^* \times \sin \delta$, $GR_{25^\circ C}$, $GR_{15^\circ C}$, T_c , $S(60)$, $m(60)$
64.MRAS.R2	ω_c	R_{09-59} , R_{MC}	$ G^* \times \sin \delta$, $GR_{25^\circ C}$, $GR_{15^\circ C}$, T_c , $S(60)$, $m(60)$

Table 16 and Table 17 summarizes whether a given blend was deemed worse, equal, or better than the target 64 virgin binder at the P20 and P40 age levels, respectively, based on the Tukey HSD analysis. At the P20 age level, the reference 58.RAP blend is deemed better than the 64 virgin binder on the basis of $|G^*| \times \sin \delta$, $S(60)$, $m(60)$ (i.e., current AASHTO M 320 specification parameters) but equal or worse on the basis of all alternative parameters. At the P40 age level, the 58.RAP has a better $S(60)$ than the 64 virgin binder and equal $|G^*| \times \sin \delta$, $m(60)$, R_{09-59} , R_{MC} , and ΔT_c At both the P20 and P40 age level. The reference 58.MRAS blend is only deemed better than the 64 virgin binder on the basis of $S(60)$ but also has equal $|G^*| \times \sin \delta$, $m(60)$, and ΔT_c values as the target virgin binder.

The 58.RAP.E1 and 58.RAP.E2 blends also have equal or better $|G^*| \times \sin \delta$, $S(60)$, and $m(60)$ compared to the 64 virgin binder at both the P20 and P40 age levels. The blends containing R1, R2, and E3 all have better $|G^*| \times \sin \delta$, $GR_{25^\circ C}$, $GR_{15^\circ C}$, ω_c , T_c , $S(60)$, and $m(60)$ values than the 64 virgin binder at the P20 age level. The blends with R1, R2, and R3 retain equal or better values of these parameters than the 64 virgin binder at the P40 age level. These blends also have equal, (and in one case corresponding to the 64.RAP.R1), better ΔT_c values than the 64 virgin binder. However, in many cases these blends have inferior R_{MC} and R_{09-59} values compared to the 64 virgin binder. At the P20 age level, all of these blends have inferior R_{MC} values than the 64 virgin binder. At the P40 age level, there are more instances where the R_{MC} and R_{09-59} values of these bends are equal to the 64 virgin binder. The 58.RAP.E1 and 58.RAP.E2 blends have inferior R_{MC} , R_{09-59} values compared to the 64 virgin binder at both the P20 and P40 age levels. In addition, the 58.RAP.E1 and 58.RAP.E2 blends have inferior ω_c , T_c , ΔT_c and values than the 64 virgin binder at the P40 age level. In many cases, the 58.E1.RAP and 58.RAP.E2 blends also have inferior values

of these parameters compared to the 64 virgin binder at the P20 age level as well as several other instances of inferior parameter values.

Table 16. Comparisons between the Rheological Properties of the Blends in Comparison to the Target PG 64-22 Virgin Binder at the P20 Age Level

Blend	Comparison to Target		
	Worse	Equal	Better
58.RAP	$GR_{15^{\circ}C}, R_{MC}, T_c$	$GR_{25^{\circ}C}, R_{09-59}, \omega_c, \Delta T_c$	$ G^* \times \sin \delta, S(60), m(60)$
58.MRAS	$GR_{25^{\circ}C}, GR_{15^{\circ}C}, R_{09-59}, R_{MC}, \omega_c, T_c$	$ G^* \times \sin \delta, m(60), \Delta T_c$	S(60)
64.RAP.R1	R_{09-59}, R_{MC}	--	$ G^* \times \sin \delta, GR_{25^{\circ}C}, GR_{15^{\circ}C}, \omega_c, T_c, S(60), m(60), \Delta T_c$
64.RAP.R2	R_{MC}	$R_{09-59}, \Delta T_c$	$ G^* \times \sin \delta, GR_{25^{\circ}C}, GR_{15^{\circ}C}, \omega_c, T_c, S(60), m(60)$
58.RAP.E1	$GR_{15^{\circ}C}, R_{09-59}, R_{MC}, \omega_c, T_c, \Delta T_c$	$GR_{25^{\circ}C}$	$ G^* \times \sin \delta, S(60), m(60)$
58.RAP.E2	R_{09-59}, R_{MC}, T_c	$GR_{25^{\circ}C}, \omega_c, \Delta T_c$	$ G^* \times \sin \delta, GR_{15^{\circ}C}, S(60), m(60)$
58.RAP.E3	R_{09-59}, R_{MC}	ΔT_c	$ G^* \times \sin \delta, GR_{25^{\circ}C}, GR_{15^{\circ}C}, \omega_c, T_c, S(60), m(60)$
64.MRAS.R1	R_{09-59}, R_{MC}	--	$ G^* \times \sin \delta, GR_{25^{\circ}C}, GR_{15^{\circ}C}, \omega_c, T_c, S(60), m(60)$
64.MRAS.R2	R_{09-59}, R_{MC}	--	$ G^* \times \sin \delta, GR_{25^{\circ}C}, GR_{15^{\circ}C}, \omega_c, T_c, S(60), m(60)$

Table 17. Comparisons between the Rheological Properties of the Blends in Comparison to the Target PG 64-22 Virgin Binder at the P40 Age Level

Blend	Comparison to Target		
	Worse	Equal	Better
58.RAP	GR _{25°C} , GR _{15°C} , ω_c , T _c	$ G^* \times \sin \delta$, R ₀₉₋₅₉ , R _{MC} , m(60), ΔT_c	S(60)
58.MRAS	GR _{25°C} , GR _{15°C} , R _{MC} , ω_c , T _c	$ G^* \times \sin \delta$, R ₀₉₋₅₉ , m(60), ΔT_c	S(60)
64.RAP.R1	--	R ₀₉₋₅₉ , R _{MC} , ΔT_c	$ G^* \times \sin \delta$, GR _{25°C} , GR _{15°C} , ω_c , T _c , S(60), m(60)
64.RAP.R2	--	R ₀₉₋₅₉ , R _{MC} , ΔT_c	$ G^* \times \sin \delta$, GR _{25°C} , GR _{15°C} , ω_c , T _c , S(60), m(60)
58.RAP.E1	R ₀₉₋₅₉ , R _{MC} , ω_c , T _c , ΔT_c	--	$ G^* \times \sin \delta$, GR _{15°C} , GR _{25°C} , S(60), m(60)
58.RAP.E2	R ₀₉₋₅₉ , R _{MC} , ω_c , T _c , ΔT_c	GR _{15°C} , m(60)	$ G^* \times \sin \delta$, GR _{25°C} , S(60)
58.RAP.E3	R _{MC}	R ₀₉₋₅₉ , ΔT_c	$ G^* \times \sin \delta$, GR _{25°C} , GR _{15°C} , ω_c , T _c , S(60), m(60)
64.MRAS.R1	R _{MC}	R ₀₉₋₅₉ , T _c	$ G^* \times \sin \delta$, GR _{25°C} , GR _{15°C} , ω_c , S(60), m(60)
64.MRAS.R2	R _{MC} , ω_c , T _c	GR _{15°C} , R ₀₉₋₅₉	$ G^* \times \sin \delta$, GR _{25°C} , S(60), m(60)

The above analysis collectively suggests that both the current practice to use a PG 58-28 binder in high RBR mixtures and the incorporation of extenders and RAs can achieve equal or better intermediate- and low-temperature performance-graded properties compared to PG 64-22 virgin binders when their dosage is selected to restore the intended high-temperature performance grade. However, the analysis showed that the blends with the additives generally maintained equal or better GR parameter values whereas the reference blends with only PG 58-28 virgin binder and recycled binder tended to have inferior values compared to the PG 64-22 virgin binder evaluated. The analysis also revealed instances where inferior ΔT_c and/or R values in both the reference blends and the blends containing the additives. The ΔT_c and R values measure the balance between stiffness and relaxation characteristics of an asphalt binder. Thus, the results suggest that both the current practice to include a PG 58-28 virgin binder as well as the addition of extenders and RAs cannot fully restore the balance of stiffness and relaxation properties of recycled binders to that of a virgin, PG 64-22 binder. This was also evident by the findings comparing the high-, intermediate-, and low-temperature characteristics of the recycled binder blends against the QA database of PG 64-22 virgin binders presented in Section 3.4.2. There, it was apparent that while the rheology of a recycled binder can be restored to the condition of PG 64-22 virgin binders in the high or low temperature regime, the properties would be notably different in the opposite temperature regime.

To further investigate the ability of the blends to restore the balance of rheological characteristics in asphalt binders, the $|G^*|$ versus δ (i.e., black space) results from intermediate-temperature grading (i.e., 25°C, 10 rad/s). Figure 22 shows the results where two points are shown for each binder/blend, corresponding to the P20 and P40 age levels. Figure 22 shows that the blends with additives all have significantly lower $|G^*|$ values than the PG 64-22 (i.e., 64) virgin binder. However, it is apparent that the δ values of the blends are not always higher than the 64 virgin binder. The blends with the extenders often display lower or similar δ values to the reference 58.RAP blend despite lower $|G^*|$ values, which suggests softening from the additive without restoration of relaxation characteristics. Increasing R values indicate lower δ values at a given modulus level. If the lines drawn were all extended to allow for comparison of the blends at an equal $|G^*|$ condition, it is apparent that the blends with recycled binder would all have lower δ values for a given $|G^*|$ value compared to the 64 binder, and thus, explaining the high number of instances where the R values of the blends were deemed inferior to the virgin binder.

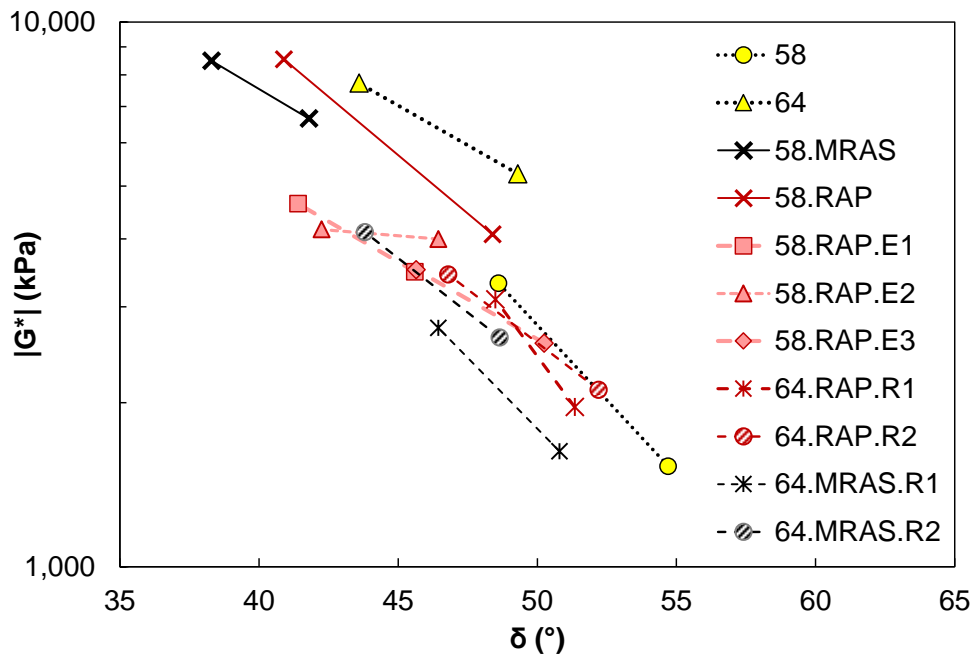


Figure 22. Relationship between $|G^*|$ and δ at 25°C, 10 rad/s at P20 and P40 age levels

3.5.3. Comparison of the Durability-Related Parameters

Correlation coefficients (r) were calculated for each possible pair of parameters to identify groups of durability-related parameters that provide similar insight regarding the relative performance of binders. Table 18 and Table 19 show the Spearman's rank correlation coefficient values among the different pairs of parameters at the P20 and P40 age levels, respectively. Pearson's correlation coefficients generally yield similar findings with the exception of a few cases where nonlinear relationships were evident that are captured by Spearman's but not Pearson's correlation coefficients. Pearson's correlation coefficient results are presented in Appendix E. The parameters $|G^*| \times \sin \delta$, $GR_{25^\circ C}$, $GR_{15^\circ C}$, ω_c , T_c are all correlated at the P20 and P40 age levels with correlation coefficients all above 0.72. The correlation coefficients among $|G^*| \times \sin \delta$, $GR_{25^\circ C}$, $GR_{15^\circ C}$ are all equal to or greater than 0.85. Moderate correlations are also evident in many cases among these parameters and $S(60)$, $m(60)$, and ΔT_c at the P20 age level but few correlations persist with these

other parameters at the P40 age level. The R_{09-59} and R_{MC} are strongly correlated at the P20 age level ($r = 0.83$) but only weakly at the P40 age level ($r = 0.50$). It was expected these parameters would be highly correlated at both age levels since they are both intended to reflect the logarithmic distance between the glassy modulus and binder modulus at the crossover point where δ equals 45° . Furthermore, it was anticipated that the R_{09-59} and ΔT_c would be correlated since the NCHRP 09-59 project suggested that either one could be used for fatigue specification (Christensen and Tran 2022). However, a correlation between R_{09-59} and ΔT_c only exists at the P40 age level ($r = -0.82$) and not the P20 age level ($r = -0.28$). The R_{09-59} and R_{MC} are also both correlated with the N_f results from the LAS test at P20 age level but only the R_{MC} is correlated with the N_f results at the P40 age level. The $S(60)$ is also positively correlated with N_f from the LAS test at both the P20 and P40 age levels, which may explain why the LAS tests often indicated the (counterintuitive) higher fatigue life at the P40 age level. The N_f results at the two strain levels evaluated are highly correlated to one another. For the study binders/blends, $S(60)$ and $m(60)$ are also highly correlated at the P20 ($r = -0.96$) and P40 ($r = -0.86$) age levels, yet ΔT_c appears to provide unique insight.

Table 18. Spearman’s Rank Correlation Coefficient Values at the P20 Age Level

Parameter	$ G^* \times \sin \delta$ (kPa)	$GR_{25^\circ C}$ (kPa)	$GR_{15^\circ C}$ (kPa)	ω_c (Hz)	T_c ($^\circ C$)	R_{MC}	R_{09-59}	$S(60)$ (MPa)	$m(60)$	ΔT_c ($^\circ C$)	N_f @ 5%
$ G^* \times \sin \delta$ (kPa)											
$GR_{25^\circ C}$ (kPa)	0.99										
$GR_{15^\circ C}$ (kPa)	0.87	0.85									
ω_c (Hz)	-0.89	-0.88	-0.97								
T_c ($^\circ C$)	0.91	0.90	0.93	-0.95							
R_{MC}	0.05	0.08	0.15	-0.26	0.32						
R_{09-59}	-0.15	-0.10	-0.16	0.00	0.07	0.83					
$S(60)$ (MPa)	0.67	0.65	0.69	-0.57	0.52	-0.40	-0.67				
$m(60)$	-0.78	-0.76	-0.84	0.74	-0.66	0.24	0.51	-0.96			
ΔT_c ($^\circ C$)	-0.70	-0.73	-0.83	0.85	-0.81	-0.37	-0.28	-0.48	0.68		
N_f @ 5%	-0.05	-0.06	0.03	-0.14	0.22	0.90	0.79	0.90	0.36	-0.22	
N_f @ 15%	-0.29	-0.32	-0.30	0.21	-0.09	0.74	0.68	-0.71	0.62	0.03	0.88

Table 19. Spearman’s Rank Correlation Coefficient Values at the P40 Age Level

Parameter	$ G^* \times \sin \delta$ (kPa)	$GR_{25^\circ C}$ (kPa)	$GR_{15^\circ C}$ (kPa)	ω_c (Hz)	T_c ($^\circ C$)	R_{MC}	R_{09-59}	$S(60)$ (MPa)	$m(60)$	ΔT_c ($^\circ C$)	N_f @ 5%
$ G^* \times \sin \delta$ (kPa)											
$GR_{25^\circ C}$ (kPa)	0.96										
$GR_{15^\circ C}$ (kPa)	0.88	0.94									
ω_c (Hz)	-0.75	-0.83	-0.82								
T_c ($^\circ C$)	0.72	0.77	0.78	-0.96							
R_{MC}	0.18	0.28	0.25	-0.71	0.74						
R_{09-59}	-0.23	-0.10	-0.03	-0.18	0.21	0.50					
$S(60)$ (MPa)	0.41	0.45	0.48	-0.28	0.15	-0.25	-0.31				
$m(60)$	-0.56	-0.63	-0.63	0.50	-0.41	-0.02	-0.09	-0.86			
ΔT_c ($^\circ C$)	-0.07	-0.18	-0.32	0.42	-0.43	-0.53	-0.82	-0.17	0.45		
N_f @ 5%	0.06	0.06	0.00	-0.46	0.55	0.76	0.21	0.76	0.32	-0.15	
N_f @ 15%	-0.02	-0.06	-0.12	-0.34	0.44	0.62	0.14	-0.44	0.35	-0.15	0.94

Correlations among the results at the P20 and P40 age levels for a given parameters were also evaluated to assess whether the P40 provides unique rheological insight compared to the P20 age level. Table 20 shows the Pearson’s and Spearman’s correlation coefficient values based on comparisons of the results of a given parameter at the P20 versus P40 age level. In general, results are highly correlated among the two age levels with the exception of the R_{09-59} . The reason for the outlier behavior in the R_{09-59} results is unknown and could not be attributed to an individual outlier

binder/blend in the results. The poor relationship in R_{09-59} may explain why the R_{MC} are correlated at the P20 but not the P40 age level. It is also noted that the correlation between the two age levels is more moderate for ΔT_c than most other parameters evaluated. Given that two potentially problematic blends (58.RAP.E1 and 58.RAP.E2) were identified through ΔT_c at the P40 age level, this finding is considered noteworthy and may indicate that the P40 age level is necessary to identify potentially problematic binder systems.

Table 20. Correlation Coefficients between P20 and P40 Age Levels

Parameter	Pearson's Correlation Coefficient	Spearman's Rank Correlation Coefficient
$ G^* \times \sin \delta$ (kPa)	0.88	0.91
$GR_{25^\circ C}$ (kPa)	0.88	0.93
$GR_{15^\circ C}$ (kPa)	0.90	0.76
ω_c (Hz)	0.85	0.87
T_c ($^\circ C$)	0.89	0.88
R_{MC}	0.82	0.92
R_{09-59}	0.38	0.48
$S(60)$ @ $-18^\circ C$ (MPa)	0.90	0.73
$m(60)$ @ $-18^\circ C$	0.83	0.80
ΔT_c ($^\circ C$)	0.74	0.67
N_f @5%	0.91	0.95
N_f @15%	0.85	0.88

To complement the correlation analysis, Table 21 summarizes the number of statistically distinct groups identified based on the Tukey HSD test results of each parameter at the P20 and P40 age levels. Comparison of the number of groups across parameters offers a measure of relative ability to discriminate the performance among the study binder systems. Additionally, comparison of the number of groups at the P20 and P40 age levels provides insight on whether better discrimination is achieved at one of the two age levels. The T_c at the P20 age level shows the highest number of unique groups of all cases evaluated. More cases were identified where there are more unique groups at the P20 than P40 age level. However, in most cases the number of groups at each level are fairly similar. Notably, the $GR_{25^\circ C}$ demonstrates better discrimination among the performance of the binders/blends evaluated at the P40 age level. Furthermore, while ΔT_c values of the study blends fall into relatively few statistically distinct groups at the P40 age level, this parameter did identify potentially problematic cases and thus, the number of statistically distinct groups may not be a direct indicator of need/viability of a parameter for specification.

Table 21. Number of Statistically Distinct Groups for Each Durability-Related Parameter

Parameter	P20	P40	Unique Groups at P20 - P40	Total No. of Binders/Blends
	Unique Groups	Unique Groups		
$ G^* \times \sin \delta$ (kPa)	5	5	0	11
GR _{25°C} (kPa)	5	7	-2	11
GR _{15°C} (kPa)	8	7	1	11
R ₀₉₋₅₉	6	4	2	11
R _{MC}	6	5	1	11
ω_c (Hz)	8	7	1	11
T _c (°C)	9	6	3	11
S(60) @ -18°C (MPa)	8	7	1	11
m(60) @ -18°C	6	6	0	11
ΔT_c (°C)	5	3	2	9

3.5.4. Summary of Findings

The majority of the rheological parameters evaluated indicate that the blends containing E3, R1, and R2 have superior durability compared to the respective reference 58.RAP or 58.MRAS and equal or superior durability compared to the 64 virgin binder evaluated. The primary exception to this finding was with respect to R values (i.e., R_{MC} and/or R₀₉₋₅₉). The blends containing E3, R1, and R2 passed recommended durability parameter criteria (including that for R₀₉₋₅₉) with the exception of T_c. However, all virgin binders and blends evaluated failed the warning limit at the P40 age level, suggesting it may be overly harsh. The blends containing E1 and E2 failed recommended criteria in several cases at the P40 age level and also exhibited parameters deemed inferior to the 64 virgin binder. Most notably, the E1 and E2 blends failed to meet the recommended minimum ΔT_c limit of -5°C at the P40 age level and generally exhibited inferior R and ΔT_c values compared to the 64 virgin binder, suggesting a potentially poorer balance in stiffness and relaxation characteristics. All study binders met the recommended limits for R₀₉₋₅₉ and thus, it is unclear if the observed trends will result in performance concerns. While the results of the rheological parameters evaluated are generally highly correlated at the P20 and P40 age levels, ΔT_c results are less correlated among the two age levels than most parameters evaluated and thus, the P40 age level is considered important for screening additives and binders. Also, while the NCHRP 09-59 project suggested that ΔT_c and R₀₉₋₅₉ provide the same insight, these parameters were not correlated at the P20 age level in this study. Furthermore, R₀₉₋₅₉ values were not correlated at the P20 and P40 age levels unlike all other parameters evaluated and poorly correlated with the R_{MC} at the P40 age level. Therefore, the need for controlling R values in binder specifications and best measure of the R value merits further investigation in future work.

Certain rheological parameters evaluated are highly correlated with each other for the study binders and thus, provided somewhat redundant insight regarding the relative durability of the binders/blends evaluated. Based on the observed correlations, only one of the parameters $|G^*| \times \sin \delta$, GR_{25°C}, GR_{15°C}, ω_c , T_c is deemed necessary. The GR_{25°C} better discriminated the performance of binders at the P40 age level than the current $|G^*| \times \sin \delta$. Also, the GR_{25°C} identified cases where the blends where the reference blends may have inferior performance compared to the 64 virgin

binder that were not identified through $|G^*| \times \sin \delta$. Thus, the $GR_{25^\circ C}$ parameter merits future consideration as an alternative intermediate-temperature binder specification parameter, especially given that it can be obtained using current intermediate-temperature AASHTO M 320 PG test results. Given that $GR_{15^\circ C}$, ω_c , and T_c require TFS testing and the construction of a corresponding master curve, they are considered less practical for adoption into specifications at this time. The LAS test revealed counterintuitive trends with respect to age level in many cases and therefore, is not recommended for implementation unless trends with respect to aging can be resolved. The standard BBR test parameters, $S(60)$ and $m(60)$, are highly correlated with one another for the study binders whereas ΔT_c provided unique insight and thus, ΔT_c merits consideration for addition to low-temperature PG binder specifications.

3.6. Effects of Recycling Agents and Extenders on the Dynamic Modulus and Cracking Performance of Long-term Aged Asphalt Mixtures

3.6.1. Asphalt Mixture Performance Test Results

The cracking performance of long-term aged laboratory-mixed asphalt mixture samples prepared according to a subset of the study blends were evaluated. These mixtures included the two reference mixtures (i.e., 58.RAP and 58.MRAS). In addition, each mixture was prepared with R1 (i.e., 64.RAP.R1 and 64.MRAS.R1) and one alternative blend. Loose asphalt mixture samples were aged in an oven at $95^\circ C$ for 7 days following short-term aging conducted in accordance with AASHTO R 30. The cracking performance was measured through AMPT dynamic modulus and cyclic fatigue tests. A long-term age condition was used for cracking evaluation given that the literature indicates additive effectiveness may diminish over the life of the pavement.

Figure 23 and Figure 24 show the dynamic modulus master curves for the RAP mixtures and MRAS mixtures, respectively. From Figure 23, it is visually evident that the reference 58.RAP and 64.RAP.R1 mixtures have similar dynamic moduli and that the 58.RAP.E2 has somewhat lower dynamic moduli. All MRAS mixtures appear to have similar dynamic moduli in Figure 24. Tukey's Honest Significant Difference (HSD) tests were conducted to evaluate the significance of dynamic modulus differences among the RAP mixtures and among the MRAS mixtures at each temperature-frequency combination using a 95 percent confidence level. The statistical test results indicate that the 58.RAP and 64.RAP.R1 mixtures have the same dynamic moduli whereas the 58.RAP.E2 mixture has distinct (lower) dynamic moduli at each temperature-frequency combination, matching visual inferences. The dynamic moduli of the 64.MRAS.R1 and 64.MRAS.R2 mixtures are deemed equal to the reference 58.MRAS mixture based on the Tukey's HSD tests. However, the 64.MRAS.R1 and 64.MRAS.R2 differ at $40^\circ C$ and both 1 Hz and 0.1 Hz loading frequencies as well as $20^\circ C$ and 0.1 Hz loading frequency based on the Tukey's HSD tests.

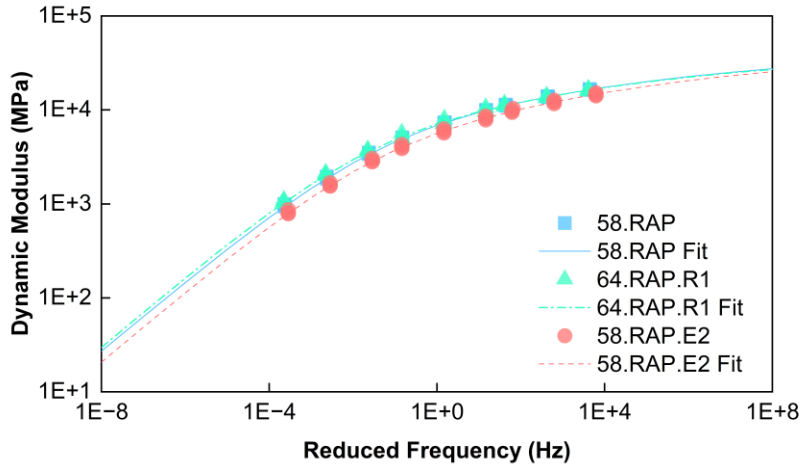


Figure 23. Dynamic modulus master curves for the RAP mixtures

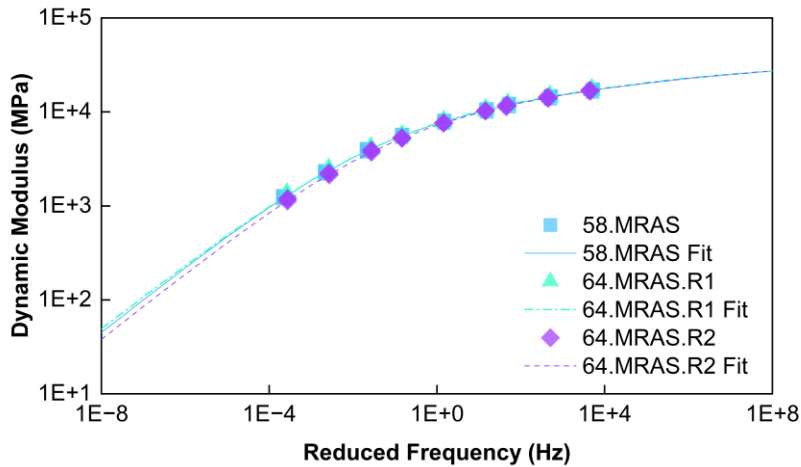


Figure 24. Dynamic modulus master curves for the MRAS mixtures

Figure 25 and Figure 26 show the damage characteristic curves for the RAP mixtures and MRAS mixtures, respectively. Figure 25 and Figure 26 reveal similar trends among the study mixtures to those observed in the dynamic modulus test results. That is, the damage characteristic curves of the MRAS mixtures are very similar. The reference 58.RAP and 64.RAP.R1 mixtures also have similar damage characteristic curves to one another but the 58.RAP.E2 mixture has a distinct damage characteristic curve, falling below the other two RAP mixtures. Lower modulus asphalt mixtures often exhibit damage characteristic curves that fall below higher modulus mixtures and thus, the observations among the RAP mixtures follow this expected trend.

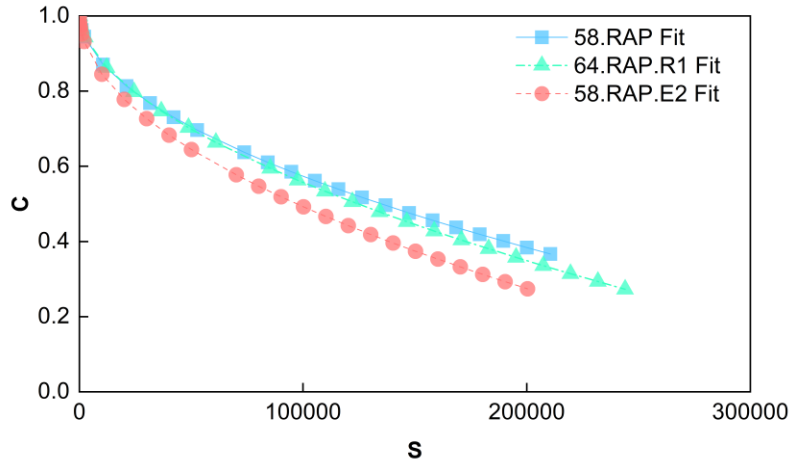


Figure 25. Damage characteristic curves for the RAP mixtures

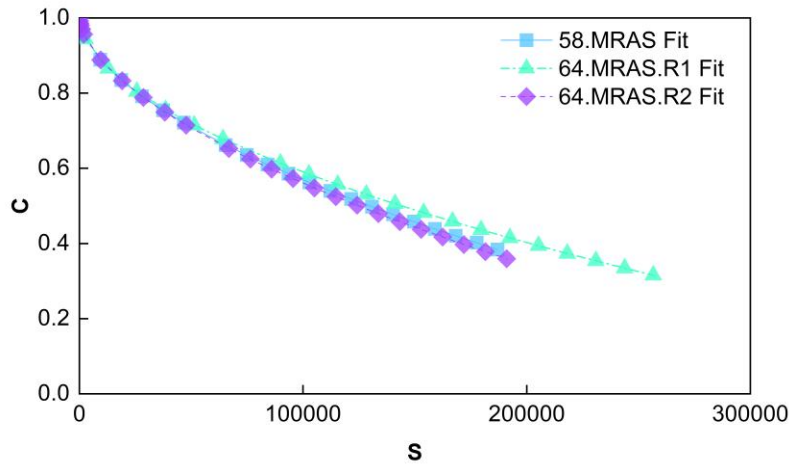


Figure 26. Damage characteristic curves for the MRAS mixtures

Figure 27 shows the D^R failure criterion results for all study mixtures. The RAP mixtures exhibit slightly higher D^R values than the MRAS mixtures. The D^R results of all RAP mixtures are statistically the same with a 95 percent confidence level. Similarly, the D^R results of all MRAS mixtures are deemed equal based on a 95 percent confidence level.

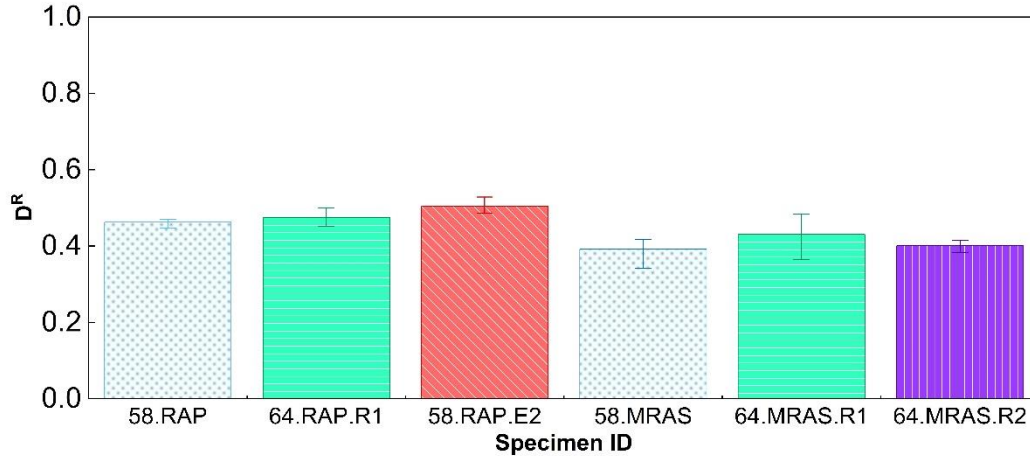


Figure 27. Failure criteria (error bars reflect the maximum and minimum individual specimen result)

Figure 28 shows the S_{app} results for all study mixtures. A higher S_{app} value indicates superior fatigue cracking performance. The RAP mixtures exhibit higher S_{app} values than the MRAS mixtures. However, no statistically significant differences in the S_{app} values among the RAP mixtures or among the MRAS mixtures are observed given a 95 percent confidence level. These results indicate in the long-term aged condition, the RA and extender modified mixtures exhibit similar fatigue performance to the reference mixtures prepared according to NCDOT’s current practice (i.e., use of a PG 58-28 virgin binder). These results suggest that the potential inferior performance of the 58.RAP.E2 blend identified in Section 3.5 did not lead to notably poorer performance in terms of S_{app} . However, mixture thermal cracking resistance was not quantified. Furthermore, studies have demonstrated diminished sensitivity of mixture performance results at long-term aged conditions compared to short-term aged conditions (Mensching et al. 2022), which may have contributed to the observed trends. It is noted that all S_{app} values pass the recommended criteria for standard traffic conditions at the short-term age level (FHWA 2019).

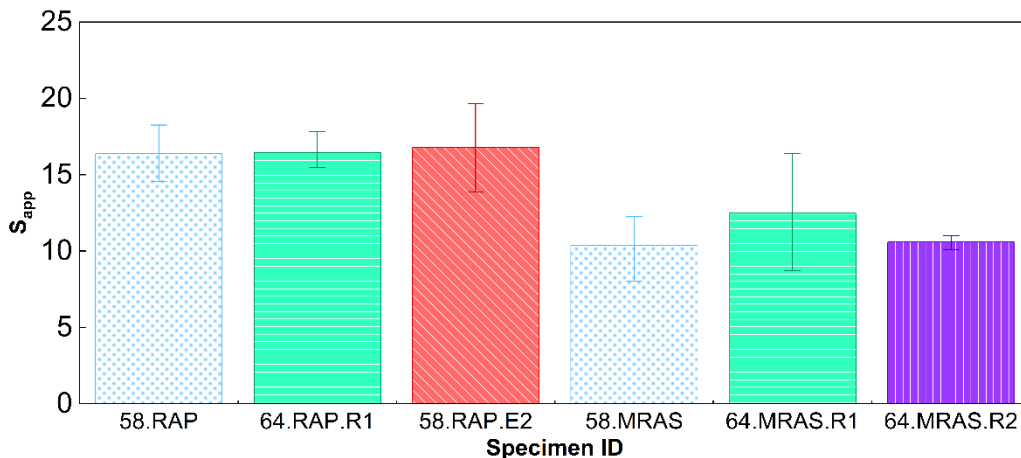


Figure 28. S_{app} results (error bars reflect the maximum and minimum individual specimen result)

3.6.2. Evaluation of the Asphalt Binders Extracted and Recovered from the Long-Term Aged Mixtures with Comparison to Binder Blends Aged for 40-hours in the PAV

In order to better understand the reason that all RAP mixtures and all MRAS mixtures exhibited similar performance, asphalt binders were extracted and recovered from the long-term aged (LTA) mixtures and characterized through TFS testing. Note that the extraction and recovery process forces complete mixing of the recycled and virgin binder in the mixture but that complete blending in the mixture prior to extraction and recovery is unlikely based on the results shown in Section 3.2. The rheological properties of the extracted and recovered binders were compared to those of the asphalt binder blends at the P40 age level. Figure 29 and Figure 30 show the asphalt binder master curves corresponding to the P40 age level and extracted and recovered from the LTA mixtures for the RAP blends and MRAS blends, respectively. Figure 29 shows that the rheology of the 58.RAP and 64.RAP.R1 blends at the LTA age level is very similar, both in terms of dynamic shear modulus and phase angle. The 58.RAP.E2 binder exhibits slightly lower dynamic shear moduli than the 58.RAP and 64.RAP.R1 blends at the P40 age level, matching trends observed in the asphalt mixture dynamic modulus test results. Figure 30 shows that all MRAS blends exhibit similar dynamic shear moduli and phase angle values at the LTA age level, consistent with the asphalt mixture dynamic modulus test results.

Figure 29 and Figure 30 also show that the LTA age level is harsher than the P40 age level as evident by the higher dynamic shear moduli and lower phase angle values of a given blend at the LTA versus P40 age level. This may indicate the LTA condition is unrealistically harsh. Furthermore, Figure 29 shows that the dynamic shear moduli and phase angle values vary among the RAP blends at the P40 age level. Similarly, Figure 30 shows that the dynamic shear moduli and phase angle values vary among the MRAS blends at the P40 age level. In both cases, the RA and extender modified blends exhibit lower dynamic shear moduli than the reference blends. This suggests that the difference between the RA and extender modified binder systems become more similar to the reference 58.RAP and 58.MRAS systems at higher long-term age levels. In other words, RA and extender effectiveness at softening binder systems and improving cracking resistance may diminish with time. Thus, if AMPT testing were conducted at a short-term or less harsh LTA condition, differences among the RAP and among the MRAS mixtures may be expected, which may contribute (at least somewhat) to prolonged pavement life. However, given that short-term aged asphalt mixture testing was not conducted, the magnitude of the benefits in terms of pavement life cannot be quantified.

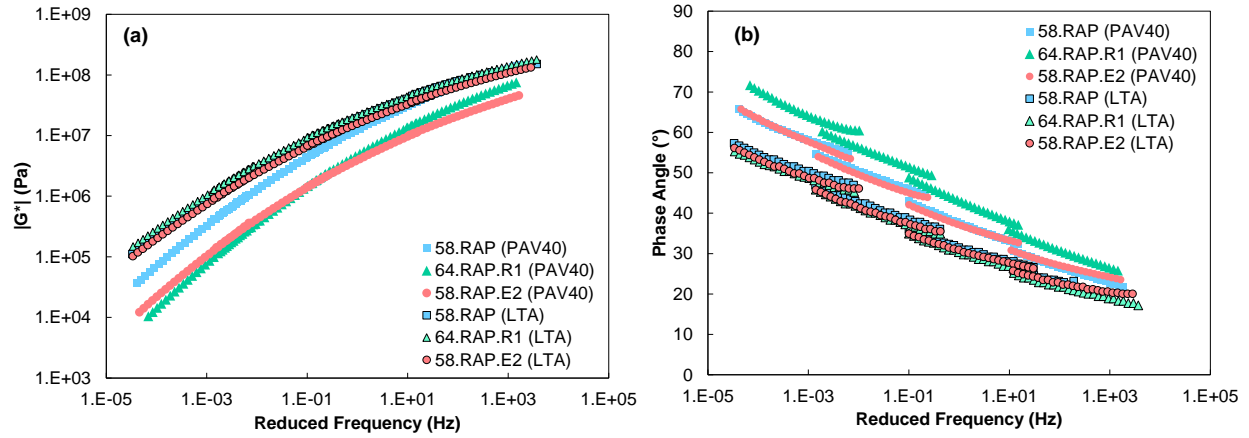


Figure 29. Comparison of PAV40 and extracted and recovered LTA binder master curves for the RAP binder blends: (a) dynamic shear modulus and (b) phase angle

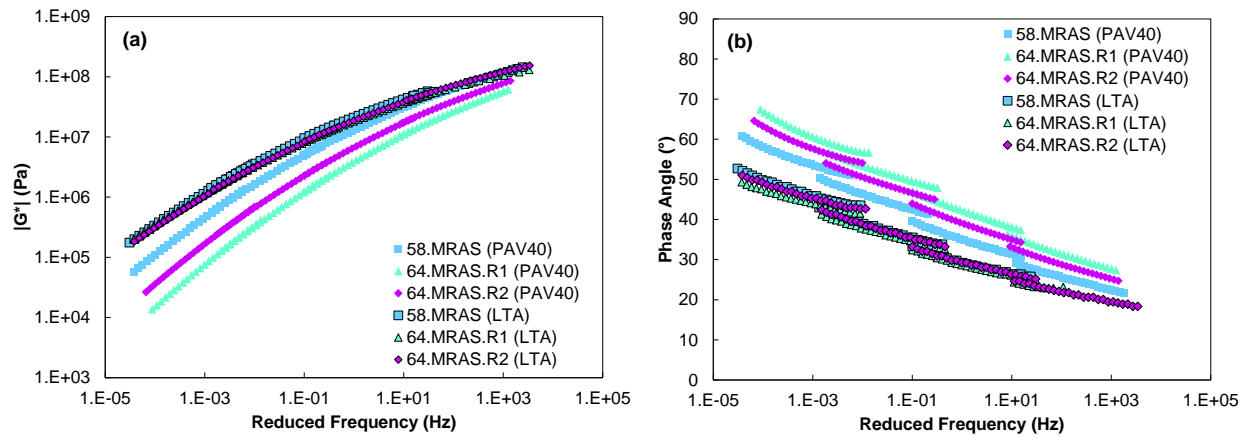


Figure 30. Comparison of PAV40 and extracted and recovered LTA binder master curves for the RAP binder blends: (a) dynamic shear modulus and (b) phase angle

4. CONCLUSIONS AND RECOMMENDATIONS

4.1. Conclusions

The following conclusions are drawn from the results of this study:

- Different recycling agent (RA) and extender products can yield different rates of change in the asphalt binder continuous high-temperature grade with additive content. However, the rate of change in asphalt binder continuous high-temperature grade with additive content for a given additive was similar for different recycled binder and virgin binder combinations.
- Testing of blends containing RAS at the original age level should be avoided as residual agglomerations of RAS may remain. It was found that RTFO aging can be used to achieve a homogenous binder blend with RAS. Testing of virgin-recycled binder blends rather than relying on linear blending theory to estimate the high-temperature grade is recommended, especially in the case of RAS binders because conducting high-temperature grading of RAS binders imparts considerable uncertainty.
- The AASHTO M 320 high-temperature grading results of verification blends prepared at selected dosages yielded considerable discrepancies with those predicted from dosage selection testing in some cases; these results suggest uncertainty in the dosage selection results of around 3°C that should be incorporated into the dosage selection procedure.
- Recycled binder contribution measurements for the two mixtures evaluated suggest complete recycled binder contribution does not exist in asphalt mixtures. The additives evaluated were ineffective at increasing recycled binder contribution. However, the PG 64-22 virgin binder evaluated yielded increased recycled binder contribution in the RAP mixture compared to the PG 58-28 virgin binder, which is speculated to be related to its higher chemical compatibility (evident in Appendix C).
- All Hamburg Wheel-Track tests conducted on asphalt mixtures prepared at additive dosages intended to achieve a continuous AASHTO M 320 grade of 64°C passed the minimum rutting criteria proposed in NCHRP Project 09-58 for the North Carolina climate conditions despite partial recycled binder contribution.
- The current practice to use a PG 58-28 virgin binder in high RBR mixtures resulted in similar intermediate- and low-temperature performance-graded properties to PG 64-22 virgin binders in North Carolina (i.e., the intended condition) for the RAP and MRAS cases evaluated. However, the current practice resulted in high-temperature performance-graded properties that were distinct from PG 64-22 virgin binders.
- The blends of virgin binder, recycled binder, and an extender or RA at a dosage selected to restore the intended high-temperature grade of 64°C display high-temperature performance-graded properties similar to virgin PG 64-22 binders. However, these systems exhibit distinct but potentially superior low- and intermediate-temperature performance-graded characteristics and other measures of binder durability compared to PG 64-22 virgin binders.
- The collective results highlight that neither the current practice to use a PG 58-28 virgin binder in high RBR mixtures or the use of extenders or RAs can fully restore rheological properties of recycled binder blends to those of PG 64-22 virgin binders. While properties in either the high or low temperature regime can be restored, the consequence will be notably different properties at the opposite temperature regime. The inability of additives to fully restore rheological properties was also identified in many cases through inferior ΔT_c and/or R values compared to a PG 64-22 virgin binder. These parameters measure the balance of relaxation

and stiffness characteristics of an asphalt. It appears that additives tend to soften binders to a greater extent than restoring relaxation characteristics.

- The majority the rheological parameters evaluated indicate that the blends containing the vacuum gas oil extender and the RAs (i.e., E3, R1, and R2) have superior durability compared to the respective reference blends of PG 58-28 virgin binder and recycled binder and equal or superior durability compared to the PG 64-22 virgin binder evaluated. These blends all had high-temperature grades between 64°C and 70°C. These blends also generally passed recommended durability parameter criteria.
- The blends containing the extenders that contain REOB (i.e., E1 and E2) failed recommended criteria for rheological parameters in several cases at the RTFO plus 40-hour PAV (P40) age level and also exhibited parameters deemed inferior to the 64 virgin binder. Most notably, these blends failed to meet the recommended minimum ΔT_c limit of -5°C at the P40 age level, suggesting potential performance concerns. This potentially inferior performance was not identified at the 20-hour PAV (P20) age level.
- The parameters $|G^*| \times \sin \delta$, Glover-Rowe (i.e., both $GR_{25^\circ C}$, $GR_{15^\circ C}$), crossover frequency (ω_c) and crossover temperature (T_c) were all correlated for the binders evaluated and thus, provided somewhat redundant information regarding the relative performance of the study binders. The values of each of these parameters were highly correlated at the standard RTFO plus 20-hour PAV (P20) and P40 age levels.
- While many cases were identified that the recycled binder blends evaluated had inferior R values compared to the PG 64-22 virgin binder, all passed recommended criteria from the NCHRP 09-59 project. Also, while the NCHRP 09-59 project suggested that ΔT_c and R_{09-59} provide the same insight, these parameters were not correlated at the P20 age level in this study. Furthermore, R_{09-59} values were not correlated at the P20 and P40 age levels unlike all other parameters evaluated and poorly correlated with the R_{MC} at the P40 age level. Therefore, the need for controlling R values in binder specifications and best measure of the R value is unclear from the results of this study.
- The LAS test revealed counterintuitive trends with respect to age level in many cases.
- The standard BBR test parameters, $S(60)$ and $m(60)$, were highly correlated with one another for the study binders whereas ΔT_c provided unique insight. The P20 and P40 results for $S(60)$ and $m(60)$ values were more highly correlated than the ΔT_c values between the two age levels.
- The long-term aged asphalt mixtures evaluated containing extenders and recycling agents all performed similarly to their corresponding reference mixture containing PG 58-28 virgin binder. However, the long-term aged mixture condition was found to be much harsher than the P40 age level based on extracted and recovered binder testing and thus, may have been overly harsh. The harsh long-term age level could have limited the sensitivity of the mixture performance results to the binder variables evaluated.

4.2. Recommendations

The following recommendations are drawn from the results of this study:

- It is recommended that the NCDOT require contractors provide extender and RA additive dosages to restore the AASHTO M 320 high-temperature grade of the blend of recycled binder, virgin binder, and additive to 67°C. This generally enables achieving equal or better durability than that of PG 64-22 virgin binders. Furthermore, this generally ensures that the binder blend will still meet a minimum high-temperature grade of 64°C given the potential uncertainty in the resultant blended binder grades from dosage selection. This dosage could be provided

based on direct experimentation of a blend of the recycled binder, virgin binder, and additive to be used in a project at a minimum of three dosages, one of which could be zero. Alternatively, the supplier could provide evidence of a calibrated relationship between additive dosage and high-temperature grade from testing of a prior blend and testing of the continuous high-temperature grade of the blend of virgin and recycled binder to be used in the project to recommend a dosage to restore the high-temperature continuous grade to 67°C. It is further suggested that the NCDOT require evidence that the blend with the additive at the selected dosage meets specified AASHTO M 320 intermediate- and low-temperature properties for PG 64-22 binders and does not yield a ΔT_c that falls below -5°C at the RTFO plus 40-hour PAV age level for product approval. It is suggested that the NCDOT monitor any projects that include an extender or RA closely to better understand their implications on long-term performance.

- It is recommended that the NCDOT consider adding a minimum ΔT_c requirement to its low-temperature performance-graded specifications for asphalt binders. Also, it is recommended that the NCDOT consider adopting the RTFO plus 40-hour PAV long-term aging procedure based on the potentially problematic cases identified through ΔT_c at this age level identified in this research project. However, it is noted that adopting the 40-hour PAV procedure would require revision of other intermediate- and low-temperature binder specification criteria, warranting additional research. It is also recommended that the NCDOT consider adopting the Glover-Rowe parameter at 25°C as an alternative to the current intermediate-temperature performance-graded specification parameter given that (1) it can be obtained using consistent testing as the current intermediate-temperature specification and (2) it demonstrated a superior ability to discriminate binder performance, particularly at the RTFO plus 40-hour PAV age level in this study. The R value may also merit future consideration given that the results indicated inferior R values were observed in recycled binder blends compared to virgin binders. However, the best method for determining R and its effect on performance merits additional research. It is also important to note that this study was limited to high recycled content mixtures, which does not cover all binder types used by the NCDOT. Polymers are not used in high recycled content mixtures but are used in RS9.5D mixtures. Polymer modified asphalts can exhibit distinct rheological behavior and performance from non-polymer modified asphalt binders. Therefore, the proposed changes to performance-graded specifications should be evaluated using a broader set of virgin binders, including both polymer-modified and unmodified asphalts prior to adoption for widespread binder specification.
- The effects of recycled binder-virgin binder compatibility on recycled binder contribution and performance merits further investigation given the results of this study.

5. IMPLEMENTATION AND TECHNOLOGY TRANSFER PLAN

The Materials and Tests Unit of the NCDOT are the primary users of the outcomes of this research. The proposed dosage selection and product approval process described in Section 4.2 can be applied to extenders and recycling agents. Furthermore, it is recommended that the NCDOT consider tracking the Glover-Rowe ($GR_{25^{\circ}C}$) parameter and NCHRP 09-59 R value (R_{09-59}) as part of QA in addition to the current intermediate-temperature specification parameter so that is viability as an alternative to the current specification can be further evaluated. This can be done using current QA test procedures. It is also recommended that the NCDOT considers allocating resources to further consider and evaluate ΔT_c and the 40-hour PAV procedure to better address binder durability within performance-graded specifications.

6. CITED REFERENCES

1. Anderson, D. A., D. W. Christensen, H. U. Bahia, R. Dongre, M. G. Sharma, C. E. Antle, and J. Button. *SHRP Report A-369: Binder Characterization and Evaluation, Volume 3: Physical Characterization*. National Research Council, Washington, D.C., 1994.
2. Anderson, R. M., G. N. King, D. I. Hanson, and P. B. Blankenship. Evaluation of the Relationship between Asphalt Binder Properties and Non-load Related Cracking. *Journal of the Association of Asphalt Paving Technologists*, Vol. 80, 2011, pp. 615-663.
3. Asphalt Institute, State-of-the-Knowledge: Use the Delta Tc Parameter to Characterize Asphalt Binder Behavior, *Asphalt Institute Information Series*, 2019.
4. Bahia, H. U., D. I. Zeng, H. Kharti, M. A. Zhai, & M. Anderson. Characterization of Modified Asphalt Binders in Superpave Mix Design, *NCHRP Report 459*, National Academies, Washington, D.C., 2001.
5. Bonaquist, R., J. Adams, and D. Anderson. Asphalt Binder Aging Methods to Accurately Reflect Asphalt Mixture Aging. *NCHRP Report 967*, National Academies, Washington, D.C., 2021.
6. Castorena, C., S. Pape, D. Mocelin, L. Xue, M. Aparicio Alvis, and M. Ravichandran. Improving the Design of RAP and RAS Mixtures. NCDOT Report 2019-21, Raleigh, N.C., 2022.
7. Christensen, D. W. *Mathematical Modeling of the Linear Viscoelastic Behavior of Asphalt Cements*. Ph.D. Dissertation, Pennsylvania State University, College Station, PA, 1992.
8. Christensen, D. W., and N. Tran. *NCHRP Report 982: Relationships Between the Fatigue Properties of Asphalt Binders and the Fatigue Performance of Asphalt Mixtures*. Transportation Research Board, Washington, D.C., 2022. <http://dx.doi.org/10.17226/26302>.
9. Daly, W.H. Relationship Between Chemical Makeup of Binders and Engineering Performance, *NCHRP Synthesis 511*, National Academies, Washington, D.C., 2017.
10. Elwardany, M., J. P. Planche, and G. King. Universal and Practical Approach to Evaluate Asphalt Binder Resistance to Thermally-induced Surface Damage. *Construction and Building Materials*, Vol. 255, 2020, pp. 119331.
11. Elwardany, M., J. P. Planche, and G. King. Proposed Changes to Asphalt Binder Specifications to Address Binder Quality-Related Thermally Induced Surface Damage. *Transportation Research Record*, Vol. 2676, No. 5, 2022, pp. 176-191.
12. Epps Martin, A., et al. The Effects of Recycling Agents on Asphalt Mixtures with High RAS and RAP Binder Ratios, *NCHRP Report 927*, National Academies, Washington, D.C., 2020.
13. FHWA, *Cyclic Fatigue Index Parameter (S_{app}) for Asphalt Performance Engineered Mixture Design*, FHWA, Washington, D.C., 2019.
14. Fini, E. H., E. W. Kalberer, A. Shahbazi, M. Basti, Z. You, H. Ozer, and Q. Aurangzeb. Chemical Characterization of Biobinder from Swine Manure: Sustainable Modifier for Asphalt Binder, *Journal of Materials in Civil Engineering*, Vol. 23, 2011, pp. 1506 -1513.
15. Glover, C. J., R. R. Davison, C. H. Domke, Y. Ruan, P. Juristyarini, D. B. Knorr, and S. H. Jung. *Development of a New Method for Assessing Asphalt Binder Durability with Field Validation*. FHWA/TX Report 05/1872-2, Texas Department of Transportation, Austin, TX, 2005.
16. Hintz, C., and H. Bahia. Simplification of Linear Amplitude Sweep Test and Specification Parameter. *Transportation Research Record*, Vol. 2370, No. 1, 2013, pp. 10-16.
17. IHS Cambridge Energy Research Associates 2010

18. Kaseer, F., A. Epps Martin, and E. Arambula-Mercado. Use of recycling agents in asphalt mixtures with high recycled materials contents in the United States: A literature review, *Construction and Building Materials*, Vol. 211, 2019, pp. 974-987.
19. Kim et al. Long-Term Aging of Asphalt Mixtures for Performance Testing and Prediction. *NCHRP Report 871*, National Academies, Washington, D.C., 2017.
20. McDaniel, R. and R.M. Anderson. Recommended Use of Reclaimed Asphalt Pavement in The Superpave Mix Design Method: Technician's Manual, *NCHRP Report 452*, National Academies, Washington, D.C., 2001.
21. Mensching, D., M. Elwardany, and V. Veginati. Evaluating the Sensitivity of Intermediate Temperature Performance Tests to Multiple Loose Mixture Aging Conditions Using the FHWA Accelerated Loading Facility's RAP/RAS Experiment, *Transportation Research Record*, No. 2676, 2022, pp. 474-485.
22. Nahar, S.N., M. Mohajeri, A. Schmets, T. Scarpas, M.F. van de Ven, and G. Schitter. First Observation of Blending Zone Morphology at Interface of Reclaimed Asphalt Binder and Virgin Binder, *Transportation Research Record*, No. 2370, 2013, pp. 1-7.
23. NCAT. NCAT Researchers Explore Multiple Uses of Rejuvenators, Asphalt Technology News, Vol. 26, No. 1 (Spring), 2014. <http://www.ncat.us/info-pubs/newsletters/spring-2014/rejuvenators.html>
24. Oldham, D., E. Fini, and E. Chailleux. Application of a bio-binder as a rejuvenator for wet processed asphalt shingles in pavement construction, *Construction and Building Materials*, Vol. 86, 2015, pp. 75-84.
25. Pape, S. E., and C. Castorena. Assessment of the impacts of sample preparation on the use of EDS for analysing recycled asphalt blending, *Journal of Microscopy*, Vol. 283 No. 3 2021, 232-242.
26. Roberts, F. Hot mix asphalt materials, mixture design and construction (3rd Ed.). *National Asphalt Pavement Association Research and Education Foundation*, Lanham, MD, 2009.
27. Rowe, G. Evaluation of the Relationship between Asphalt Binder Properties and Non-load Related Cracking. *Journal of the Association of Asphalt Paving Technologists, Prepared Discussion*, 2011, Vol. 80, pp. 649-663.
28. Rowe, G. M., and M. J. Sharrock. Alternate Shift Factor Relationships for Describing Temperature Dependency of Viscoelastic Behavior of Asphalt Materials. *Transportation Research Record: Journal of the Transportation Research Board*, 2011. Volume 2207: <http://dx.doi.org/10.3141/2207-16>.
29. Safaei, F., C. Castorena, and Y. R. Kim. Linking Asphalt Binder Fatigue to Asphalt Mixture Fatigue Performance using Viscoelastic Continuum Damage Modeling. *Mechanics of Time-Dependent Materials*, Vol. 20, No. 3, 2016, pp. 299-323, doi: 10.1007/s11043-016-9304-1.
30. Safaei, F., and C. Castorena. Temperature Effects in Linear Amplitude Sweep Testing and Analysis. *Transportation Research Record*, Vol. 2574, No. 1, 2016, pp. 92-100.
31. Wright, L., A. Kanabar, E. Moul, S. Rubab, and S. Hesp. Oxidative Aging of Asphalt Cements from and Ontario Pavement Trial, *International Journal of Pavement Engineering*, Vol. 4, No. 5, 2011, pp. 259-267.
32. Yang, K., R. Li, C. Castorena, and B. S. Underwood. Correlation of asphalt binder linear viscoelasticity parameters and the ranking consistency related to fatigue cracking resistance. *Construction and Building Materials*, Vol. 322, 2022, pp. 126450.

33. Yang, K., R. Li, B. S. Underwood, and C. Castorena. Effect of Laboratory Oxidative Aging on Dynamic Shear Rheometer Measures of Asphalt Binder Fatigue Cracking Resistance. *Construction and Building Materials*, Vol. 337, 2022.

APPENDIX A: DETAILED LITERATURE REVIEW

INTRODUCTION

The use of asphalt mixtures containing high Recycled Binder Replacements (RBRs) is increasing. Recycled binders are oxidized and thus, harder and more susceptible to cracking than virgin binders. Consequently, the use of higher recycled content mixtures has prompted heightened interest in recycling agents and necessitated the use of asphalt extenders to produce softer virgin binder grades. Recycling agents include a wide-range of both softening agents and rejuvenators that are intended to restore the physical and chemical properties of aged asphalt binders. Petroleum-based extender products have been in existence for a long time. Non-petroleum based products have been more recently introduced (e.g., bio-oils). This report consists of a review of relevant literature pertaining to the use of recycling agents and extenders, including changes to asphalt binders that are induced by oxidative aging, current recycling agent and extender products in use, performance concerns associated with the use of these products and shortcomings of the current specifications, potential means of improving binder characterization to enable screening of extenders and recycling agents, and dosage selection procedures.

CHANGES IN ASPHALT BINDERS WITH OXIDATIVE AGING

Asphalt binder is regarded as a colloid, consisting of highly polar asphaltenes dispersed in a soluble phase, consisting of saturates, aromatics, and resins. The resins are polar and serve to peptize the asphaltenes in the aromatics and saturates. The balance of the Saturates, Aromatics, Resins, and Asphaltenes (SARA) components affects the rheological properties of asphalt binders. Oxidative aging is a process that changes the microstructural and chemical composition of asphalt binders. Oxygen reacts with polar components of asphalt, converting polar aromatics and resins to asphaltenes (Petersen 2009). This is seen in Saturates, Aromatics, Resins, and Asphaltenes (SARA) fractionation as a loss of aromatics and resins, and a corresponding increase in asphaltenes. The loss of molecules in the maltene phase causes the asphaltenes to agglomerate, as the maltene phase is no longer providing adequate dispersion, and the viscosity and brittleness of the asphalt increases. Consequently, aging leads to hardening and embrittlement of asphalt binders. There are limits to working with SARA-type fractionation. As an individual process it cannot characterize aging. The simple mass proportion changes measured do not fully capture the chemical reactions taking place (Petersen 2009).

There are specific chemical functional groups that are formed upon oxidative aging, including sulfoxides and carbonyls. Fourier transform infrared spectroscopy (FTIR) can be used to track the formation of sulfoxides and carbonyls at wavenumbers of 1700 cm^{-1} and 1030 cm^{-1} , respectively. In addition to the sites for oxidation, additional molecules such as vanadium can also indicate aging. However, it should be noted that while some vanadium-containing molecules can catalyze oxidation, others do not (Petersen 2009).

The molecular size distribution within asphalt binders also evolves with aging. As a binder ages, a greater number of large molecules are produced and thus, examining the proportion of large size molecules (LSM) is a proportion that has been used to quantify aging (Li 2020).

The consequence of the chemical and microstructural changes on the performance grades (PGs) of asphalt binders is evident by increases in the low and high temperature grades. Table 22 shows a comparison between reclaimed material binder grades and virgin binder grades used in various

states (Epps-Martin et al. 2019). It can be seen that the high and low temperature grades of the reclaimed materials exceeds that of the virgin, due to oxidative aging.

Table 22. Comparison of Virgin Binder to Recycled Materials (Epps-Martin et al. 2019)

Material	Source	PG	Continuous PGH (°C)	Continuous PGL (°C)	ΔT_c (°C)
Virgin/Base Binders	TX	64-22	68.2	-24.6	-4.6
	NH	64-28	66.9	-28.0	+1.2
	NV	64-28P ^a	65.6	-30.7	-3.6
	IN	64-22	66.2	-25.3	-1.2
	IN	58-28	59.9	-28.2	-8.0
	MN	58-28	58.6	-28.0	+0.1
	WI	58-28	59.4	-28.6	-3.4
	WI	52-34	52.3	-34.2	+0.4
	DE	64-28	66.5	-29.0	+0.1
Recycled Materials	TX	—	106.6	-2.4	-9.8
	IN	88-10	90.4	-13.7	-6.2
	NV	82-16	84.4	-20.4	-3.4
	NH	88-16	90.2	-20.6	-2.1
	WI	82-10	83.5	-10.9	-7.3
	DE	82-10	86.2	-13.8	-4.4
	TX	—	130.7	—	—
	IN	—	123.3	—	—
	DE	—	146.0	—	—
	TX	—	178.0	—	—
CA	—	166.0	—	—	

Note: — = not available because RAS binders were very stiff and did not meet the m-value criteria (>0.3), even at high testing temperatures.

^a Polymer-modified binder.

Restoring Binder Compatibility

Simply restoring the PG of an aged binder by adding a soft virgin binder, extender, and/or recycling agent may not ensure that the properties of the binder have been restored to an unaged state. Several researchers have postulated that restoring the chemical compatibility of the binder is important to ensure adequate long-term performance when using reclaimed materials. Chemical compatibility refers to the extent of microstructure in an asphalt binder. Microstructure can arise due to the formation of asphaltene clusters and/or the crystallization of waxes within the saturates phase. Binders with poor compatibility have been shown to be prone to oxidative age hardening (Petersen 2009). Thus, if a binder softens but does not restore compatibility, it may be prone to oxidation induced hardening.

One means of examining chemical compatibility is by using colloidal instability also referred to as the Gaestel index (Kleizine 2019). The Gaestel index (I_c) can be calculated by using the concentrations of saturates (S_a), aromatics (A_r), resins (R_e), and asphaltenes (A_s) using Equation (1). As I_c increases, there tends to be an increase in the binder compatibility under the premise that having a high amount of resins and asphaltenes relative to asphaltenes and saturates helps prevent the formation of asphaltene clusters and crystallized wax formation (Kleiziene et al. 2019). The inverse of I_c , termed the colloidal instability index (CII), is also often reported as an alternative to I_c .

$$I_c = \frac{(A_r + R_e)}{(S_a + A_s)} \times 100\% \quad (13)$$

The automated flocculation tritrimeter (AFT) is another means to evaluate binder compatibility (Chandio et al. 2015, Yang et al. 2016). AFT measures the peptizability of the binder by measuring the flocculation behavior of asphaltenes in an asphalt. The peptizability evaluates the ability of the maltenes to prevent the formation of asphaltene clusters. Thus, better peptization would indicate a higher compatibility. This method works by finding asphaltene peptizability (P_a) and solvating power of oil (P_o) and solvency characteristics of maltene. A higher P_a indicates the asphaltenes are more peptized. A higher P_o indicates higher solvation by the maltenes. These values are used in Equation (14) below to give overall peptizability. Typically, P values fall between 2.5 and five (Chandio et al. 2015).

$$P = \frac{P_o}{1 - P_a} \quad (14)$$

In the AFT experiment, the asphalt is dissolved in a solvent and titration of the sample is carried out using a precipitant to estimate the onset point of asphaltene flocculation. To measure P_o and P_a , the asphalt is diluted by a solvent using varying concentrations of solvent and titrated. At each dilution concentration, the flocculation ratio (FR) is measured. FR is the fraction of volume of solvent to the total volume of solvent-titrant mixture at flocculation onset point during titration. The dilution concentration is the ratio of the mass of the asphalt to the volume of titrant and solvent at the onset of flocculation. FR versus C is plotted and used to determine FR_{Max} and C_{min} as shown in Figure 31 and P_a and P_o are calculated using Equation (15) and Equation (16), respectively.

$$P_a = 1 - FR_{Max} \quad (15)$$

$$P_o = FR_{Max} \times \left[\left(\frac{1}{C_{min}} \right) + 1 \right] \quad (16)$$

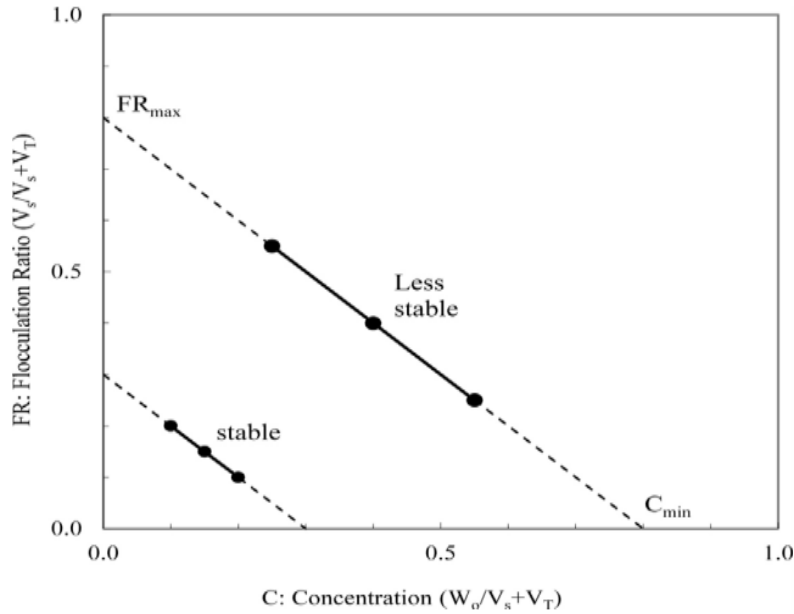


Figure 31. AFT analysis (Chandio et al. 2015)

ADDITIVE TYPES

Recycling Agents

Recycling agents are a class of materials used to improve the cracking resistance and, in some cases, workability of RAP and RAS mixtures without adversely affecting rutting resistance (Epps Martin et al. 2015). Recycling agents are often separated into two classes of materials: softening agents and rejuvenators. Softening agents are soft asphalt binders or other additives that simply lower the viscosity of the blended binder. Rejuvenators are additives that are intended to restore physical and chemical properties of the unaged binder (Daly 2017). Many types of recycling agents are used in practice, as outlined in Table 23 (NCAT 2014). The composition of rejuvenators is typically proprietary (Daly 2017).

Table 23. Types of Rejuvenators (NCAT 2014)

Category	Description
Paraffinic Oils	Refined used lubricating oils
Aromatic Extracts	Refined crude oil products with polar aromatic components
Naphthenic Oils	Engineered hydrocarbons
Vegetable Oils	Triglycerides and fatty acids
Tall Oils	Paper industry by-products, same chemical family as liquid antistripping agents and emulsifiers

Kaseer et al. (2019) conducted an extensive review of the effect of recycling agents on the performance of recycled binder blends and asphalt mixtures and found significant variation among different products, potentially due to differences in rejuvenation mechanisms. The mechanisms driving the “rejuvenation” caused by recycling agents are generally poorly quantified. Previous researchers have suggested the ideal methods for rejuvenation, such as Nahar et al. (2013), who suggested addition of volatile and light constituents lost during aging, and Roberts et al. (2009), who preferred oils comprised of aromatics and resins to restore the I_c . It has also been suggested that rejuvenators containing waxes should be avoided due to their tendency to crystallize and lead to cracking at low temperatures (Roberts et al. 2009). Epps Martin et al. (2019) postulated that some recycling agents may work by reducing the size of asphaltene agglomerations, possibly by breaking apart strong polar bonds or aromatic interactions. Other products may simply work by improving the dispersive power of the maltene phase to lower the viscosity and minimize additional asphaltene agglomeration. To assess compatibility, Epps-Martin et al. (2019) tested mixtures rejuvenated with tall oil using a modified SARA fractionation technique with additional separation of the asphaltenes, and found that while rheological tests showed improvement, the SARA fractionation and additional asphaltene information did not show clear benefits of the rejuvenator. It was determined that the SARA analysis could neither prove nor disprove whether the asphaltene agglomerates were reduced in size (Epps-Martin et al. 2019).

Currently, specifications pertaining to recycling agents are sparse and variable (Daly 2017). Epps-Martin et al. (2019) distributed a survey to state highway agencies to identify the laboratory tests used in practice to characterize asphalt binders modified by recycling agents. The results of their survey are presented in Figure 32, which demonstrates a wide variation in practices, with 40 percent of agencies that use recycling agents performing no characterization of the recycling agent itself or of the recycling agent blended with asphalt. As of 2015, 83 percent of state highway

agencies did not allow the use of recycling agents in surface mixtures (Epps Martin et al. 2019). It is inferred that the limited use of recycling agents is largely a result the lack of robust specifications.

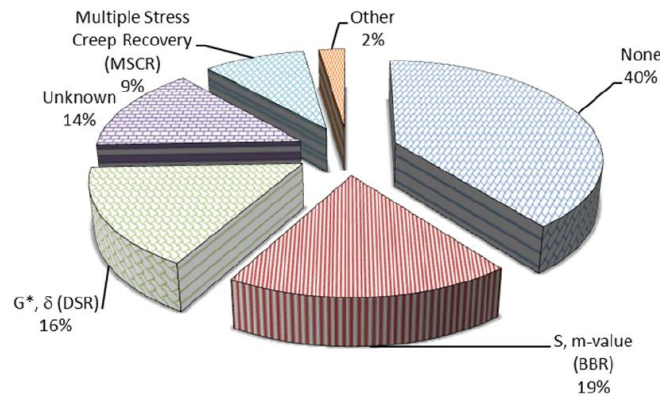


Figure 32. National survey results of laboratory tests used in practice to characterize the properties of asphalt binders modified by recycling agents (Epps Martin et al. 2019).

Extenders

Extenders are often needed to meet asphalt binder grade requirements due to recent changes in petroleum refining and the need for softer virgin binder grades to meet pay grade requirements. While additional extenders are available, this review focuses on two major classes of extenders that have been gaining interest in recent years: bio-based materials and REOB.

Bio-based Materials

The uncertainty of liquid asphalt supply and spike in price that occurred in 2008 prompted increased interest in non-petroleum based extenders. Bio-based materials constitute the majority of non-petroleum based extenders (Daly 2017). Efforts have been made to directly use biological materials and waste as asphalt modifiers, including waste cooking vegetable oil (Wen et al. 2013), lignin (McCready and Williams 2007), and soy fatty acids (Seidel and Haddock 2012). Additionally, efforts have been made to use bio-oil produced from thermo-chemical conversion of biomass as “bio-binders” using a variety of feedstocks, including agricultural byproducts (Ratouf and Williams 2010) and animal manure (Fini et al. 2011). While bio-based materials have been primarily proposed for use as extenders, it should be noted that bio-binder have also been proposed for use as recycling agents (Oldham et al. 2015). The literature on the characterization of asphalt modified by bio-based materials has primarily focused on rheological characterization with little relatively little attention given to long-term oxidative aging and performance within asphalt mixtures (Daly 2017). Su et al. (2018) conducted an extensive review of bio-binders, including soybean oil, palm oil, vegetable oil, engine oil residue combined with an unmodified binder and subjected to short-term aging and found effective softening from all products. It was also found that the bio-binder can potentially lead to a reduction of compaction temperature (Sun et al. 2016). This could be caused by the increase of maltenes; saturates, resins, and aromatics which would dilute the hardening effect of asphaltenes (Sun et al. 2016). While the literature suggests promising performance benefits from the use of bio-based extenders, their composition can differ significantly from asphalt, which suggests that the metrics used within the current PG system may be insufficient to adequately capture performance concerns. For example, Fini et al. (2011) found that bio-binders derived from swine manure have very low molecular weight and relatively high

oxygen content compared to asphalt binder. Williams and Ratouf (2010) found that the bio-binders produced from pyrolysis of agricultural products exhibit significant volatilization and oxidation compared to asphalt. Yang et al. (2016) also noted concerning levels of age-induced hardening in bio-oil modified binders.

Re-refined Engine Oil Bottoms (REOB)

REOB, also known as Vacuum Tower Asphalt Extender (VTAE), is defined as “the non-distillable residuum from a vacuum tower in a used oil re-refinery” (Asphalt Institute 2016). REOB has been used as an extender to soften asphalt since the 1980s, with typical dosage rates falling between 4 and 8 percent (Asphalt Institute 2016). The increasing use of softer virgin asphalt binders to meet grade requirements in RAP and RAS mixtures has prompted increased use of REOB in recent years (Asphalt Institute 2016). Research has demonstrated that REOB can exacerbate oxidation induced embrittlement, which led 10 states to ban its use as of 2016 (Asphalt Institute 2016). In response to the heightened use and concern regarding REOB, the Asphalt Institute prepared a state of the knowledge report on the use of REOB/VTAE in 2016 (Asphalt Institute 2016). Their review highlights that the oxidation induced embrittlement caused by REOB may not be adequately captured using conventional Rolling Thin Film Oven (RTFO) plus 20-hour PAV aging coupled with standard Dynamic Shear Rheometer (DSR) and Bending Beam Rheometer (BBR) test parameters. Rather, it was found that the detrimental effects of REOB were only captured after prolonged PAV aging coupled with the characterization of properties that more directly relate to ductility. Also, Fatigue tests conducted on numerous comparative asphalt mixtures without and with VTAE demonstrated an overall reduction in fatigue life of mixtures with VTAE compared to those without. No significant change in rutting performance with VTAE modification was noted (Wielinski et al. 2015).

The presence of REOB can be inferred within asphalt binder by the detection of metals. X-ray fluorescence (XRF) can be used to determine the REOB content of an asphalt binder (ASTM D6481-14). XRF examines the average intensities of elements and can compare the results to what should be expected, significant differences point to a sample having REOB (Karki and Zhou 2017). The XRF functions by exciting electrons with x-rays. When the x-ray is sent through a sample an electron moves from the outer layer of an atom and moves to the inner layer. This sends out a certain wavelength that can be perceived by the test as a specific atom ranging from fluorine to uranium (Karki and Zhou 2017). XRFs have two detectors, one is filled with P10 gas and can identify longer wavelengths, while another is a scintillation detector and identifies shorter wavelengths. The machine calculates the number of times each wavelength is counted, and this gives a chemical breakdown of the sample.

The simultaneous detection of calcium, zinc, copper, and molybdenum are used to detect REOB and infer its concentration (Asphalt Institute 2016). Alternatively, ash testing is used in Canada to detect the presence of REOB; binders with greater than 0.8 percent ash contain significant REOB and are prohibited in Ontario (Marks 2015). Detecting REOB using XRF was also part of a study by the Texas Department of Transportation (Barborak 2016). Texas DOT focused on matching sulfur versus vanadium of known intensities from samples without REOB and compared those values to binders that may or may not have contained REOB. For identifying REOB the XRF was looking for the atoms of Ca, Cu, MO, ZN, K, P, S, V, Fe, Ni, and Si. These atoms were identified by a study done for Texas DOT.

BINDER PERFORMANCE CHARACTERIZATION CONCERNS

Bahia et al. (2001) found that modified and unmodified binders often demonstrate similar properties according to AASHTO M 320 Superpave PG but drastically different cracking performance. The need for an improved procedure to mimic field aging coupled with a test method to capture binder cracking resistance are also highlighted by the recent solicitation and funding of three NCHRP projects; NCHRP 9-60: *Addressing Impacts of Changes in Asphalt Binder Formulation and Manufacture on Pavement Performance through Changes in Asphalt Binder Specifications*, NCHRP 9-59: *Relating Asphalt Binder Fatigue Properties to Asphalt Mixture Fatigue Performance*, and NCHRP 9-61: *Short- and Long-Term Binder Aging Methods to Accurately Reflect Aging in Asphalt Mixtures*.

Cracking Susceptibility

Recent efforts that have investigated recycling agents and extenders have largely focused on non-load related cracking (i.e., thermal and block cracking). Findings suggest that current Bending Beam Rheometer (BBR) stiffness (i.e., $S(60)$) and relaxation rate (i.e., $m(60)$) parameters are insufficient to capture the potential negative effects of recycling agents and extenders on cracking susceptibility (Anderson et al. 2011). There has been growing interest in the identification of an easy-to-measure rheological parameter that captures the ductility of the binder to adequately capture non-load related cracking performance (Asphalt Institute 2016).

In addition, fatigue resistance is a primary concern when using high recycled content mixtures. Thus, the characterization of the fatigue resistance of binders is a necessary first step to designing appropriate asphalt binder blends. However, it has been demonstrated that the current Superpave binder PG intermediate temperature parameter to address fatigue resistance (i.e., $|G^*| \cdot \sin \delta$) lacks relationship to asphalt mixture and pavement performance when modified binders are used (Bahia et al. 2001). The current Superpave intermediate temperature DSR test consists of sinusoidal loading at a small strain amplitude over very few loading cycles. Therefore, it lacks the ability to evaluate actual cracking resistance and has been deemed insufficient to preclude fatigue resistant binders from use in practice.

Long-term Aging

Recent research suggests that binder test results from 40-hours of PAV conditioning is a better means of gauging field performance after five or more years in service than standard 20-hour PAV aging (Asphalt Institute 2016). Research has demonstrated that embrittlement in modified binders can be captured by binder conditioning in the PAV for 40 hours but not with the standard 20 hours (Bennert 2015, Reinke et al. 2015). Concerns have been raised regarding the additional time burden of the extended PAV aging procedure. However, a reduction in the binder film thickness within the PAV and/or increasing the aging temperature can be used to alleviate this concern, which is the focus of NCHRP 09-61. The NCHRP 09-61 project is refining short- and long-term laboratory aging procedures for asphalt binders. The authors are proposing no changes to the RTFO but is proposing several changes to the PAV (Bonaquist 2017, Bonaquist 2020). The refined long-term aging procedure will consist of a PAV procedure, retaining the standard air pressure of 2.1 MPa and 20 hour duration but decreasing the binder film thickness by using 12.5 g per pan rather than 50 g per pan and using elevated temperature compared to the current procedure. The aging temperatures are currently being calibrated as a function of climatic conditions to reflect 12 years of field aging using 26 binders; this level of field aging was selected based on the analysis

of LTPP SPS 8 projects which showed an average time to sustained transverse cracking of 12 years. The revised procedure is anticipated to induce a greater extent of aging compared to the current PAV procedure, which was developed to reflect five to seven years of in-service aging.

Aging

Current Superpave PG specifications (AASHTO M 320 and AASHTO M 332) simulate short- and long-term aging of asphalt binder using the RTFO and PAV, respectively. Recent studies show that the current 20-hour PAV procedure provides insufficient oxidation to mimic the effects of prolonged field aging (Glover et al. 2005, Wright et al. 2011). Standard PAV aging has also been found to be insufficient to capture the negative effects of additives. Significant attention has been given to binders that contain re-refined engine oil bottoms (REOB) because they contribute to the premature cracking of pavements as a result of embrittlement (Asphalt Institute 2016). Furthermore, it has been cautioned that the aging susceptibility of bio-materials has not been well-studied (Daly 2017) and preliminary evaluation indicates potential concerns. Kaseer et al. (2019) reported that numerous studies have reported a loss of recycling agent effectiveness with long-term aging, the extent of which depends upon the type and dose of the recycling agent.

POTENTIAL METHODS FOR IMPROVED BINDER CHARACTERIZATION

Cracking Resistance

The *delta T critical* (ΔT_c), which is equal to the difference between the low-temperature critical PG specification temperatures for $S(60)$ and $m(60)$, has been given considerable attention in recent years for capturing the effects of embrittlement on pavement cracking potential. The parameter was first introduced by Anderson et al. (2011) who observed a strong correlation between ΔT_c and pavement block cracking; correspondingly, the authors postulated that ΔT_c is a good indicator of asphalt binder ductility at low temperature. They found that the value of ΔT_c decreases with oxidative aging and thus, trends with aging level may be helpful to identifying binders susceptible to oxidative embrittlement. Subsequently, researchers have found that the parameter can be used to identify problems associated with REOB, with values falling below -5°C indicating concern (Asphalt Institute 2016). The parameter could be implemented into practice relatively easily because it can be calculated using the results of standard BBR testing used for PG determination.

A survey distributed to a task force of 14 members from different state agencies was used to gain perspective on agencies' opinions and use of (ΔT_c). The majority agreed it is an indicator of age related cracking. However, the task force was more split on its use as an effective specification parameter. Two of the 14 respondents did not find enough data to support using ΔT_c as a binder parameter while the majority conditionally supported it due to the fact that it is needed to evaluate the quality of asphalt binders (Asphalt Institute 2019). Of the 12 members that support using ΔT_c , seven members have a current specification, indicated in Table 24 (Asphalt Institute 2019).

Table 24. Agencies and their Selected Parameter

Agency	ΔT_c Requirement	PAV Aging Duration, hrs	Status
Florida DOT	≥ -5.0	20	Current
Utah DOT	≥ -2.0	20	Current
PANYNJ	≥ -5.0	40	Current
Vermont DOT	≥ -5.0	40	Current
Maryland DOT	≥ -5.0	40	Current
Kansas DOT	≥ -5.0	40	Current
Ontario MTO	≥ -5.0	20	Current
Texas DOT	≥ -6.0	20	Current
Oklahoma DOT	≥ -6.0	20	2020
Delaware DOT	≥ -5.0	40	2020

The base value of ΔT_c can be either positive or negative depending on the binder used. If a binder is positive then the low-temperature grade it is governed by its creep stiffness whereas if it is negative it is governed by the m-value. There are many properties that can affect ΔT_c . Aging causes the ΔT_c value to decrease and typically become negative. Therefore, reclaimed binders tend to have a more negative ΔT_c than that of virgin binder. There is a linear relationship between the amount of binder being replaced with RAP and RAS and the decrease in ΔT_c which can be seen below in Figure 33 (Asphalt Institute 2019).

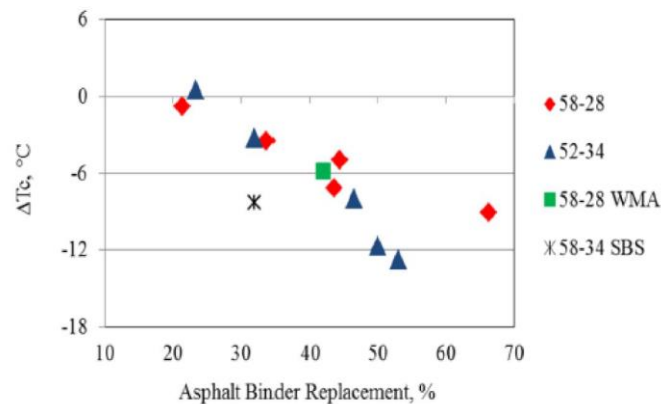


Figure 33. Relationship between RAP/RAS replacement and ΔT_c (Asphalt Institute 2019)

Researchers have demonstrated that several alternative rheological parameters related to brittleness can be derived from the DSR (Glover 2005, Rowe 2011, Rowe et al. 2016, Christensen and Tran 2019). These parameters have been primarily proposed for capturing resistance to non-load associated cracking but also have promise for identifying asphalt binders susceptible to fatigue cracking. Glover (2005) first proposed a rheological parameter as an indicator of ductility that could be determined using DSR testing rather than cumbersome force-ductility testing. Rowe (2011) simplified the Glover parameter as $|G^*| \cdot (\cos\delta)^2 / \sin\delta$; this parameter is called the Glover-Rowe (G-R) parameter. Anderson et al. (2011) demonstrated that the G-R parameter correlates with pavement durability (block cracking) when evaluated at 15°C and 0.0008 Hz (0.005 rad/s), with a higher G-R value indicative of lower ductility. Based on the correlations observed between the G-R parameter and pavement block cracking, Anderson et al. (2011) proposed that a value of 180 kPa corresponds to damage onset whereas a value exceeding 450 kPa corresponds to

significant cracking. Rowe et al. (2013) proposed measuring the G-R parameter based on construction of a master curve from frequency sweep testing at 5°C, 15°C, and 25°C in the DSR using the standard 8-mm parallel-plate geometry and interpolating to find the value of G-R at 15°C and 0.005 rad/sec.

The NCHRP 09-59 project proposed the replacement of the current intermediate temperature specification with the G-R parameter (i.e., $|G^*/\cos^2\delta/\sin\delta|$) and the addition of the R-value (determined using standard Bending Beam Rheometer (BBR) testing) to address fatigue cracking (Christensen and Tran 2019). The R-value is the logarithmic difference between the glassy modulus and dynamic share modulus at the reduced frequency where the phase angle equals 45°.

The NCHRP 09-60 project has evaluated the ability of rheological properties to reflect block cracking potential (Planche et al. 2018, Elwardany et al. 2020). Properties considered include those proposed by the NCHRP 09-59 project as well as ΔT_c (i.e., the difference between the *S*- and *m*-based low-temperature critical PG specification temperatures). In addition, the NCHRP 09-60 project has established a DSR-based parameter to use as a surrogate for ΔT_c , called T_{ve} and defined as the difference between the glass transition temperature and crossover temperature. In addition, the Asphalt Binder Cracking Device (ABCD) was employed. The ABCD involves casting a sample of asphalt inside an instrumented ring before cooling the sample to induce thermal contraction until the sample fractures; the critical fracture temperature is reported. It was found that consideration of failure properties, achieved by means of the ABCD was necessary to discriminate between the performance of modified binders. Linear viscoelastic properties, including ΔT_c and those proposed by the NCHRP 09-59 project failed to discriminate between the performance of modified binders.

Other studies have also suggested that asphalt binder failure properties are necessary to capture mixture cracking resistance. Consequently, a several fracture mechanics-based and continuum damage-based test methods have been proposed to quantify binder failure properties, as summarized in Table 25 under the categories of fracture mechanics-based and continuum damage-based tests. The Double Edge Notch Tension (DENT) and Single Edge Notch Bending (SENB) tests use notched direct tension and BBR geometries, respectively, and revised loading schemes to capture fracture mechanics-based properties. The LAS and time sweep tests consist of subjecting asphalt binder samples to repeated loading in the DSR using the standard 8-mm parallel plate geometry. Changes in loading resistance with respect to number of loading cycles are used to evaluate damage resistance and determine fatigue failure. The time sweep consists of loading whereas the LAS includes systematically increasing amplitudes to accelerate damage. The glass bead composite test also includes repeated loading in the DSR but uses a standard composite torsion bar of glass beads mixed with binder to recreates a state of stress as closely as possible to a real asphalt mixture. Similarly, the poker chip test attempts to reflect the state of a binder film in an asphalt mixture. In the poker chip test, a confined film to monotonic tension to measure tensile strength.

Table 25. Summary of Binder Cracking Indicators

Property/Test	Fatigue Cracking	Thermal Cracking	Block Cracking	References
<i>Linear Viscoelastic Parameters</i>				
G-R	X		X	Rowe 2011, Christensen and Tran (2019)
R-Value	X		X	Christensen and Tran (2019)
ΔT_c		X	X	Anderson et al. (2011)
T_{ve}			X	Planche et al. (2018)
<i>Fracture Mechanics-Based Tests</i>				
DENT	X	X		AASHTO TP 113
ABCD		X		AASHTO TP 92
SENB		X		Velasquez et al. (2011)
<i>Continuum Damage-Based Tests</i>				
LAS	X			AASHTO TP 101
Time Sweep	X			Bahia et al. (2001)
Glass Bead Composite	X			Motamed et al. (2013)
Poker Chip	X			Sultana et al. (2014)

DOSAGE SELECTION

In addition to having adequate metrics to evaluate the performance of binders, a corresponding dosage selection procedure for recycling agents and extenders would be beneficial. Currently, the typical practice for dosage selection is to use the manufacturer’s recommendations (Kaseer et al. 2019). This approach is questionable in cases where a single product is combined with different materials (e.g., virgin binder, RAP, RAS) of drastically different properties and concentrations. Therefore, there is a need for a method to select and/or verify additive dosages that can be used by agencies and contractors based upon the target virgin binder properties, which will vary as a function of the type of recycled material included within the mixture (i.e., RAP and/or RAS) and their proportion within the asphalt mixture (i.e., RBR%).

Significant effort has been dedicated to the development of a robust procedure for recycling agent dosage selection in NCHRP 09-58 (Epps-Martin et al. 2019). They have considered three means of dosage selection: (1) restore low-temperature PG, verify high-temperature PG, (2) achieve $\Delta T_c = -5.0$ after 20 hours of PAV aging, and (3) restore high-temperature grade. Method 1 was found to yield the lowest recycling agent dosages. Method 2 resulted in the highest recycling agent dosages and corresponding high-temperature grades that could indicate rutting issues. In contrast, Method 3 allows as much recycling agent as possible without compromising rutting resistance below a certain threshold. Method 3 was found to restore the low-temperature PG at least to that of the target binder. Therefore, the NCHRP 09-58 research team is proposed the use of Method 3 in practice.

To implement Method 3 in practice, the NCHRP 09-58 project proposed a two step approach. First, the high-temperature performance grade of the virgin binder and reclaimed binder blend is calculated using Equation (17) based on the high temperature grades of the constituent binders and the blend ratios used. Then, the recycling agent dosage is calculated using Equation (18).

$$PGH_{Blend} = (RAP_{BR} \times PGH_{RAP}) + (RAS_{BR} \times PGH_{RAS}) + (B_{BR} \times PGH_{Base})$$

(17)

where: PGH_{Blend} : Pavement Grade Blend, RAP_{RBR} : Binder Ratio of RAP, PGH_{RAP} : Pavement Grade of RAP, RAS_{RBR} : Binder Ratio of RAS, PGH_{RAS} : Pavement Grade of RAS, B_{RBR} : Binder Ratio of Virgin Binder, and PGH_{Base} : Pavement Grade of Virgin Binder.

$$RecyclingAgent(\%) = \frac{(PGH_{Blend} - PGH_{Target})}{SlopeRate}$$

(18)

where: PGH_{Blend} : Pavement Grade of Virgin Binder Blend with RAP/RAS, PGH_{Target} : Pavement Grade Target of binder blend, $SlopeRate$: Reduction Rate of PG based on type of rejuvenator used, which was found to be equal to 1.38 for aromatic extracts and 1.82 for tall oils, vegetable oils, reacted bio-based oils; however, material specific values can be derived.

The suggested $SlopeRate$ values were derived from the linear relationship between recycling agent does and PGH when using virgin binders with grades between 64°C and 70°C and various reclaimed materials; the results used to obtain the $SlopeRate$ values are shown in Figure 34 and Figure 35 for aromatic extracts and other recycling agent types, respectively.

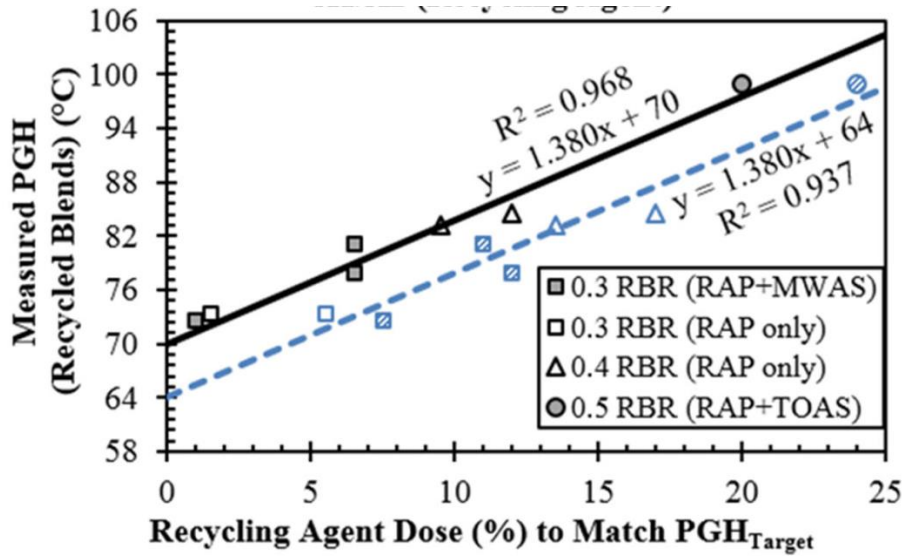


Figure 34. Rejuvenator dosage for aromatic extract (Epps-Martin et al. 2019)

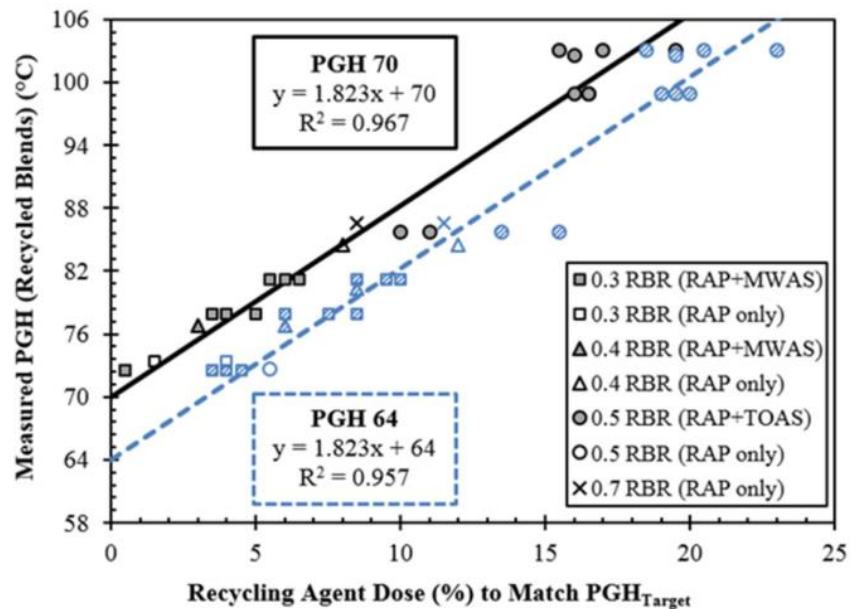


Figure 35. Recycling agent dosages combined for tail oils, vegetable oils, and reacted bio-based oils (Epps-Martin et al. 2019)

A critical component of a dosage selection procedure that NCHRP 9-58 does not consider is the appropriate assumption of the recycled binder contribution, which defines the target virgin binder properties. The results of the NCHRP Project 09-12 (McDaniel and Anderson 2001) indicate that the assumption of complete activation of recycled binder becomes invalid when the asphalt binder replacement ratio exceeds 40 percent. It was demonstrated that following the assumption of complete blending led to select virgin binders for very high recycled binder contents yielded mixtures that were prone to rutting, which is consistent with expectations if the virgin and recycled binders do not fully blend. Thus, the target virgin binder properties used in a dosage selection procedure should be established based on the *activated* binder replacement ratio (i.e., the recycled binder that mobilizes and blends with the virgin binder).

References

1. Anderson, R. M., G. N. King, D. I. Hanson, and P. B. Blankenship. Evaluation of the Relationship between Asphalt Binder Properties and Non-load Related Cracking. *Journal of the Association of Asphalt Paving Technologists*, Vol. 80, 2011, pp. 615-663.
2. Asphalt Institute, State of the Knowledge: The Use of REOB/VTAE in Asphalt, *Asphalt Institute Information Series No. 240 (IS-240)*, 2019.
3. Asphalt Institute, State-of-the-Knowledge: Use the Delta Tc Parameter to Characterize Asphalt Binder Behavior, *Asphalt Institute Information Series* 2019.
4. Bahia, H. U., D. I. Zeng, H. Kharti, M. A. Zhai, & M. Anderson. Characterization of Modified Asphalt Binders in Superpave Mix Design, *NCHRP Report 459*, National Academies, Washington, D.C., 2001.
5. Barborak, R., C. Coward, and R. Lee. Detection and Estimation of Re-Refined Engine Oil Bottoms in Asphalt Binders: Texas Department of Transportation's Approach with Wavelength Dispersive X-Ray Fluorescence Spectroscopy, *Transportation Research Record*, No. 2574, 2016, pp. 48-56.

6. Bennert, T. Asphalt Binder and Mixture Properties Produced with REOB Modified Asphalt Binders, Presentation at the Asphalt Binder Expert Task Group Meeting, Fall River, MA, 2015.
7. Bonaquist, R. Short- and Long-Term Binder Aging Methods to Accurately Reflect Aging in Asphalt Mixtures, *NCHRP 09-61 Interim Report*, National Academies, Washington, D.C., 2017.
8. Bonaquist, R. NCHRP 9-61 Update: Short- and Long-Term Binder Aging Methods to Accurately Reflect Aging in Asphalt Mixtures, Presented at the 99th Annual Meeting of the Transportation Research Board, Washington, D.C., 2020.
9. Christensen, D. & N. Tran. Relating Asphalt Binder Fatigue Properties to Asphalt Mixture Fatigue Performance, *NCHRP 09-59 Draft Final Report*, National Academies, Washington, D.C., 2019.
10. Chandio, Z., M. Ramasamy, and H.B. Mukhtar. Temperature effects on solubility of asphaltenes in crude oils. *Chemical Engineering Research and Design*, Vol. 94, 2015, pp. 573-583
11. Daly, W.H. Relationship Between Chemical Makeup of Binders and Engineering Performance, *NCHRP Synthesis 511*, National Academies, Washington, D.C., 2017.
12. Elwardany, M., J.P. Planche, and G. King. A Tale of Two Deltas: Towards a Universal Blind Framework for Asphalt Durability, Presented at the 99th Annual Meeting of the Transportation Research Board, Washington, D.C., 2020.
13. Epps Martin, A., et al. The Effects of Recycling Agents on Asphalt Mixtures with High RAS and RAP Binder Ratios, *NCHRP Report 927*, National Academies, Washington, D.C., 2019.
14. Fini, E. H., E. W. Kalberer, A. Shahbazi, M. Basti, Z. You, H. Ozer, and Q. Aurangzeb. Chemical Characterization of Biobinder from Swine Manure: Sustainable Modifier for Asphalt Binder, *Journal of Materials in Civil Engineering*, Vol. 23, 2011, pp. 1506 -1513.
15. Glover, C. Development of a New Method for Assessing Asphalt Binder Durability with Field Validation, *Report FHWA/TX-05/1872-2*, Texas Transportation Institute, College Station, TX, 2005.
16. Karki, P., and F. Zhou, Systematic Method for Quantifying Re-Refined Engine Oil Bottom Content in Binders: Using X-Ray Fluorescence Spectroscopy, *Transportation Research Record*, No. 2632, 2017, pp. 52-59.
17. Kaseer, F., A. Epps Martin, and E. Arambula-Mercado. Use of recycling agents in asphalt mixtures with high recycled materials contents in the United States: A literature review, *Construction and Building Materials*, Vol. 211, 2019, pp. 974-987.
18. Kleizine, R., M. Panasenkiene, and A. Vaitukus. Effect of Aging on Chemical Composition and Rheological Properties of Neat and Modified Bitumen, *Materials*, Vol. 12, 2019.
19. Li, J., Feipeng, X., Amir Khanina, Serji, N. High temperature rheological characteristics of plasma-treated crumb rubber modified binders, *Construction and Building Materials*, Vol. 236, 2020.
20. McDaniel, R. and R.M. Anderson. Recommended Use of Reclaimed Asphalt Pavement in The Superpave Mix Design Method: Technician's Manual, *NCHRP Report 452*, National Academies, Washington, DC, 2001.
21. Motamed, A., A. Bhasin, and A. Izadi. Evaluating Fatigue-Cracking Resistance of Asphalt Binders in a Standardized Composite Using Continuum Damage Theory, Vol. 25, No. 9, 2013, pp. 1209-1219.

22. Nahar, S.N., M. Mohajeri, A. Schmets, T. Scarpas, M.F. van de Ven, and G. Schitter. First Observation of Blending Zone Morphology at Interface of Reclaimed Asphalt Binder and Virgin Binder, *Transportation Research Record, Transportation Research Board*, No. 2370, 2013, pp. 1-7.
23. NCAT. NCAT Researchers Explore Multiple Uses of Rejuvenators, *Asphalt Technology News*, Vol. 26, No. 1 (Spring), 2014, <http://www.ncat.us/info-pubs/newsletters/spring-2014/rejuvenators.html>.
24. Oldham, D., E. Fini, and E. Chailleux. Application of a bio-binder as a rejuvenator for wet processed asphalt shingles in pavement construction, *Construction and Building Materials*, Vol. 86, 2015, pp. 75-84.
25. Peterson, J.C. A Review of the Fundamentals of Asphalt Oxidation, *TRB Circular E-C140*, Transportation Research Board, Washington, D.C., 2009.
26. Planche, J. P., M. E. Elwardany, C. Rodezno, and D. Christensen. *NCHRP 09-60 Interim Report*, National Academies, Washington, D.C., 2018.
27. Ratouf, M. and R.C. Williams. Temperature Susceptibility of a Non Petroleum Binder as a Paving Material, *Transportation Research Record*, No. 2180, 2010, pp. 9-18.
28. Reinke, G., A. Hanz, D. Herlitzka, S. Engber, and M. Ryan. Further Investigations into the Impact of REOB and Parrafinic Oils on the Performance of Bituminous Mixtures, Presentation at the Asphalt Binder Expert Task Group Meeting, Fall River, MA, 2015
29. Roberts, F. Hot mix asphalt materials, mixture design and construction (3rd Ed.). *National Asphalt Pavement Association Research and Education Foundation*, Lanham, MD, 2009.
30. Rowe, G. M., M. J. Sharrock, and S. Raposo. Cracking and Linear Viscoelastic Binder Properties. 8th *RILEM International Conference on Mechanisms of Cracking and Debonding in Pavements*, Vol. 13, 2016, pp. 3-8.
31. Rowe, G. Prepared Discussion for Evaluation of the Relationship between Asphalt Binder Properties and Non-load Related Cracking. *Journal of the Association of Asphalt Paving Technologists*, Vol. 80, 2011, pp. 615-663.
32. Su, N. F. Xiao, J. Wang, L. Cong, and S. Amirkhani. Production and applications of bio-asphalts – A Review. *Construction and Building Materials*, Vol. 183, 2018, pp. 578-591.
33. Sultana, S., and A. Bhasin. Effect of chemical composition on rheology and mechanical properties of asphalt binder, *Construction and Building Materials*, Vol. 72, 2014, pp. 293-300.
34. Sun, Z., J. Yi, Y. Huang, D. Feng, D., and C. Guo. Properties of asphalt binder modified by bio-oil derived from waste cooking oil, *Construction and Building Materials*, Vol. 102, 2016, pp. 496-504
35. Velasquez, R., H. Tabatabaee, and H. U. Bahia. Low Temperature Cracking Characterization of Asphalt Binders by Means of the Single-Edge Notch Bending (SENB) Test, *Journal of the Association of Asphalt Paving Technologists*, Vol. 80, 2011, pp. 583-613.
36. Wen, H., S. Bhusal, and B. Wen. Laboratory Evaluation of Waste Cooking Oil-Based Bioasphalt as Sustainable Binder for Hot-Mix Asphalt, *Transportation Research Board E-Circular E-165*, August, 2012, pp. 49-60.
37. Wielinski, J., A. Kriech, A. Horton, T. Reece, and G. Huber. Laboratory Evaluation of Vacuum Tower Asphalt Extenders Impact on HMA Fatigue Resistance and Asphalt Binder Aging, Proceedings of the 94th Annual Meeting of the Transportation Research Board, Washington, D.C., 2015.

38. Wright, L., A. Kanabar, E. Moul, S. Rubab, and S. Hesp. Oxidative Aging of Asphalt Cements from and Ontario Pavement Trial, *International Journal of Pavement Engineering*, Vol. 4, No. 5, 2011, pp. 259-267.
39. Yang, X., J. J. Mills-Beale, and Z. You. Chemical characterization and oxidative aging of bio-asphalt and its compatibility with petroleum asphalt, *Journal of Cleaner Production*, Vol. 142, 2016, pp. 1837-1847.

APPENDIX B: DEVELOPMENT OF PRACTICAL ALGORITHMS TO CONSTRUCT ASPHALT BINDER MASTER CURVES AND CALCULATE CHRISTENSEN ANDERSON (CA) MODEL PARAMETERS

INTRODUCTION

Master curves are used to describe the time and temperature dependence of the rheological behavior of asphalt binders. Master curves are constructed by conducting rheological measurements over a range of frequencies (or times) and temperatures. The set of measurements (e.g., modulus, phase angle) at a given temperature is called an isotherm. For thermorheologically simple materials, such as asphalt binder, isotherms can be shifted along the log frequency (or log time) axis by temperature-dependent shift factors to form a smooth and continuous ‘master curve’. Models are fit to represent the master curve and shift factors to understand the overall rheological behavior of asphalt binders and readily obtain properties at any desired temperature and frequency (or time) combination.

The Strategic Highway Research Program (SHRP) considered the use of master curves as the basis for providing rational specification parameters (Anderson et al. 1994). The effort yielded the Christensen-Anderson (CA) model (Christensen 1992), which persists as the most widely applied asphalt binder master curve model today. The CA model is a phenomenological model applied to describe the reduced frequency (ω_R) dependence of asphalt binder dynamic shear modulus ($|G^*$) and phase angle (δ) and is given in Equations (19) and (20).

$$|G^*|(\omega) = G_g \left[1 + \left(\frac{\omega_c}{\omega_R} \right)^{(\log 2/R)} \right]^{-R/\log 2} \quad (19)$$

$$\delta(\omega) = \frac{90}{\left[1 + \left(\frac{\omega_R}{\omega_c} \right)^{\log 2/R} \right]} \quad (20)$$

where G_g = glassy modulus, often assumed to equal 1 GPa, which is supported by experimental evidence from asphalt binders (Christensen 1992) and is also commonly accepted for other organic materials (Ferry 1980); ω_c = crossover frequency, equal to the reduced frequency where the phase angle equals 45°; and R = rheological index, equal to the logarithmic distance between G_g and $|G^*|$ at ω_c .

The $|G^*|$ model was derived from the cumulative form of a skewed logistic function (Christensen 1992). The δ was derived from earlier work by Dickinson and Witt (1974) that indicates δ is directly proportional to the first derivative of $\log |G^*|$ with respect to $\log \omega_R$ (Christensen 1992).

The CA model parameters themselves have been proposed as potential measures to evaluate asphalt binders (Christensen 1992). The ω_c defines the point where the storage and loss moduli are equal and thus, constitutes a transition point from elastic- to viscous-dominated behavior. As asphalt binders undergo oxidative aging, the ω_c decreases and the R value increases. While single-point measurements were ultimately adopted for asphalt binder specification during SHRP, recent studies suggest master curve-based parameters may better capture the cracking resistance of asphalt binders than the current specification parameters. Studies suggest that the R value in the

CA model is an indicator of asphalt binder cracking potential. Rowe and Sharrock (2016) demonstrated a positive correlation between asphalt binder R values and bending beam fatigue life results of asphalt mixtures. Furthermore, Christensen and Tran (2022) recently proposed that the R value of an asphalt binder is an indicator of its fatigue strain capacity. Cucionalon et al. (2019) introduced another master curve-based parameter closely related to ω_c , termed the cross over temperature, equal to the temperature where $\delta = 45^\circ$. The authors proposed the crossover temperature as both a parameter for tracking asphalt binder aging and a measure of rheological balance in terms of rutting and age-induced embrittlement when combined with a binder's high-temperature grade.

Master curves are also applied to calculate parameters indicative of asphalt binder ductility. Glover et al. (2005) first proposed a rheological parameter as an indicator of ductility that could be determined using DSR testing rather than the more cumbersome force-ductility testing. For unmodified asphalt binders, the Glover parameter is highly correlated with force-ductility tests conducted at 15°C and a loading rate of 1 cm/min when evaluated at 15°C and 0.005 rad/s, with a higher G-R value indicative of lower ductility. Rowe (2011) subsequently simplified the Glover parameter to yield the so-called Glover-Rowe (G-R) parameter, equal to $|G^*| \cdot (\cos \delta)^2 / \sin \delta$. Anderson et al. (2011) demonstrated that the G-R parameter correlates with pavement block cracking when evaluated at 15°C and 0.005 rad/s. Directly measuring the G-R parameter at 0.005 rad/s is not practical or feasible given the slow loading rate. Therefore, Glover et al. (2005) proposed evaluating the parameter at 44.7°C and 10 rad/s, which yielded approximately equivalent results as those based on 15°C and 0.005 rad/s based on time-temperature equivalencies. However, Anderson et al. (2011) demonstrated that a single time-temperature equivalency is not valid for all binders and therefore, that the G-R parameters obtained from a master curve are more highly correlated with force-ductility results. Therefore, the authors proposed the use of temperature-frequency sweep testing coupled with a master curve model to obtain the G-R parameter. Asphalt binder master curves also offer a potential basis for predicting asphalt mixture behavior on the basis of asphalt mixture constituents (Olard and Di Benedetto 2003, Zeng et al. 2001).

An impediment to the more widespread implementation of master curves and associated parameters is the lack of standardized procedures constructing and modeling asphalt binder master curves. Likewise, there are very limited accounts in the literature of the implications of the chosen method for constructing asphalt binder master curves and determining CA model parameter values on the resultant model accuracy and values of associated calculated parameters. Standardization is necessary to ensure the repeatability and reproducibility of master curve results if adopted in future specifications. Correspondingly, an effort was undertaken to establish robust algorithms for constructing multiple methods of modeling asphalt binder master curves, comparing the different methods directly, and fitting the CA model to oscillatory Dynamic Shear Rheometer (DSR) test data that are easily implementable in Microsoft Excel®. The resultant algorithms were used in latter tasks to interpret the acquired rheological data.

METHODOLOGY

Materials and Test Procedures

Table 26 summarizes the asphalt binders and temperature-frequency sweep test procedures used in this study. The test results used in this study includes two groups of binders, denoted A and B. The Group A binders coincide with those evaluated within this research project and encompass

two typical virgin binders as well as blends of virgin binder with recycled binder, and in some cases additives. The additives included in the Group A binders include both a recycling agent (RA) and extender (E). The recycled binder sources included reclaimed asphalt pavement (RAP) and recycled asphalt shingles (RAS) binders from North Carolina. The performance grades (PG) reported in Table 26 correspond to binder system tested. For example, binder 4 is a blend of virgin binder, RAP binder, and an RA and the PG of this blend is 64-28. Tests results of the Group A binders were acquired through this project. The Group B binders are all polymer-modified and the corresponding temperature-frequency sweep tests were acquired in a previous research effort (Gundla and Underwood 2020). Temperature-frequency sweep testing was conducted on each binder after undergoing Rolling Thin Film Oven (RTFO) and Pressure Aging Vessel (PAV) aging in accordance with AASHTO T 240 and R 28, respectively. This age level is denoted P20. Additional age levels were also used for select binders, encompassing original (O), RTFO (R), and RTFO plus 40 hours of aging in the PAV (P40) conditions. Collectively, the experimental plan yielded a broad range of asphalt binder types and characteristics. Test results are identified by the binder code followed by the age level. For example, 8|P20 results correspond to the PG 70V-16 binder from Group B tested at the standard RTFO + 20-hour PAV age level.

Temperature-frequency sweep testing was conducted using the 8-mm parallel plate geometry in a DSR. Testing adhered to AASHTO T 315. A minimum of two replicate tests were conducted for each binder and age level combination. Replicates were run until repeatability was evaluated and verified to meet AASHTO T 315 precision limits. The average test results for a given binder and age level combination were used to construct the master curves.

Table 26. Summary of the Asphalt Binders and Test Procedures

Group	Code	PG	Additive	Recycled Binder	Test Temp. (°C)	Frequency Range (Hz)	Strain Amplitude	Age Levels
A	1	58-28	--	--	5, 20, 35, 50	0.1 to 10	1.0% at 50 °C, 35 °C 0.1% at 20 °C, 5 °C	O, R, P20
	2	64-22	--	--				O, R, P20, P40
	3	70-22	--	RAP				P20, P40
	4	64-28	RA	RAP				O, R, P20, P40
	5	64-28	Extender	RAP				R, P20
	6	64-34	RA	RAS				P40
B	7	64V-22	Polymer	--	10, 20, 30, 40, 54	0.1 to 30	0.5%	P20
	8	70V-16	Polymer	--				P20
	9	76-22	Polymer	--				P20

-- Not included

Test Analysis

Data Screening

As the test frequency increases at a given test temperature, the $|G^*|$ is expected to increase and the δ is expected to decrease. However, it is common for δ data acquired at high frequencies to exhibit so-called ‘feathering’ that deviates from these trends. Feathering can be visually observed and used

to identify and remove spurious data when the relationship between $|G^*|$ and phase angle (so-called the ‘black space’ is examined) (Marasteanu and Anderson 2001). Herein, an initial filter was applied to identify and remove spurious data from the temperature-frequency sweep test results prior to constructing asphalt binder master curves. Data points at each isotherm are removed if the measurement exhibited a higher δ than the previous data point acquired at a lower frequency. Figure 36 shows a black space diagram where feathers are visually evident for 4|O (i.e., binder 4 at the original age level) before trimming that are trimmed by the filter to form a smoother black space curve. A second data filter following the recommendations of Marasteanu and Anderson (2001) was also tried after applying the initial filter. Marasteanu and Anderson (2001) proposed that measurements that deviate substantially from the expected proportionality of $|G^*|$ and δ constitute erroneous measurements. To apply the filter, the slope of $\log |G^*|$ with respect to \log of the frequency (ω) was calculated for each data point using the point of interest and the two nearest points. This slope was divided by the quantity of $\delta/90$. If the calculated value was less than 0.95 or greater than 1.05, it was removed. However, in all cases, all data passed the second filter criteria after removal of spurious data according to the first filter, making it an extraneous addition. Many of the temperature-frequency sweep tests did not contain spurious data. Spurious data was most common in the polymer-modified asphalt binders and the unmodified binders tested at the highest test temperature.

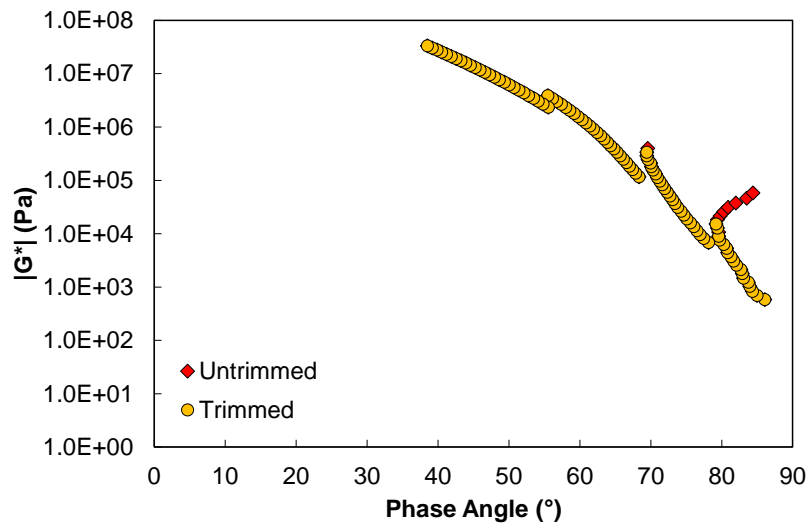


Figure 36. Example of the effects of data screening for binder 4|O

Master Curve Construction

There are two methods for constructing master curves, termed ‘free shifting’ and ‘constrained shifting’ (Rowe and Sharrock 2011). In the free shifting method, the isotherms are shifted horizontally along the log frequency or time axis to form a smooth, continuous master curve prior to and independent of determining the master curve model parameters. In the constrained shifting method, models are selected to describe both the master curve and time-temperature shift factors. The shift factor and master curve model parameters are then optimized simultaneously. Both methods are commonly applied to asphalt materials and Marasteanu (1999) demonstrated that both can yield satisfactory master curves. The free shifting approach is adopted herein because optimizing numerous model coefficients simultaneously, as required in the constrained

optimization approach, can lead to results that are dependent on the initial values assigned to the parameters and constraints of the optimization.

Gordon and Shaw (1994) proposed a robust free-shifting algorithm for creating master curves that has been successfully applied to asphalt binders (Rowe and Sharrock 2011). In the method, isotherms are shifted using a pairwise approach. Initially, a linear fit of each isotherm is used to estimate the shift factor between each isotherm in a given pair. Then, the shift factors are updated iteratively using weighted least square polynomial fits of the isotherms. Implementation of the method requires rather sophisticated software and cannot be readily implemented in Excel. Marasteanu (1999) employed an alternative free shifting method to calculate shift factors based on storage and loss moduli that also required software to implement. Therefore, a simpler approach is devised herein, termed pairwise interpolation.

The pairwise interpolation approaches first determines a shift factor (a_T) for each successive pair of isotherms that reflects the shift factor for the higher temperature isotherm with temperature equal to T_H using a reference temperature equal to the lower temperature isotherm with temperature equal to T_L . For example, if the data includes test temperatures of 5°C, 20°C, 35°C, and 50°C, this would involve determining the shift from 5°C to 20°C, from 20°C to 35°C, and from 35°C to 50°C. Then, these shift factors are used to calculate the final shift factors relative to the desired reference temperature. Note that application of the pairwise interpolation approach requires overlap in the range of property values among successive isotherms. In contrast, the Gordon and Shaw (1994) method does not require overlap in the range of values among successive isotherms.

The following steps describe how to determine the shift factor factors using the pairwise interpolation method. The steps are written including storage modulus ($G' = |G^*| \times \cos \delta$). However, the steps were applied to both G' and loss modulus ($G'' = |G^*| \times \sin \delta$) for each binder and then averaged to determine the final shift factors; this approach is adopted to incorporate and balance $|G^*|$ and phase angle considerations. Note that Marasteanu (1999) also considered both storage and loss moduli when free shifting data to construct asphalt binder master curves.

1. Identify the minimum measurement frequency at T_H for which the corresponding G' value falls above the minimum property value measured at T_L . Denote this frequency ω_m and the G' value at this frequency $G'(T_H, \omega_m)$.
2. Calculate the equivalent frequency at T_L that will yield $G'(T_H, \omega_m)$ using linear interpolation of $\log G'$ versus \log frequency for two nearest data points, termed the equivalent frequency (ω_e). To do so, identify the measurement at T_L with the closest G' value lower than $G'(T_H, \omega_m)$ and the measurement with the closest G' value higher than $G'(T_H, \omega_m)$, denoted points 1 and 2, respectively. Then, calculate the equivalent frequency at the T_L (ω_e) using Equation (21).

$$\log \omega_e = \log \omega_1 + (\log G'(T_H, \omega_m) - \log G'(T_L, \omega_1)) \times \frac{\log \omega_2 - \log \omega_1}{\log G'(T_L, \omega_2) - \log G'(T_L, \omega_1)} \quad (21)$$

3. Calculate the logarithm of the shift factor ($\log a_T$) based on the equivalent frequency using Equation (22).

$$\log a_T = \log \left(\frac{\omega_e}{\omega_m} \right) \quad (22)$$

4. Repeat Steps 2 and 3 for each measurement frequency at T_H that is greater than ω_m (replacing ω_m in Equations (21) and (22) with the ω of interest).
5. Average the calculated $\log a_T$ values and report as the $\log a_T(T_H, T_{ref} = T_L)$ value for the isotherm pair; this $\log a_T$ defines the time-temperature shift factor at T_H for a reference temperature (T_{ref}) equal to T_L .
6. Select one of the test temperatures as the reference temperature for constructing the master curve. The $\log a_T$ at this temperature equals zero. Use the $\log a_T$ values from Step 1 to calculate the shift factors at the other test temperatures based on the values from Step 1 and the corresponding direction and distance from the reference temperature. For example, if the temperature-frequency sweep included test temperatures of 5°C, 20°C, 35°C, and 50°C, the $\log a_T(50, T_{ref} = 20) = \log a_T(35, T_{ref} = 20) + \log a_T(50, T_{ref} = 35)$ and the $\log a_T(5, T_{ref} = 20) = -\log a_T(20, T_{ref} = 5)$.

The pairwise interpolation method was applied to construct master curves herein and the resultant $\log a_T$ values were compared to those determined using the RHEA software v2.1.2, which implements the Gordon and Shaw (1994) method. To enable the most direct comparison with the pairwise interpolation method, the $\log a_T$ values reported from RHEA were determined using the average of those calculated from G' and G'' . A reference temperature of 20°C was used in all cases. The $\log a_T$ results from the pairwise interpolation method were used for subsequent calculation of the master curve model coefficients.

Shift Factor Model

Equation (23) was used to model the time-temperature shift factors. Equation (23) is included in AASHTO R 62 as a suitable model for describing the temperature-dependence of shift factors for asphalt mixtures and also works well for asphalt binders. The model coefficients a and b were determined using the LINEST function in Excel, which uses an objective least squares method to calculate linear or polynomial model coefficients. A shift factor model R^2 of 1.00 was achieved in all cases; note that alternative shift factors models may be more appropriate if considering low temperatures where the binder approaches glassy behavior (Rowe and Sharrock 2011).

$$\log a_T(T) = a(T - T_{ref})^2 + b(T - T_{ref}) \quad (23)$$

Master Curve Model

The CA model given in Equations (19) and (20) includes three model parameters: G_g , ω_c and R . The G_g in Equations (19) was assumed to equal 1 GPa in this study because testing was conducted at a minimum temperature of 5°C, which did not permit measurement of the binder response in a glassy state. Testing at lower temperatures was avoided for two reasons: (1) most DSRs used for asphalt binder testing are not equipped to cool the asphalt below 0°C and (2) while temperature-control systems can be upgraded for most rheometers to permit testing at lower temperatures, upper torque limits and instrument compliance effects can pose challenges when testing at lower temperatures. However, it is noted that past studies that have performed testing at temperature approaching the glass transition temperature have reported G_g values can differ among asphalt binders (Sui et al. 2010).

Measures were taken when determining the ω_c and R values in Equations (19) and (20) to ensure that they retain the underlying principle of the CA model; that is that the ω_c and R values reflect the reduced frequency and logarithmic distance of the $|G^*|$ from the glassy modulus (assumed to be 1 GPa in this study) at the point where $\delta = 45^\circ$. If both parameters are simultaneously and freely

optimized using a least squares approach, the ω_c and therefore, R value may not reflect the point where $\delta = 45^\circ$. Also, the simultaneous optimization of parameters can yield results that are sensitive to the initial values assigned to the parameters and the constraints of the optimization. A single method was applied to determine ω_c value in all cases whereas several different methods were evaluated for subsequently calculating the R value, termed the linear regression (LR), Average, and least squares optimization (LSO) herein.

Anderson et al. (1994) proposed simple methods to estimate the ω_c and R values in the CA model given in Equations (19) and (20). To estimate ω_c , the authors proposed fitting a line to $\log \omega_c$ versus $\log \tan \delta$ for $\tan \delta$ values falling between 0.5 and 2 wherein the relationship is generally linear as evident by Figure 37. The intercept of this line is ω_c (i.e., reduced frequency where $\delta = 45^\circ$ and therefore, $\log \tan \delta = 0$). This method was used to determine all ω_c values herein with the additional constraint of only considering values for which $|G^*|$ exceeds 10^5 Pa based on the results of Christensen (1992) which suggests that the CA model can fail to accurately reflect binder behavior when the $|G^*|$ falls below this limit.

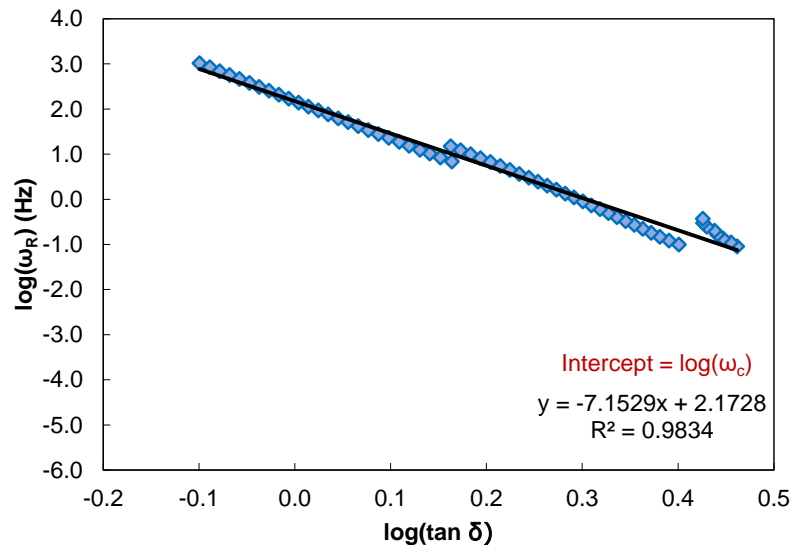


Figure 37. Example of relationship used to determine ω_c for binder 4|O

Linear Regression: Anderson et al. (1994) proposed that the R value can be estimated from fitting a line to $\log (\log |G^*|)$ versus $\tan \delta$, which is also generally linear for $\tan \delta$ values falling between 0.5 and 2. In this case, the intercept of the line is equal to $\log R$. The method suggested by Anderson et al. (1994), termed the ‘LR’ method herein, was used to estimate R values for all binders evaluated; similar to the calculation of ω_c , only data with $\tan \delta$ values falling between 0.5 and 2 and $|G^*|$ greater than 10^5 Pa were considered when implementing the LR method to calculate R . Figure 38 shows an example of the graph used to calculate R according to the LR method.

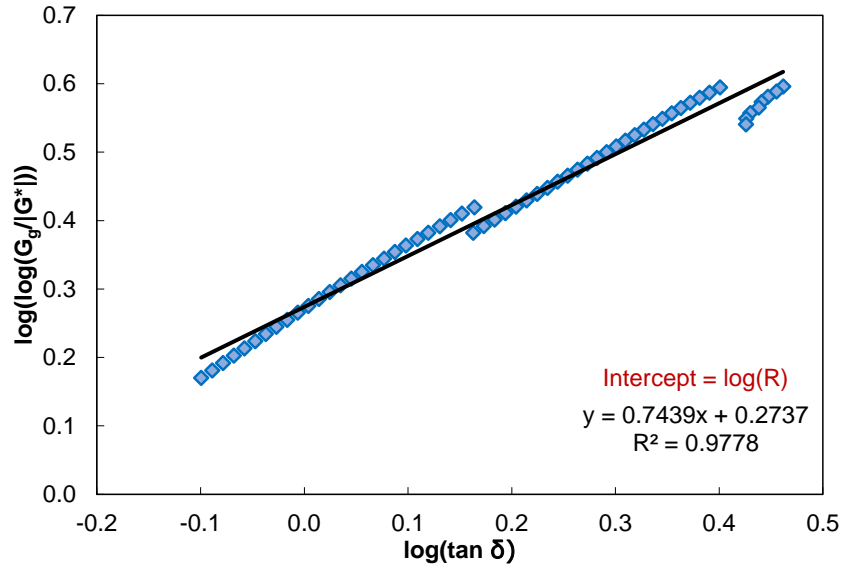


Figure 38. Example relationship used to determine R in the LR method

Average: As part of the NCHRP 09-59 Project, Christensen and Tran (2022) recently proposed that the R value can be calculated from Equation (24) using measurements of $|G^*|$ and δ obtained at a single temperature and frequency so long as the resultant $|G^*|$ exceeds 10^6 Pa and G_g is assumed to equal 1 GPa. Equation (24) is a direct derivation from the CA model. While Christensen and Tran (2022) suggested a single measurement point can determine R , the R values herein were determined by averaging the R values calculated using Equation (24) at all temperature and frequency combinations for which $|G^*|$ exceeded 10^6 Pa.

$$R = \log(2) \frac{\log(|G^*|/G_g)}{\log(1 - \delta/90)} \quad (24)$$

Figure 39 shows three examples that are illustrative of the three trends observed when calculating R according to Equation (24). In original and RTFO aged binders evaluated, the calculated R value did not vary with the measured $|G^*|$ (e.g., binder 1|O). In polymer-modified asphalts, the calculated R value fluctuated randomly over a small range (e.g., binder 9|P20). Unmodified binders at the P20 and P40 conditions generally exhibited a decreasing trend with respect to $|G^*|$ (e.g., binder 6|P40). These latter cases suggest that the data does not perfectly conform to the CA model. However, the model may still provide acceptable accuracy.

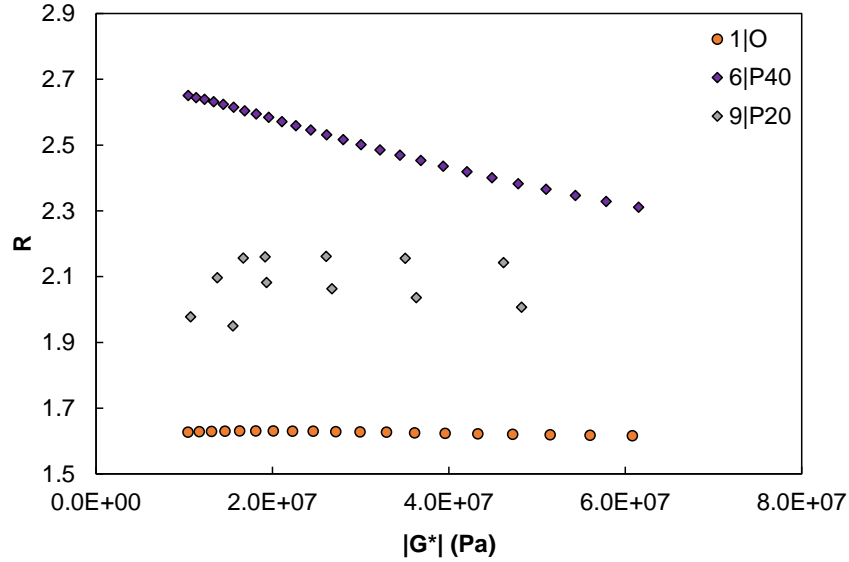


Figure 39. Examples of trends of R values calculated according to Equation (6) with respect to $|G^*|$

LSO: Two least squares optimizations (LSO) were also applied to determine R values after previously determining the ω_c as described above. The optimization of only one parameter alleviates concerns associated with the simultaneous optimization of model parameters that were previously discussed. Least squares optimizations were carried out using Microsoft Excel Solver to minimize the two objective functions defined in Equations (25) and (26), termed the LSO log and LSO approaches, respectively. In both cases, the squared errors for both G' and G'' are summed in an effort to balance the resultant $|G^*|$ and δ model accuracy. In Equation (25), the sum of squared errors is calculated on the basis of $\log G'$ and $\log G''$ values because the basis for the CA model is the phenomenological observation of the shape of the $|G^*|$ master curve in logarithmic space. The errors are computed based on the arithmetic values in Equation (26). An initial value of 2.00 was assigned to R when performing the numerical optimizations.

$$Error = \sum_{i=1}^n [\log(G'_{measured,i}) - \log(G'_{predicted,i})]^2 + [\log(G''_{measured,i}) - \log(G''_{predicted,i})]^2 \quad (25)$$

$$Error = \sum_{i=1}^n [G'_{measured,i} - G'_{predicted,i}]^2 + [G''_{measured,i} - G''_{predicted,i}]^2 \quad (26)$$

where $G'_{measured}$ = measured G' value, $G'_{predicted}$ = G' value predicted by the master curve model, $G''_{measured}$ = measured G'' value, $G''_{predicted}$ = G'' value predicted by the master curve model, and n = number of data points.

Evaluation of the Master Curve Model Results

Several criteria were used to evaluate the ability of the CA model to represent asphalt binder rheological behavior over the measurement range and to compare the different approaches for calculating the R value. The coefficient of determination (R^2) values of the models were calculated for both $|G^*|$ and δ models. The normalized root mean squared error (RMSE(%)) of the $|G^*|$ model was also calculated as defined in Equation (27), which reflects the ratio of the model RMSE to the standard deviation of the logarithm of the average $|G^*|$ results.

$$RMSE(\%) = \frac{\sqrt{\frac{1}{n} \sum_{i=1}^n (\log |G^*|_{predicted,i} - \log |G^*|_{measured,i})^2}}{\sqrt{\frac{1}{n} \sum_{i=1}^n (\log |\bar{G}^*| - \log |G^*|_{measured,i})^2}} \times 100\% \quad (27)$$

where: $|G^*|_{measured}$ = measured $|G^*|$ value, $|G^*|_{predicted}$ = $|G^*|$ value predicted by the master curve model, and $|\bar{G}^*|$ = average $|G^*|$ value.

AASHTO R 84, which is a standard practice for developing asphalt mixture dynamic modulus master curves, specifies that the master curve RMSE(%) should be less than 5 percent, which is adopted herein to evaluate asphalt binder $|G^*|$ master curve model results. The R^2 and mean absolute percent error (MAPE) were chosen to evaluate δ master curve model accuracy. Note that AASHTO R 84 does not include specifications for constructing or evaluating asphalt mixture δ master curves and the MAPE was thought to constitute an intuitive measure of the model accuracy. The fit statistics were calculated in two ways: (1) including all data that was not omitted in the data screening process and (2) also omitting data corresponding to $|G^*|$ values falling below 10^5 Pa based on precedent in the literature that suggests the CA model only accurately reflects binder behavior for higher $|G^*|$ values (Christensen 1992). In addition, the G-R parameter values were calculated at 15°C and 0.005 rad/s using the CA and shift factor models to evaluate the effects of the differences in the R values calculated according to the various methods on a practical application of master curves.

RESULTS

Evaluation of the Pairwise Interpolation Approach for Constructing Master Curves

Figure 40 shows the comparison between the $\log a_T$ values determined according to the Gordon and Shaw method (1994) and pairwise interpolation method developed herein. The results indicate that the two methods yield very similar $\log a_T$ values with an average difference of approximately two percent. The best agreement between the two methods is observed at the higher temperature isotherms. A small bias from the line of equality (LOE) is observed for the $\log a_T$ values at 5°C and 10°C, where the pairwise interpolation method resulted in slightly smaller $\log a_T$ values than the Gordon and Shaw (1994) method. The maximum difference in $\log a_T$ values observed among the two methods was 4.2 percent, coinciding with the results of binder 8|P20 at 10°C. It is noted that the percent difference between $\log a_T$ values calculated from the Gordon and Shaw (1994) and pairwise interpolation method were found to increase slightly as the age level increased for a given asphalt binder but this increase was generally less than one percent.

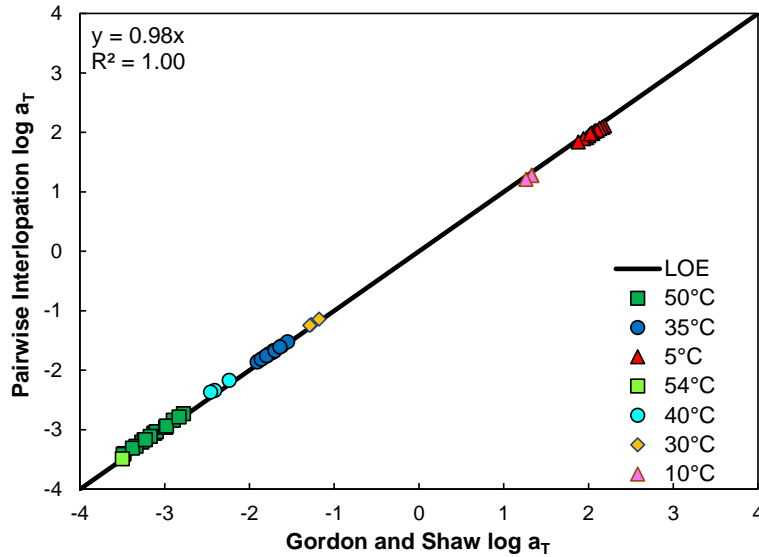


Figure 40. Comparison of $\log a_T$ values determined using the Gordon and Shaw (1994) and pairwise interpolation methods

Evaluation of the CA Model Results

Table 27 summarizes CA model ω_c and R parameter values determined after applying the $\log a_T$ values calculated using the pairwise interpolation method to construct $|G^*|$ and δ master curves. The R values are also shown graphically in Figure 41. In all cases, the results for a given binder tested at multiple age levels follow the expected trend of a decrease in ω_c and increase in R value (Christensen 1992). The R values calculated by the different approaches are generally similar for a given binder. The two LSO approaches yield the most similar R values results among the four methods evaluated with the Average method generally exhibiting the most distinct result. The binder age level appears to have a small effect on the sensitivity of the R value to the method of calculation with the more heavily aged materials generally displaying slightly higher variation than lesser aged materials. The maximum discrepancy in R values determined from the four methods coincides with binder 8|P20, a polymer-modified binder, where the percent difference between the maximum and minimum calculates R values is 12 percent. The higher sensitivity of the R values to the method of calculation in more highly aged and polymer-modified binders was expected because these were the cases where the R values calculated using Equation (24) were found to vary with respect to $|G^*|$ as discussed within the methodology. Nevertheless, the differences in the R values calculated using the different methods are generally quite small. The average percentage difference between the highest and lowest R value calculated for a given binder and age level combination across the different methods is four percent. When the Average method is neglected, this average percent difference reduces to 2.4 percent and the maximum observed difference reduces to 4.2 percent.

Table 27. Summary of the CA Model Parameters

Binder	Age	ω_c	LR <i>R</i>	Average <i>R</i>	LSO <i>R</i>	LSO log <i>R</i>
1	O	176.87	1.63	1.63	1.63	1.68
1	R	56.79	1.75	1.79	1.77	1.79
1	P20	6.25	2.08	2.17	2.13	2.14
2	O	45.29	1.62	1.68	1.65	1.69
2	R	11.15	1.76	1.82	1.82	1.78
2	P20	1.26	2.01	2.13	2.08	2.08
2	P40	0.23	2.30	2.49	2.37	2.36
3	P20	0.83	2.09	2.12	2.15	2.15
3	P40	0.09	2.31	2.31	2.36	2.37
4	O	148.88	1.88	1.86	1.87	1.90
4	R	28.09	1.98	1.99	2.00	2.00
4	P20	3.13	2.25	2.33	2.29	2.30
4	P40	0.71	2.35	2.43	2.40	2.40
5	R	7.75	2.02	2.06	2.06	2.06
5	P20	1.11	2.24	2.29	2.29	2.29
6	P40	0.45	2.52	2.50	2.55	2.56
7	P20	2.00	2.28	2.22	2.30	2.29
8	P20	0.11	2.69	2.38	2.65	2.69
9	P20	0.48	2.06	2.08	2.08	2.10

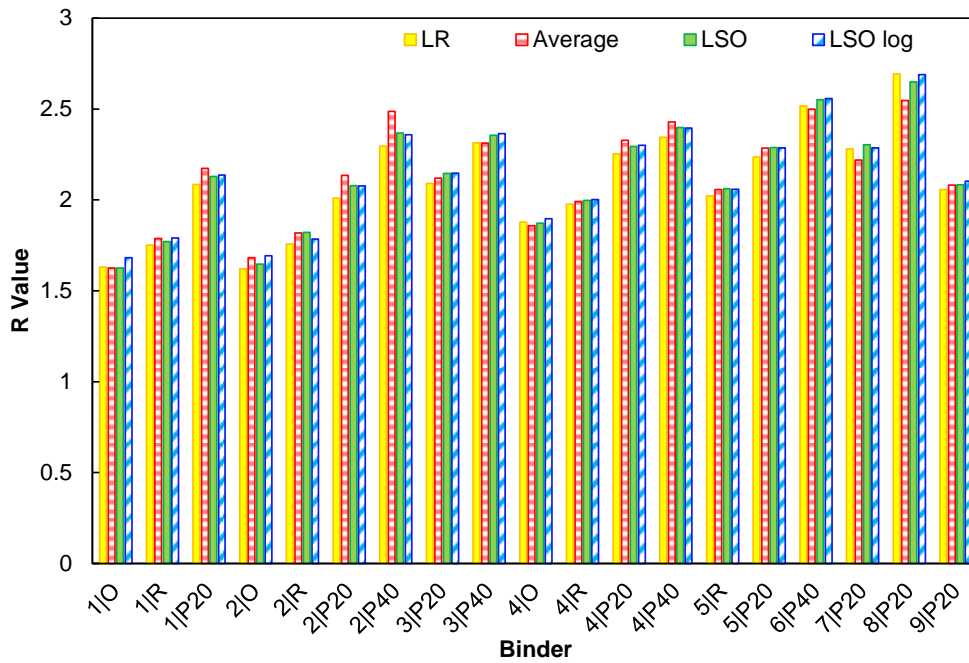


Figure 41. R values

Example master curves are shown for binder 4|P40 and 8|P20 in Figure 42 and Figure 43, respectively. These examples show that, in general, the CA model visually agrees with the measured data. Figure 42 is illustrative of most cases observed wherein small discrepancies between the measured data and model predicts are apparent in the $|G^*|$ and δ master curves at low reduced frequencies in Figure 42, which matches expectations based on the literature (Christensen 1992). In Figure 42, it is difficult to visually distinguish among the different methods used to calculate the CA model R value which was the case for most binders evaluated. The differences among the different methods is somewhat more apparent in Figure 43, which constitutes the case that exhibited the largest variation in R values calculated from the different methods. In Figure 43, the CA model predictions from the Average method are most distinct. This was a case where the R value calculated according to Equation (24) fluctuated with respect to $|G^*|$. Figure 42 and Figure 43 also reveal that the application of time-temperature superposition results in a smoother $|G^*|$ master curve than δ , which matches expectations based on previous studies (Rowe and Sharrock 2011).

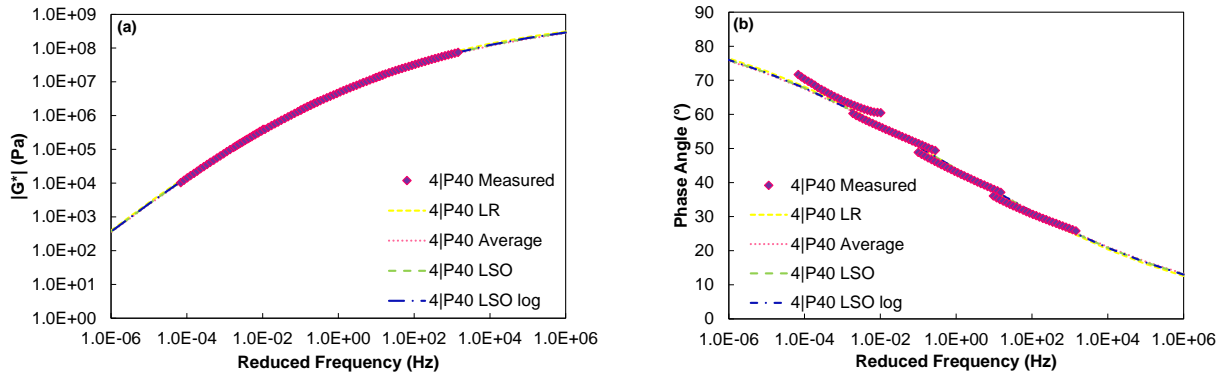


Figure 42 Master curves for binder 4|P40: (a) $|G^*|$ and (b) δ

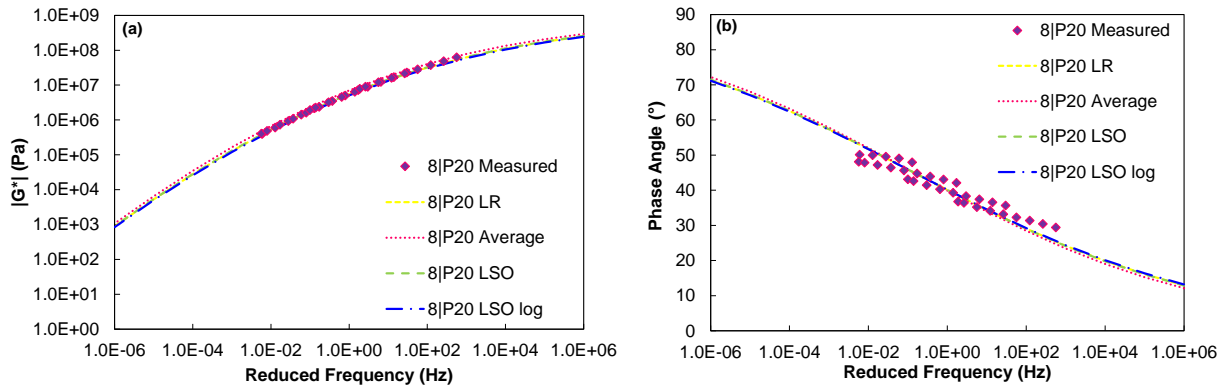


Figure 43. Master curves for binder 8|P20: (a) $|G^*|$ and (b) δ

To further evaluate the CA model results, the CA model predictions of $|G^*|$ and δ are plotted against the measured values in Figure 44. Group A and B binders are plotted separately to better allow for visually distinguishing trends among polymer-modified (i.e., Group B) and unmodified binders (i.e., Group A). To reduce clutter in these graphs, only select test frequencies are plotted in Figure 44. For Group A binders, results corresponding test frequencies of 0.15 Hz, 1.35 Hz, and 10 Hz are plotted from each test temperature whereas for the Group B binders, the selected test

frequencies are 0.1 Hz, 1.4 Hz, 6.5 Hz. Note that different frequencies were used in the two groups of binders and thus, similar but not identical frequencies are plotted for Groups A and B.

Figure 44 (a) and (b) shows that the $|G^*|$ results generally fall very close to LOE. Somewhat higher deviation from the LOE is apparent in the few points where $|G^*|$ falls below approximately 10^4 Pa. The literature suggests that CA model accuracy is best when $|G^*|$ exceeds 10^5 Pa (Christensen 1992). For both groups of binders, it is apparent that the Average method for calculating the R value generally yields poorer $|G^*|$ model accuracy compared to the other methods. In the case of the Group A binders, the Average method tends to underestimate $|G^*|$ whereas for the Group B binders, it tends to overestimate $|G^*|$. Figure 44 (c) shows that the δ model results for the binders without polymer modification (Group A) are very close to the LOE, indicating high accuracy, when the δ is below 70° whereas for polymer-modified asphalt binders, deviation from the LOE begins to occur when the δ exceeds 60° . Visually, it is difficult to distinguish among the CA model predictions of δ obtained from the different R calculation methods. Generally, the data where the δ model accuracy tends to diminish coincide with $|G^*|$ values falling below 10^5 Pa and thus, the data generally assign to align with the literature (Christensen 1992). One alternative to the CA model to potentially improve model accuracy at low $|G^*|$ values is the Christensen-Anderson-Marasteanu (CAM) model (Marasteanu 1999), which incorporates an additional model parameter to allow for better capturing how fast or slow $\log |G^*|$ versus $\log \omega_R$ data converge to the glassy and equilibrium asymptotes.

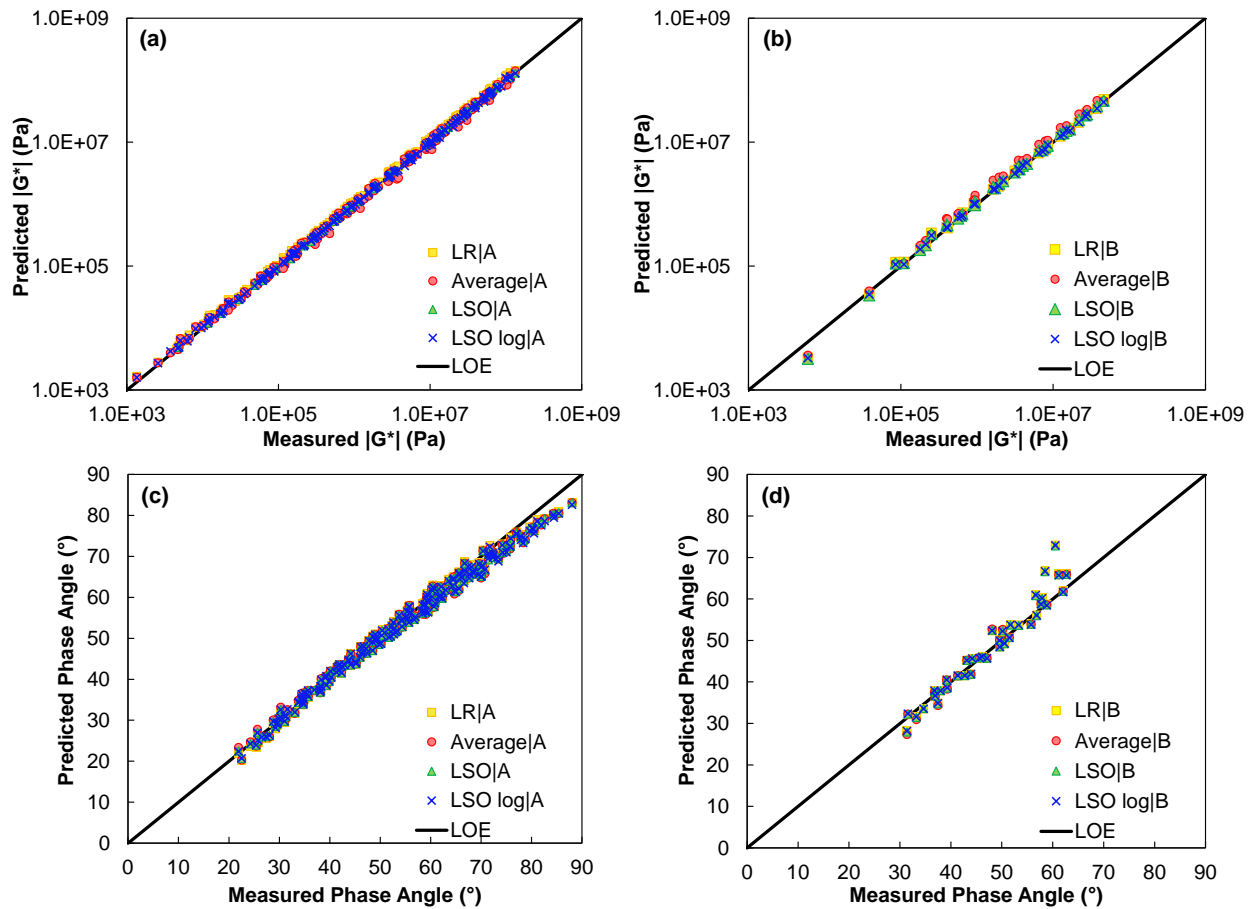


Figure 44. Comparison of the measured and predicted (a) $|G^*|$ values for the Group A binders, (b) $|G^*|$ values for the Group B binders, (c) δ for the Group A binders, and (d) δ for the Group B binders.

The CA model fit statistics for $|G^*|$ and δ are presented in Table 3 through Table 6. Tables 3 and 4 show the $|G^*|$ fit statistics, including all data and neglecting data where $|G^*|$ falls below 10^5 Pa, respectively. Tables 5 and 6 show the δ fit statistics, including all data and neglecting data where $|G^*|$ falls below 10^5 Pa, respectively. Note that all model fit statistics are calculated using only data that was retained after screening. The $|G^*|$ model fit statistics reflect visual observations in Figure 9 for the Average method, suggesting it is inferior to the other approaches. In general, the LSO method to calculate R yields the highest R^2 and lowest RMSE(%) values for the CA model for $|G^*|$. However, it is noted that the RMSE(%) values corresponding to the LR method are comparable to those from the LSO method in many cases and the maximum RMSE(%) is only slightly higher for LR method when all data is considered (5.81 vs. 5.75) and only data where $|G^*|$ exceeds 10^5 Pa (3.91 vs. 2.85). The LR method is considered practically advantageous in that it does not require numerical optimization and therefore, could more easily be specified than the LSO and LSO log methods. Both the LSO and LR methods provide acceptable RMSE(%) values based on the AASHTO R 84 criterion (for asphalt mixture dynamic modulus master curves) when data where $|G^*|$ falls below 10^5 Pa is omitted. These methods both yield R^2 values of 0.97 or higher when all data is included and yield values of 1.00 when data where $|G^*|$ falls below 10^5 Pa is

excluded for both unmodified and polymer-modified binders. Comparison of the fit statistics in Tables 3 and 4 does demonstrate an improvement in model accuracy when $|G^*|$ data falling below 10^5 Pa is omitted. For example, the average RMSE(%) decreases from 3.22 to 2.49 for the LR method and from 1.87 to 1.02 for the LSO method.

The four methods for calculating R values yield comparable model fit statistics for δ with average MAPE values of approximately three percent when all data is included and approximately two percent when data corresponding to $|G^*|$ values falling below 10^5 Pa is omitted. The R^2 values are generally lower for δ than $|G^*|$ and the poorest fit statistics for both $|G^*|$ and δ generally coincide with the polymer-modified binders (i.e., binders 7, 8, and 9).

Table 28. |G*| Model Fit Statistics Including All Data

Binder	Age Level	LR		Average		LSO		LSO log	
		R ²	RMSE	R ²	RMSE	R ²	RMSE	R ²	RMSE
1	O	1.00	3.83%	1.00	3.93%	1.00	3.93%	0.98	3.26%
1	R	1.00	2.03%	1.00	1.38%	1.00	1.52%	1.00	1.40%
1	P20	0.99	2.70%	0.99	2.66%	1.00	1.03%	1.00	1.12%
2	O	1.00	3.98%	0.99	2.79%	1.00	3.23%	0.99	2.83%
2	R	0.98	1.76%	1.00	2.25%	1.00	2.41%	0.99	1.24%
2	P20	0.98	3.81%	0.98	3.98%	1.00	1.07%	1.00	1.03%
2	P40	0.97	4.20%	0.91	9.35%	1.00	1.93%	1.00	1.63%
3	P20	0.98	2.70%	1.00	2.66%	1.00	1.03%	1.00	1.12%
3	P40	0.99	3.93%	0.99	3.96%	1.00	1.03%	1.00	0.73%
4	O	1.00	0.98%	1.00	1.64%	1.00	1.15%	1.00	0.96%
4	R	1.00	1.42%	1.00	0.81%	1.00	0.69%	1.00	0.69%
4	P20	0.99	2.80%	0.99	2.10%	1.00	0.73%	1.00	0.77%
4	P40	0.99	3.34%	0.99	2.53%	1.00	0.70%	1.00	0.64%
5	R	0.99	2.09%	1.00	0.77%	1.00	0.82%	1.00	0.77%
5	P20	0.99	3.27%	1.00	0.65%	1.00	0.70%	1.00	0.67%
6	P40	0.99	3.09%	0.99	4.36%	1.00	0.78%	1.00	0.65%
7	P20	1.00	5.78%	0.96	7.94%	1.00	5.75%	1.00	5.72%
8	P20	0.98	3.72%	0.94	12.03%	1.00	2.85%	0.98	7.45%
9	P20	1.00	5.81%	1.00	4.26%	1.00	4.24%	1.00	3.71%
		Max	5.81%	Max	12.03%	Max	5.75%	Max	7.45%
		Mean	3.22%	Mean	3.69%	Mean	1.87%	Mean	1.91%

Table 29. |G*| Model Fit Statistics Excluding |G*| values Below 10⁵ Pa

Binder	Age Level	LR		Average		LSO		LSO log	
		R ²	RMSE	R ²	RMSE	R ²	RMSE	R ²	RMSE
1	O	1.00	1.19%	1.00	1.28%	1.00	1.29%	1.00	1.52%
1	R	1.00	1.01%	1.00	0.62%	1.00	0.41%	1.00	0.72%
1	P20	1.00	1.99%	1.00	2.42%	1.00	0.39%	1.00	0.70%
2	O	1.00	1.95%	1.00	1.44%	1.00	1.19%	1.00	1.76%
2	R	1.00	1.74%	1.00	2.07%	1.00	2.21%	1.00	1.18%
2	P20	1.00	3.29%	1.00	3.92%	1.00	0.83%	1.00	0.76%
2	P40	1.00	3.42%	1.00	9.16%	1.00	1.71%	1.00	1.21%
3	P20	1.00	3.61%	1.00	1.89%	1.00	0.64%	1.00	0.62%
3	P40	1.00	3.84%	1.00	3.87%	1.00	1.03%	1.00	0.71%
4	O	1.00	0.56%	1.00	1.15%	1.00	0.70%	1.00	0.77%
4	R	1.00	1.22%	1.00	0.62%	1.00	0.49%	1.00	0.51%
4	P20	1.00	2.36%	1.00	2.02%	1.00	0.37%	1.00	0.54%
4	P40	1.00	2.99%	1.00	2.45%	1.00	0.62%	1.00	0.53%
5	R	1.00	2.03%	1.00	0.39%	1.00	0.34%	1.00	0.37%
5	P20	1.00	3.02%	1.00	0.59%	1.00	0.64%	1.00	0.61%
6	P40	1.00	2.95%	1.00	4.15%	1.00	0.78%	1.00	0.63%
7	P20	1.00	2.43%	1.00	6.66%	1.00	1.00%	1.00	1.98%
8	P20	1.00	3.70%	1.00	11.26%	1.00	2.85%	1.00	7.27%
9	P20	1.00	3.91%	1.00	1.89%	1.00	1.87%	1.00	1.49%
		Max	3.91%	Max	11.26%	Max	2.85%	Max	7.27%
		Mean	2.49%	Mean	3.04%	Mean	1.02%	Mean	1.26%

Table 30. δ Model Fit Statistics Including All Data

Binder	Age Level	LR		Average		LSO		LSO log	
		R ²	MAPE						
1	O	0.95	3.41%	0.95	3.36%	0.95	3.36%	0.93	4.01%
1	R	0.98	2.25%	0.97	2.51%	0.98	2.38%	0.97	2.54%
1	P20	0.98	2.54%	0.97	3.01%	0.97	2.77%	0.97	2.81%
2	O	0.97	3.33%	0.96	4.10%	0.97	3.67%	0.95	4.23%
2	R	0.99	1.83%	0.99	1.88%	0.99	1.89%	0.99	1.83%
2	P20	0.99	2.32%	0.98	3.31%	0.99	2.72%	0.99	2.70%
2	P40	0.98	2.93%	0.96	5.09%	0.98	3.78%	0.98	3.66%
3	P20	0.98	2.54%	0.97	3.01%	0.97	2.77%	0.97	2.81%
3	P40	0.99	2.71%	0.99	2.71%	0.99	2.42%	0.99	2.37%
4	O	0.97	2.22%	0.97	2.09%	0.97	2.18%	0.97	2.34%
4	R	0.99	1.75%	0.99	1.75%	0.99	1.75%	0.99	1.75%
4	P20	0.99	2.02%	0.98	2.18%	0.99	2.09%	0.99	2.10%
4	P40	0.99	2.24%	0.99	2.40%	0.99	2.32%	0.99	2.31%
5	R	0.99	2.20%	0.99	2.18%	0.99	2.18%	0.99	2.18%
5	P20	0.99	2.46%	0.99	2.45%	0.99	2.45%	0.99	2.45%
6	P40	0.99	2.26%	0.99	2.31%	0.99	2.19%	0.99	2.18%
7	P20	0.86	5.31%	0.85	5.73%	0.87	5.16%	0.86	5.27%
8	P20	0.90	5.24%	0.89	5.80%	0.90	5.28%	0.90	5.09%
9	P20	0.97	2.42%	0.98	2.39%	0.98	2.39%	0.98	2.37%
		Max	5.31%	Max	5.80%	Max	5.28%	Max	5.27%
		Mean	2.87%	Mean	3.21%	Mean	2.95%	Mean	3.01%

Table 31. δ Model Fit Statistics Excluding Data Corresponding to $|G^*|$ values Below 10^5 Pa

Binder	Age Level	LR		Average		LSO		LSO log	
		R ²	MAPE						
1	O	0.98	1.44%	0.99	1.42%	0.99	1.42%	0.98	1.75%
1	R	1.00	1.05%	0.99	1.13%	1.00	1.09%	0.99	1.14%
1	P20	1.00	1.36%	0.99	1.50%	1.00	1.41%	0.99	1.43%
2	O	0.99	2.03%	0.98	2.50%	0.98	2.24%	0.98	2.58%
2	R	1.00	1.45%	1.00	1.34%	1.00	1.34%	1.00	1.38%
2	P20	0.99	1.84%	0.99	2.58%	0.99	2.09%	0.99	2.08%
2	P40	0.99	2.36%	0.98	4.28%	0.99	3.11%	0.99	3.01%
3	P20	0.99	2.22%	0.99	2.09%	0.99	2.00%	0.99	1.99%
3	P40	0.99	2.65%	0.99	2.65%	0.99	2.39%	0.99	2.34%
4	O	0.99	1.03%	0.99	1.00%	0.99	1.02%	0.99	1.06%
4	R	1.00	1.25%	1.00	1.21%	1.00	1.19%	1.00	1.18%
4	P20	0.99	1.40%	0.99	1.40%	0.99	1.38%	0.99	1.38%
4	P40	0.99	1.87%	0.99	1.89%	0.99	1.86%	0.99	1.86%
5	R	0.99	1.66%	0.99	1.53%	0.99	1.52%	0.99	1.53%
5	P20	0.99	2.12%	0.99	2.02%	0.99	2.01%	0.99	2.01%
6	P40	0.99	2.19%	0.99	2.24%	0.99	2.09%	0.99	2.07%
7	P20	0.98	2.73%	0.97	3.01%	0.98	2.63%	0.98	2.70%
8	P20	0.91	4.96%	0.89	5.50%	0.91	5.00%	0.91	4.82%
9	P20	0.98	2.33%	0.98	2.29%	0.98	2.29%	0.98	2.26%
		Max	4.96%	Max	5.50%	Max	5.00%	Max	4.82%
		Mean	2.00%	Mean	2.19%	Mean	2.00%	Mean	2.03%

To further compare the different methods for calculating R values on a practical application of master curves, G-R parameter values were calculated at 15°C and 0.005 rad/s (0.0008 Hz) using the time-temperature shift model and CA model results. As discussed, the G-R parameter evaluated at this condition has been proposed as an indicator of ductility (Anderson et al. 2011). The temperature-frequency combination of 15°C and 0.005 rad/s coincides with reduced frequencies near the lower end of the measured data, coinciding within the measurement range of the highest temperature isotherm in most cases. Recall that generally the CA model fits are poorest at low reduced frequencies, corresponding to low $|G^*|$ values and high δ values and thus, constitute a condition where the highest discrepancies among model fits may be expected. In 9 out of the 19 binders evaluated, the predicted $|G^*|$ fell below 10^5 Pa and/or δ value was above 70° at the reduced frequency corresponding to 15°C and 0.005 rad/s. In the case of one binder, 8|P20, the reduced frequency δ corresponding to 15°C and 0.005 rad/s was outside the accepted measurement range after the screening of spurious data. In all other cases, the corresponding reduced frequency was within the measurement range.

Figure 45 presents the G-R value results where trends for a given binder generally match those for the R values shown in Figure 41. In general, the results obtained when using the Average method to calculate R are most distinct from the other methods. Binders 2|P20, 2|P40, and 8|P20 showed notable sensitivity in R values to the method of calculation, which persists in the G-R results. While differences exist, the rankings of the binders evaluated on the basis of G-R does not change with

the method used to calculate the R value. The average percent difference in G-R values for a given binder calculated using the LSO and LR methods is 5.17% when calculated on an arithmetic basis and 1.59% when calculated on a logarithmic basis.

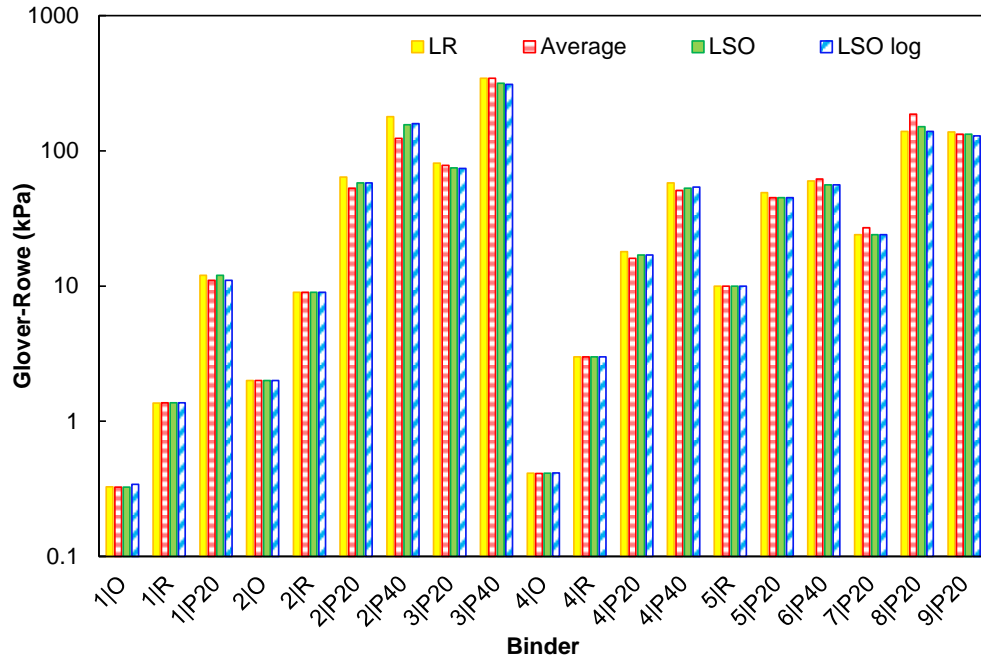


Figure 45. Glover-Rowe values calculated at 15°C and 0.005 rad/s using the shift factor and CA models

CONCLUSIONS AND RECOMMENDATIONS

The following conclusions and recommendations are drawn from the results of this study:

- The pairwise interpolation for constructing asphalt binder master curves developed herein yields good agreement with the Gordon and Shaw (1994) method. The pairwise interpolation method can be more easily implemented than the Gordon and Shaw method but does require that there is overlap in the range of storage and loss moduli in successive isotherms.
- Rheological measurements where δ increases as the measurement frequency increases should be removed from temperature-frequency sweep data prior to constructing master curves.
- The relationship between reduced frequency and $\tan \delta$ in logarithmic space over $\tan \delta$ values spanning from 0.2 to 0.5 is generally linear and can be used to determine the crossover frequency as proposed by Anderson et al. (1994).
- Calculating the CA model R value on the basis of measurements at a single temperature-frequency combination as proposed by Christensen and Tran (2022) or the average over a range of temperature-frequency combinations should be avoided because the calculated R value can vary with the temperature-frequency combination in long-term aged and polymer-modified asphalts, which leads to poorer $|G^*|$ model predictions than alternative methods.
- Solving for the CA model R value using least squares optimization using a previously determined ω_c values on the basis of log storage and log loss moduli values generally yields slightly poorer model accuracy than when computing the squared errors without logarithmic

transforms. Least squares optimization to minimize the sum of squared errors for storage and loss moduli was found to yield the highest model accuracy among the methods evaluated.

- The relationship between $\log(\log |G^*|)$ and $\tan \delta$ is generally linear for $\tan \delta$ values falling between 0.5 and 2 and can be used to estimate the CA Model R value. This approach provided acceptable and comparable model accuracy to least squares optimization in most of the cases evaluated and thus, constitutes a viable alternative to numerical optimization.
- Based on the asphalt binders evaluated in this study, the CA model can accurately reflect asphalt binder rheological behavior when the $|G^*|$ exceeds 10^5 Pa and δ is less than 70° for unmodified asphalts or less than 60° for polymer-modified asphalts.
- This effort focused on identifying practically implementable methods to construct asphalt binder master curves and determine CA model parameters. Research is also needed to develop standardized procedures for temperature-frequency sweep testing.

REFERENCES

1. Anderson, D. A., D. W. Christensen, H. U. Bahia, R. Dongre, M. G. Sharma, C. E. Antle, and J. Button. *SHRP Report A-369: Binder Characterization and Evaluation, Volume 3: Physical Characterization*. National Research Council, Washington, D.C., 1994.
2. Anderson, R. M., G. N. King, D. I. Hanson, and P. B. Blankenship. Evaluation of the Relationship between Asphalt Binder Properties and Non-load Related Cracking. *Journal of the Association of Asphalt Paving Technologists*, Vol. 80, 2011, pp. 615-663.
3. Christensen, D. W. *Mathematical Modeling of the Linear Viscoelastic Behavior of Asphalt Cements*. Ph.D. Dissertation, Pennsylvania State University, College Station, PA, 1992.
4. Christensen, D. W., and N. Tran. *NCHRP Report 982: Relationships Between the Fatigue Properties of Asphalt Binders and the Fatigue Performance of Asphalt Mixtures*. Transportation Research Board, Washington, D.C., 2022. <http://dx.doi.org/10.17226/26302>.
5. Cucalon, L. G., F. Kaseer, E. Arambula-Mercado, A. E. Martin, N. Morian, S. Pournoman, and E. Hajj. The Crossover Temperature: Significance and Application Towards Engineering Balanced Recycled Binder Blends. *Road Materials and Pavement Design*. 2019, Vol. 20, No. 6: <http://dx.doi.org/10.1080/14680629.2018.1447504>.
6. Dickinson, E. J., and H. P. Witt. The Dynamic Shear Modulus of Paving Asphalts as a Function of Frequency. *Transactions of the Society of Rheology*, 1974, Vol. 18, No. 4, pp. 591-606.
7. Ferry, J. D. *Viscoelastic Properties of Polymers*. Wiley, New York, NY, 1980.
8. Glover, C. J., R. R. Davison, C. H. Domke, Y. Ruan, P. Juristyarini, D. B. Knorr, and S. H. Jung. *Development of a New Method for Assessing Asphalt Binder Durability with Field Validation*. FHWA/TX Report 05/1872-2, Texas Department of Transportation, Austin, TX, 2005.
9. Gordon, G. V., and M. T. Shaw. *Computer Programs for Rheologists*. Hanser/Gardner, 1994.
10. Gundla, A., and B. S. Underwood. Molecular Weight Distribution of Asphalt Binders from Laser Desorption Mass Spectroscopy (LDMS) Technique and its Relationship to Linear Viscoelastic Relaxation Spectra. *Fuel*, 2020. Volume 262: <http://dx.doi.org/10.1016/j.fuel.2019.116444>.
11. Marasteanu, M. O. *Inter-conversions of the Linear Viscoelastic Functions Used for the Rheological Characterization of Asphalt Binders*, Ph.D. Dissertation, The Pennsylvania State University, College Station, PA, 1999.

12. Marasteanu, M. O., Anderson, D. A., "Techniques for Determining Errors in Asphalt Binders Rheological Data," *Transportation Research Record*, No. 1766, 2001, pp. 32-39.
13. Olard, F., and H. Di Benedetto. General "2S2P1D" Model and Relation between the Linear Viscoelastic Behaviors of Bituminous Binders and Mixtures. *Road Materials and Pavement Design*. 2003. Vol. 4, No. 2: <http://dx.doi.org/10.1080/14680629.2003.9689946>.
14. Rowe, G. Evaluation of the Relationship between Asphalt Binder Properties and Non-load Related Cracking. *Journal of the Association of Asphalt Paving Technologists, Prepared Discussion*, 2011, Vol. 80, pp. 649-663.
15. Rowe, G. M., and M. J. Sharrock. Alternate Shift Factor Relationships for Describing Temperature Dependency of Viscoelastic Behavior of Asphalt Materials. *Transportation Research Record: Journal of the Transportation Research Board*, 2011. Volume 2207: <http://dx.doi.org/10.3141/2207-16>.
16. Rowe, G. M., and M. J. Sharrock. Cracking of Asphalt Pavements and the Development of Specifications with Rheological Measurements. *Proceedings of the 6th Eurasphalt and Eurobitume Congress*, 2016. <http://dx.doi.org/10.14311/EE.2016.215>.
17. Sui, C., M. J. Farrar, W. H. Tuminello, and T. F. Turner. "New Techniques for Measuring Low-Temperature Properties of Asphalt Binders with Small Amounts of Material," *Transportation Research Record: Journal of the Transportation Research Board*, No. 2179, 2010, pp. 23-38.
18. Zeng, M., H. U. Bahia, H. Zhai, M. R. Anderson, and P. Turner. Rheological Modeling of Modified Asphalt Binders and Mixtures. *Journal of the Association of Asphalt Paving Technologists*, Vol. 70, 2001, pp. 403-441.

APPENDIX C: SATURATES, AROMATICS, RESINS, AND ASPHALTENE (SARA) ANALYSIS OF THE IMPACTS OF ADDITIVES

INTRODUCTION

To complement the rheological evaluation of the asphalt binders and blends, the effects of the additives on the composition of asphalt binders was evaluated using Saturates, Aromatics, Resins, and Asphaltenes (SARA) analysis of virgin binders, RAP binder, and select blends at the RTFO and RTFO plus 40-hour PAV (P40) age levels. The analysis was conducted in an effort to understand the mechanisms by which additives alter binder rheology.

MATERIALS AND METHODS

SARA analysis was conducted on the following binders/blends detailed in Section 2.5 at both the RTFO and P20 age levels: PG 58-28 (58) and PG 64-22 (64) virgin binders, the RAP binder (at the RTFO age level only), 58.RAP, 58.RAP.E1, 58.RAP.E2, 64.RAP.R1, and 64.RAP.R2. The asphaltenes content of each binder/blend was determined through precipitation of the binder in a solution of n-heptane. Subsequently, the maltene fraction (that remained in solution) was applied to rods for Iatroscan analysis. The Iatroscan (NTS 2023) was used to determine the breakdown of saturates, aromatics, and resins. Five rods were analyzed in the Iatroscan per binder/blend. In a few cases, one rod was lost due to contamination. The SARA results were used to calculate the Colloidal Instability Index (CII), defined in Equation (28). A higher CII indicates less compatible microstructure in the binder, which is often associated with higher age hardening susceptibility and potentially poorer durability (Epps Martin et al. 2020). Tukey's Honest Significant Different (HSD) tests were conducted to identify SARA results with statistically equal means by means of the Tukey-Kramer method using a confidence level of 95 percent.

$$CII = \frac{\text{Saturates} + \text{Asphaltenes}}{\text{Aromatics} + \text{Resins}} \times 100\% \quad (28)$$

RESULTS AND ANALYSIS

Figure 46 and Table 32 show the SARA results. An estimate of the SARA composition of a blend of the 64 virgin binder and RAP binder at the RTFO age level is included to enable an evaluation of the effect of the R1 and R2 additives on composition. The estimated was obtained using the rule of mixtures (i.e., a weighted average) of the 64 virgin binder and RAP binder results. The accuracy of this approach was verified for the 58.RAP blend where 58 virgin binder and RAP binder results as well as the blend result were available. The comparison between the estimates and measurements are shown in Table 33. The rule of mixtures yields very close agreement to the measured results at the RTFO age level. The rule of mixtures could not be applied to predict the composition of the 64.RAP blend at the P40 age level since RAP SARA results at the P40 were not obtained.

Figure 46 show that the saturates and resins content of a given binder/blend do not change substantially with age level in comparison to the aromatics and asphaltenes. Tukey HSD analysis indicates all binders indicates statistically significant changes in aromatics and asphaltenes contents with aging from the RTFO to P40 condition. Tukey HSD results indicate that differences

in saturates content with age level for a given binder/blend are generally statistically insignificant. For the resins fraction, it was more varied if the content differed significantly at the two age levels for a given binder/blend. The 58.RAP, 64.RAP, and 58.RAP.E1 did not experience a significant change in resins content from the RTFO to P40 age level whereas the other binders/blends did. The 58.RAP.E1 and 58.RAP.E2 blends have distinct saturates, resins, and CII values compared to the 64.RAP.R1 and 64.RAP.R2 blends, suggesting inferior compatibility. However, the 58.RAP blend also has notably poorer compatibility than the 64.RAP blend based on the CII and thus, it is difficult to infer if this a result of differences among the extenders and RAs or due to the differences in the 58 versus 64 virgin binders from Figure 46 and Table 32. The RAP binder has notably higher asphaltenes content than the virgin binders and blends but a similar CII value to the 58.RAP, 58.RAP.E1, and 58.RAP.E2 blends at the P40 age level. The 58 virgin binder, 58.RAP.E1, and 58.RAP.E2 exhibited relatively poor ΔT_c values at the P40 age level compared to other binders and blends evaluated, which may be associated with their poor CII values.

Table 32. SARA Results

Binder/Blend	Asphaltenes (%)	Resins (%)	Aromatics (%)	Saturates (%)	CII (%)
58 (RTFO)	18.1	25.6	48.2	8.1	35.5
58 (P40)	23.4	30.6	37.4	8.7	47.2
58.RAP (RTFO)	22.4	30.0	40.9	6.7	41
58.RAP (P40)	27.3	31.6	33.9	7.2	52.7
58.RAP.E1 (RTFO)	21.2	34.4	34.5	9.9	45.1
58.RAP.E1 (P40)	25.7	34.5	30.0	9.7	54.9
58.RAP.E2 (RTFO)	22.4	29.8	39.3	8.4	44.6
58.RAP.E2 (P40)	26.5	32.3	33.4	7.9	52.4
64 (RTFO)	16.7	35.0	42	6.3	29.9
64 (P40)	21.2	39.7	34.2	4.9	35.3
64.RAP (RTFO) (Estimate)	21.8	36.6	36.2	5.3	37.2
64.RAP.R1 (RTFO)	21.8	39.2	33.1	5.9	38.3
64.RAP.R1 (P40)	25.6	41.3	27.0	6.0	46.3
64.RAP.R2 (RTFO)	20.7	42.9	32.2	4.2	33.2
64.RAP.R2 (P40)	26.0	44.4	25.3	4.2	43.3
RAP	31.0	38.3	27.0	3.6	53.0

Table 33. Comparison of Estimate and Measurement of SARA Fractions for 58.RAP

Determination	Asphaltenes (%)	Resins (%)	Aromatics (%)	Saturates (%)	CII (%)
RTFO Estimated	22.7	30.2	40.6	6.5	41.3
RTFO Measured	22.4	30.0	40.9	6.7	41.0

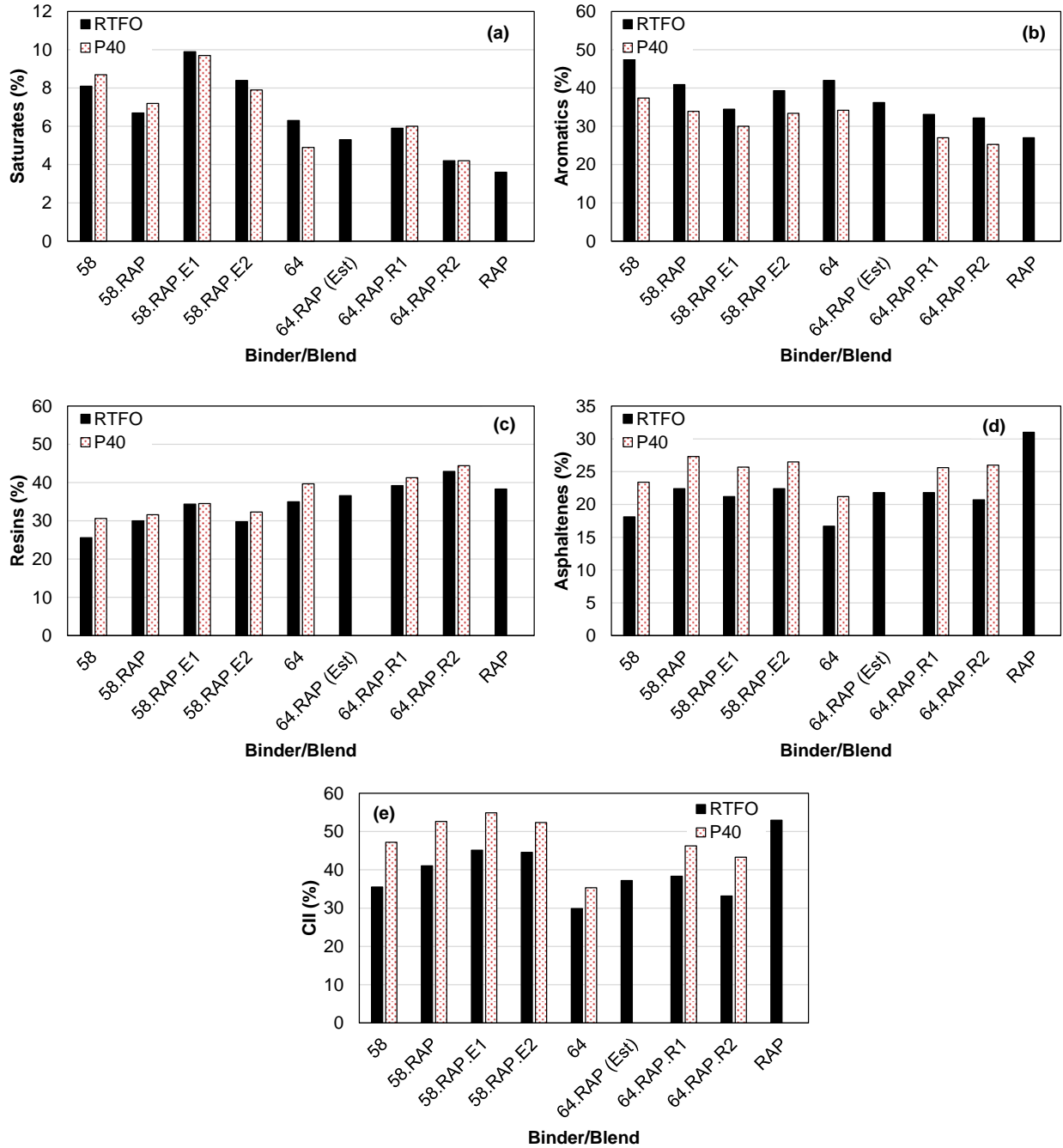


Figure 46. SARA results

To further evaluate the impact of the additives on the SARA composition of binder blends, Table 34 and Table 35 show the changes imparted by the additives on the SARA composition of the blends of the 58.RAP and 64.RAP, respectively. The values in Table 34 and Table 35 were calculated by the taking the content of a given fraction in the blend with the additive and subtracting the content of that same fraction in the respective reference (58.RAP or 64.RAP). Cases that reflect statistically significant changes are identified by the * following the reported value. Note that the statistical significance in asphaltene results could not be evaluated since replicate asphaltene content results were not available. Table 34 and Table 35 show that the E1, R1, and R2 additives increased the resins content and decreased the aromatics content of the respected reference blend. Additives E1 and E2 also increased the saturates content whereas the R2 additive decreased the saturates content. The effects of E1 and E2 on the SARA composition of the 58.RAP were more pronounced at the RTFO age level compared to the P40 age level. The additives had relatively little effect on the asphaltenes content at the RTFO age level. Some cases indicate a small decrease in asphaltene content due to the addition of the additive. The difference in asphaltenes content between the 58.RAP.E1 and 58.RAP.E2 blends and the reference 58.RAP were higher at the P40 than P20 age level, indicating the additives may slightly hinder the increase in asphaltene content with long-term aging. However, the differences in asphaltene content at the P40 age level are small and thus may be insignificant. The E1 and E2 additives increased the CII at the RTFO age level whereas the R2 additive decreased the CII value relative to the reference blend. A higher CII value is associated with poorer chemical compatibility and thus, it is possible the increase in CII in the E1 and E2 blends could have contributed to their poor ΔT_c values. However, the poor ΔT_c values were observed at the P40 age level where the effect of E2 on CII is deemed insignificant and thus, it is difficult to make a very clear link between the SARA results and rheological results. Also notable, the R1 and R2 blends performed very similarly rheologically despite their different effects on CII.

Table 34. Change with Respect to Reference 58.RAP

Blend	Asphaltenes (%)	Resins (%)	Aromatics (%)	Saturates (%)	CII (%)
58.RAP.E1 (RTFO)	-1.2	4.4*	-6.4*	3.2*	4.1*
58.RAP.E1 (P40)	-1.6	2.9*	-3.9*	2.5*	2.2*
58.RAP.E2 (RTFO)	0.0	-0.2	-1.6	1.7*	3.5*
58.RAP.E2 (P40)	-0.8	0.7	-0.5	0.7	-0.3

Table 35. Change with Respect to Reference 64.RAP

Blend	Asphaltenes (%)	Resins (%)	Aromatics (%)	Saturates (%)	CII (%)
64.RAP.R1 (RTFO)	0.0	2.6*	-3.1*	0.6	1.1
64.RAP.R2 (RTFO)	-1.1	6.3*	-4.0*	-1.1*	-4.0*

SUMMARY OF FINDINGS

The E1 and E2 additives both increased the saturates content of the blend of recycled and virgin binder. The E1, R1, and R2 additives all depleted the aromatics content and added to the resins content of the blend of recycled and virgin binder. Only minor impacts of the additives on the asphaltenes contents were observed. The 58.RAP.E1 and 58.RAP.E2 exhibited relatively poor

compatibility on the basis of CII values compared to the 64.RAP.R1 and 64.RAP.R2 blends as well as the 64 virgin binder, which potentially helps explain the inferior rheology of these blends identified through several rheological indicators of binder durability, notably ΔT_c at the P40 age level. The E1 and E2 additives were found to negatively affect CII but also the 58 virgin binder had a poorer CII (and poorer ΔT_c) than the 64 virgin binder so it is unclear to what extent the additives versus virgin binder affected the rheological performance. Also, while the R1 and R2 blends performed similarly rheological, the two additives had notably different effects on CII, further making it difficult to draw defined links between the SARA and rheological results. It is noted that the NCHRP 09-58 project was also unable to draw clear inferences between the effects of additives on the SARA and their corresponding effects on rheology (Epps Martin et al. 2020). Thus, the mechanisms by which additives alter the rheology of asphalt binders merits further investigation in future research.

REFERENCE

1. Epps Martin, A., et al. The Effects of Recycling Agents on Asphalt Mixtures with High RAS and RAP Binder Ratios, *NCHRP Report 927*, National Academies, Washington, D.C., 2020.
2. NTS America Corporation. (n.d.). SARA Method. Retrieved April 29, 2023, from <https://www.iatrosan.com/sara-method>

APPENDIX D: PREDICTION OF BINDER BLEND PROPERTIES USING VIRGIN BLENDS AND RECYCLED BINDER PROPERTIES

INTRODUCTION

Given that extraction, recovery, and testing of recycled binders or blends containing recycled binder is cumbersome, the ability to screen the performance of binders using testing of the virgin binder blended with additives alone was evaluated. Accordingly, blends of virgin binder and additives were prepared at dosages to reflect their relative proportions in the blends containing virgin binder, additive, and recycled binder detailed in Table 6. The blending process aligned with that described in Section 2.2.1. The DSR AASHTO M 320 performance-graded properties of the virgin blends were determined, consistent with the testing detailed in Section 3.5. Subsequently, the ability to predict the rheological properties of the blends of virgin binder, recycled binder, and additives on the basis of properties of the recycled binder and properties of the blend of virgin binder and additive was assessed using micromechanical and mixing models.

BACKGROUND

Limited efforts have been made to understand the blending of virgin binder, recycled binder, and RAs and extenders from a predictive modeling perspective. Recently, Sharma et al. (2022) studied the applicability of eight different mixing rules to recycled binder blends. Promising results were reported. However, although the study used three RAP sources, only one virgin binder (high PG 76), and one material designated as an RA were evaluated. The material designated as an RA was a softer asphalt binder (high PG 64) rather than what is typically designated as an RA. Savarnya et al. (2022) developed a ternary blend mixing formulation, including the RA, virgin binder, and recycled binder rheology, to predict the recycled binder blend rheology including what are conventionally regarded as RAs by indirectly determining the dynamic viscoelastic properties of the RA products from rotational viscosity measurements and applying the Cox-Merz principle. Promising results were obtained but the characterization of RA rheology may be impractical.

Herein, the ability to predict the AASHTO M 320 performance-graded properties of blends of recycled binder, virgin binder, and an RA or extender on the basis of the properties of the recycled binder and the blend of virgin binder and an RA or extender is evaluated. The rationale behind this approach is that the NCDOT currently, implicitly presumes recycled binder characteristics when specifying virgin binder grades on the basis of the mixture RBR. It is inferred this is because it is impractical to require extracted and recovered recycled binder testing on a routine basis. If ability to predict recycled binder blend properties on the basis of the recycled binder and the blend of virgin binder and an additive is viable, it could potentially allow for specification of the properties of blends of virgin binder and additive that must be achieved as a function of RBR. These specifications could be established on the basis of the predictive model and assumed, representative recycled binder properties such that the blend of the virgin binder, additive, and assumed recycled binder properties achieves the desired AASHTO M 320 performance grade.

MATERIALS AND METHODS

Blends of a subset of the study virgin binders and additives were prepared at dosages to reflect their relative proportions in the blends containing virgin binder, additive, and recycled binder

detailed in Table 6. The corresponding blends evaluated are detailed in Table 36. Note that two 64.R2 blends are listed. The 64.R2-a blend was prepared to reflect the virgin system in the 64.RAP.R2 blend whereas the 64.R2-b blend was prepared to reflect the virgin system in the 64.MRAS.R2 blend. The blending process and aging procedures for the virgin blends aligned with that described in Section 2.2.1. The AASHTO M 320 performance-graded DSR-based properties of the virgin blends were determined, consistent with the testing detailed in Section 3.5.

Table 36. Summary of Blends Evaluated

Blend	Additive Content (%)
64.R1	8.6
64.R2-a	8.9
58.E1	10.9
58.E2	6.0
64.RAP.R1	5.5
64.RAP.R2	5.5
58.RAP.E1	7.0
58.RAP.E2	3.9
64.R2-b	9.1
64.MRAS.R2	7.4

THEORETICAL BACKGROUND

Several micromechanical and mixing models were evaluated for the prediction of the blend of virgin binder, recycled binder, and additives on the basis of measurements of the properties of the recycled binder and the blend of virgin binder and additive.

Micromechanical models

The recycled binder blend can be seen as a composite of three constituents: (a) virgin binder, (b) RAP binder, and (c) additive. One simplification for the application of micromechanics principles can be to consider the “virgin binder + RA” blend as one constituent and RAP binder as another constituent within micromechanical models. Three micromechanical models were chosen for evaluation as described below:

1. Paul’s model

Paul’s model is a simple mathematical framework that is used to analyze the mechanical behavior of composite materials. The model is based on the concept that the composite material can be viewed as a homogenized material with effective properties that are determined by the properties of its constituent materials and the way in which they are arranged and interact with one another. The model is popularly known as rule of mixtures. The rule of mixture states that the effective properties of the composite material (G_{blend}) can be determined by a weighted average (w_n) of the properties of its constituent materials (G_n) as shown in Equation (29).

$$G_{blend} = \sum_{N=1}^n w_n G_n \quad (29)$$

2. Elshelby’s model

Eshelby's model is a theoretical model for the behavior of elastic materials with small defects, such as rigid inclusions or voids. Specifically, Eshelby developed a model that enables the calculation of the ratio of the composite modulus (in the present case, the recycled binder blend) to the matrix modulus (which is "virgin binder + additive" blend in the study case), as given by Equation (30), which is a function of the composite modulus (G_c), matrix modulus (G_m), and particulate modulus (G_p) (which refers to the recycled binder in the present case). The term ν_m represents the Poisson's ratio of the matrix (assumed to equal 0.5) and C_v is the volumetric concentration of the particulates, which is RBR in the present case.

$$\frac{G_c}{G_m} = 1 - \frac{15(1-\nu_m) \left(1 - \frac{G_p}{G_m}\right)}{7 - 5\nu_m + 2(4 - 5\nu_m) \frac{G_p}{G_m} C_v}$$

(30)

3. Hashin's model

Hashin's model was derived for the shear moduli of composites by considering the change in strain energy in a homogeneous body due to the inclusion of non-homogeneities. The model assumes that the particles are spherical, and that the action of the surrounding heterogeneous medium on any one inclusion is transmitted via a spherical shell that is wholly contained in the matrix. Hashin's model for the ratio between the shear modulus of the composite (G_c) to the matrix (G_m) is presented in Equation (31). The variables have the same definitions as that of Eshelby's model described above.

$$\frac{G_c}{G_m} = 1 - \frac{15(1-\nu_m) \left(1 - \frac{G_p}{G_m}\right) C_v}{7 - 5\nu_m + 2(4 - 5\nu_m) \left[\frac{G_p}{G_m} - \left(\frac{G_p}{G_m} - 1\right) C_v \right]}$$

(31)

Mixing models

Centeno et al. (2011) have evaluated the use of mixing rules for predicting the property of petroleum-crude blends and virgin and RAP binder blends. However, the use of "virgin binder + additive" blends in these rules and its utility in predicting the viscoelastic properties of recycled binder blends remain to be assessed. In order to address this research gap, several models were considered for evaluation in this study. Given the diversity of mixing rules available in the literature, only those rules were selected which have shown some promise in the literature. These rules are briefly discussed below:

1. Arrhenius model

The Arrhenius model (1887) has been used to predict the dynamic shear modulus ($|G^*|$) of binder blends. Three variations of Arrhenius model have been developed in terms of the norm $|G^*|$ and are given in Equations (32), (33), and (34). Equation (32) predicts the $|G^*|$ of the blend of the binder and additive (denoted $|G^*|_{Binder + RA}$) on the basis of the binder $|G^*|_{binder}$ and additive $|G^*|_{RA}$. Equation (33) predicts the $|G^*|$ of the blend of recycled binder, virgin binder, and

additive (denoted $|G^*|_{Binder+RAP+RA}$) on the basis of the $|G^*|$ values of the individual components. Equation (34) predicts the $|G^*|_{Binder+RAP+RA}$ based on the $|G^*|_{Binder+RA}$ and $|G^*|_{RAP}$ of the recycled binder (denoted $|G^*|_{RAP}$). The parameters a , b , and c reflect the mass proportions of the constituents in the blend.

a. Recycling agent prediction model

$$\log |G^*|_{Binder+RA} = a'' \log |G^*|_{Binder} + c'' \log |G^*|_{RA} \quad (32)$$

b. Ternary prediction model

$$\log |G^*|_{Binder+RAP+RA} = a' \log |G^*|_{Binder} + b' \log |G^*|_{RAP} + c' \log |G^*|_{RA} \quad (33)$$

c. Binary prediction model

$$\log |G^*|_{Binder+RAP+RA} = a \log |G^*|_{Binder+RA} + b \log |G^*|_{RAP} \quad (34)$$

2. Reciprocal rule

The reciprocal rule is a variation of the Paul's model, as shown in Equation (35) with $n = -1$ as shown in Equation (36).

$$|G^*|_{Binder+RAP+RA}^n = a |G^*|_{RAP}^n + (1-a) |G^*|_{Binder+RA}^n \quad (35)$$

$$\frac{1}{|G^*|_{Binder+RAP+RA}} = \frac{a}{|G^*|_{RAP}} + \frac{(1-a)}{|G^*|_{Binder+RA}} \quad (36)$$

It is considered to be a better physical representation of the blend than Paul's model as it represents the property of an infinitely layered mixture between the two heterogeneous fluids.

3. Kendall and Monroe model

The Kendal and Monroe (1917) model is also considered a variation of the simple mixing law (Equation (35)) such that $n = 1/3$ as shown in Equation (37) and has been used by several researchers in the past for asphalt binder and RAP binder blend predictions.

$$|G^*|_{Binder+RAP+RA} = \left(a |G^*|_{Binder+RA}^{\frac{1}{3}} + b |G^*|_{RAP}^{\frac{1}{3}} \right)^3 \quad (37)$$

4. Grunberg and Nissan model

The Grunberg and Nissan model has shown promise for the prediction of recycled binder blend properties in the literature (Sharma et al. 2021.) It is an extension of the Arrhenius model by means of the addition of an interaction parameter (Grunberg and Nissan 1949). Equation (38) shows the general form of Grunberg and Nissan model.

$$\log |G^*|_{Binder+RAP+RA} = a \log |G^*|_{Binder+RA} + b \log |G^*|_{RAP} + a \times b \times d \quad (38)$$

where d is the interaction parameter.

5. Taylor's model

Taylor's (1932) model, shown in Equation (39), has been used to relate the norm of the complex shear modulus of the blend with the corresponding property of the continuous phase, which is assumed to be the "virgin binder + RA" blend and dispersed phase, which is considered to be the RAP binder. where φ refers to the RBR.

$$\frac{|G^*|_{blend}}{|G^*|_{continuous}} = 1 + 2.5\varphi \left(\frac{|G^*|_{dispersed} + 0.4|G^*|_{continuous}}{|G^*|_{dispersed} + |G^*|_{continuous}} \right) \quad (39)$$

RESULTS

Micromechanical models

The ability of the micromechanical models to predict $|G^*|$ at 58°C was evaluated for the RAP blends. The results are shown in Figure 47. It was found that Paul's model and Eshelby's model over predicted $|G^*|$ while Hashin's model under predicted it. The possible explanation can be the difference in the mixing mechanisms of the virgin binder, RAP binder, and RAs, but also the underlying model assumptions as these models consistent over predicted or under predicted across all the tested blends. Several other conditions were also tested but similar results were found. Given the limited dataset, no conclusive evidence was found about the suitability of these three micromechanical models for modeling recycled binder blends.

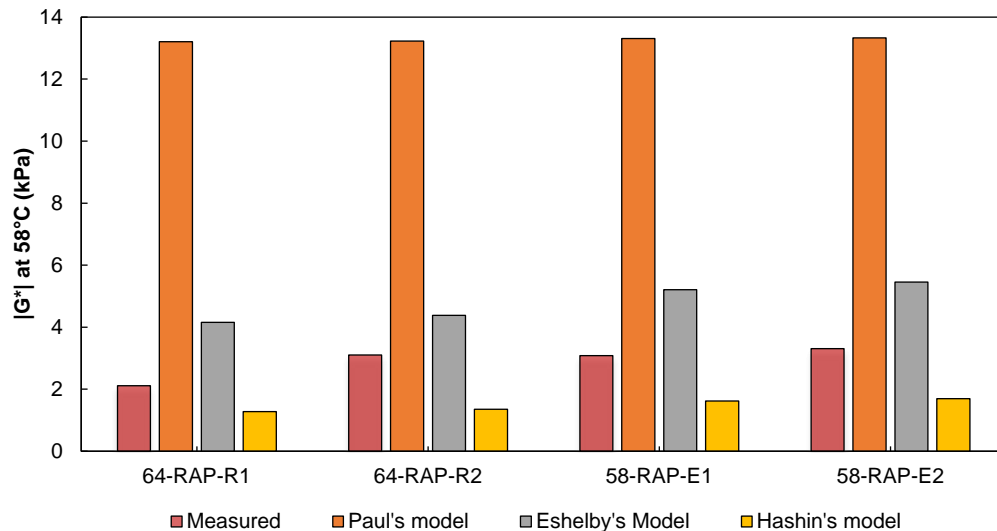


Figure 47. Micromechanical model predictions for the norm of complex shear modulus at 58°C

Mixing Models

Evaluation of mixing models

Initially, all the models were evaluated for predicting the $|G^*|$ at 58°C. One thing to note that binary form of the Arrhenius model was used while the interaction parameter for Grunberg and Nissan model was obtained by least-square error fitting for each individual blend. The results are shown in Figure 48, which shows the Kendal and Monroe model highly over predicted while Reciprocal

rule and Taylor’s model significantly under predicted the $|G^*|$. Only Arrhenius and Grunberg and Nissan models showed promising results and were considered for further evaluation along with Kendal and Monroe model for comparison purposes.

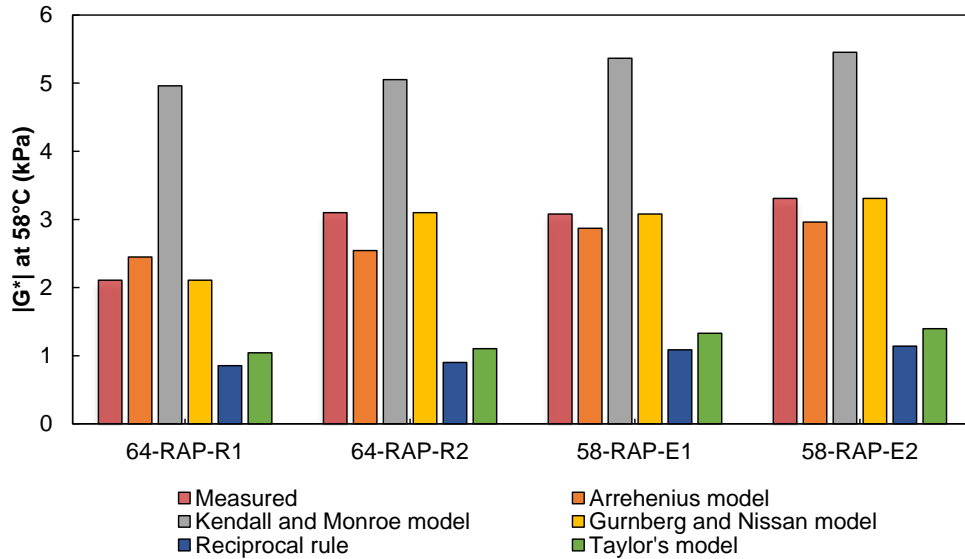


Figure 48. Mixing model predictions for the norm of complex shear modulus at 58°C

To further evaluate the Arrhenius model, the binary and ternary formulations were compared for two test conditions of 58°C and 64°C. Given the nature of these formulations, the value of the model parameters as shown in Table 37, is calculated from the proportions of the blend constituents and remain same for each blend.

Table 37. Model Parameters for Arrhenius Model

Blend	Model Parameters						
	a''	c''	a'	b'	c'	a	b
64.RAP.R1	0.9212	0.0788	0.6104	0.3374	0.0521	0.6626	0.3374
64.RAP.R2	0.9187	0.0813	0.6093	0.3368	0.0539	0.6632	0.3368
58.RAP.E1	0.9016	0.0984	0.6019	0.3327	0.0654	0.6673	0.3327
58.RAP.E2	0.9436	0.0564	0.6198	0.3426	0.0375	0.6574	0.3426

As expected, the binary and ternary models result in same predictions due to the nature of model formulations and the underlying assumption of no interactions. Figure 49 and Figure 50 show the results for both binary and ternary Arrhenius models for 58°C and 64°C respectively.

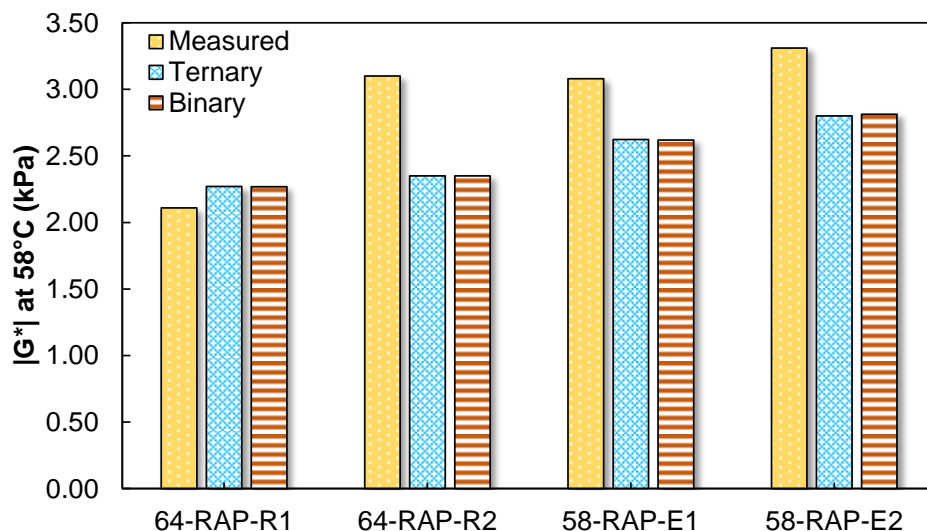


Figure 49. Arrehenius model predictions for the norm of complex shear modulus at 58°C

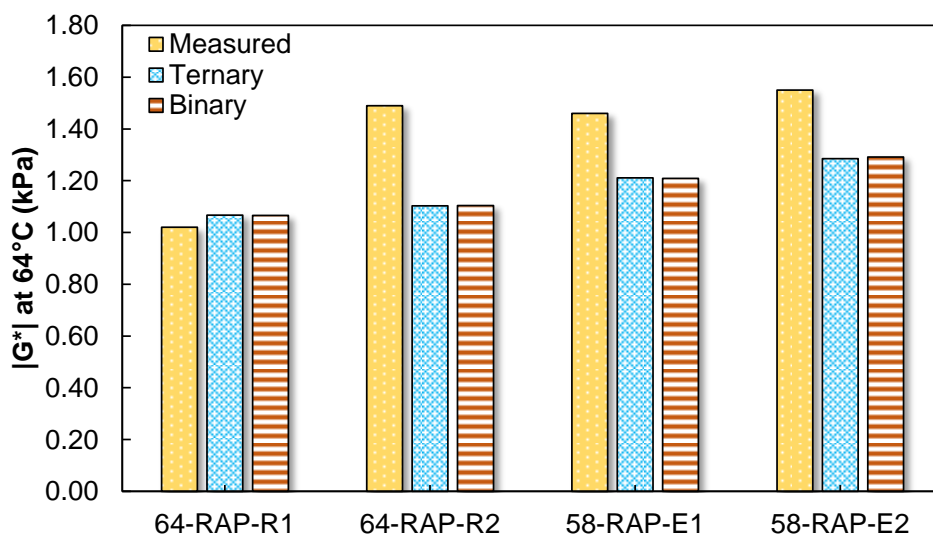


Figure 50. Arrehenius model predictions for the norm of complex shear modulus at 64°C

In order to compare Grunberg and Nissan model for a fixed value of the interaction parameter, d , instead of using any fitting procedure and understand how it impacts the model predictions, a value of 0.3 based on the literature and preliminary analysis done in the current study, was assumed across the four RAP blends at 64°C. Figure 51 shows the comparison of predictions from the three models with the measured value and it can be clearly seen that Kendal and Monroe model over predicts in all cases while the binary Arrehenius model under predicts across three blends. It is interesting to note that Grunberg and Nissan model gives close predictions for most blends as compared to the other models. This can be attributed to the inclusion of the interaction parameter (d) in its formulation.

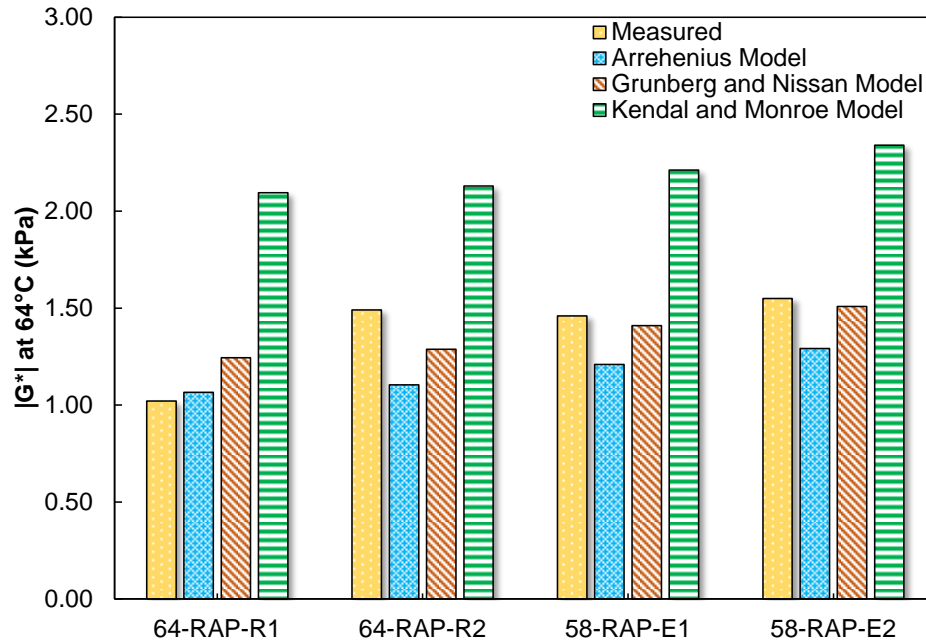


Figure 51. Comparison of model predictions for $|G^*|$ at 64°C

Mixing models for different aging conditions

To evaluate the three models for different aging conditions, three parameters were chosen. First, the $|G^*|$ at 64°C in the original unaged state, second, the $|G^*|$ at 64°C in the RTFO-aged state, and third, then, the $|G^*|$ at 25°C in the PAV-aged state. For Grunberg and Nissan model, the value of the interaction parameter assumed varied with the aging state, as shown in Table 38. It should be noted that the value initially assumed for the preliminary analysis was 0.3 as discussed in the previous section. However, it was observed that the predictions of the model can be improved by defining values as a function of the aging condition. In the subsequent sections, additional analysis is presented to investigate alternative values of the interaction parameter.

Table 38. Assumed Value of Interaction Parameter for Grunberg and Nissan Model

S.No.	Aging condition	Value of interaction parameter (d)
1	Unaged	0.35
2	Short-term aged (RTFO)	0.35
3	Long-term aged (PAV 20hrs)	0.5

Figure 52 shows the model predictions for original unaged conditions for the $|G^*|$ at 64°C. It can be seen that Kendal and Monroe model over predicts for all the blends by nearly 50% for 64.RAP.R2, 58.RAP.E1, and 58.RAP.E2, and by almost 100% in case of 64.RAP.R1 blend. The Arrehenius model under predicts by around 20% for 64.RAP.R2, 58.RAP.E1, and 58.RAP.E2, but is comparatively more accurate for 64.RAP.R1. In case of Grunberg and Nissan model, the model over predicts for 64.RAP.R1 by almost 25%, and predicts other blends quite well except 64.RAP.R2 which is under predicted by close to 10%. For RTFO aged state shown in Figure 53, Arrehenius model and Grunberg and Nissan model mostly under predict but the former does it by almost 25% in the worst case while the latter does it by around 10% in the worst case, which is

consistent with the predictions in original unaged state. Kendal and Monroe again over predicts by almost 85% in the worst case. Finally, in the PAV-aged state, the predictions are done for the $|G^*|$ at 25°C as shown in Figure 54. It must be noted that the value of the interaction parameter for the PAV-aged condition is taken as 0.5 as already presented in Table 38 above. It is interesting to note that Kendal and Monroe model does fairly well in predicting the intermediate temperature properties at 25°C, as shown in Figure 54. Grunberg and Nissan model also shows promising predictions with the worst under prediction being less than 20% as opposed to Arrhenius model which under predicts by close to 40% in the worst case. An attempt was made to use these models to predict the phase angle at high and intermediate temperatures. However, the results were not very promising. Given that phase angle is used as part of the calculation of Superpave parameters for rutting and fatigue performance in practice, these models were used to predict the Superpave parameters at high and intermediate temperatures.

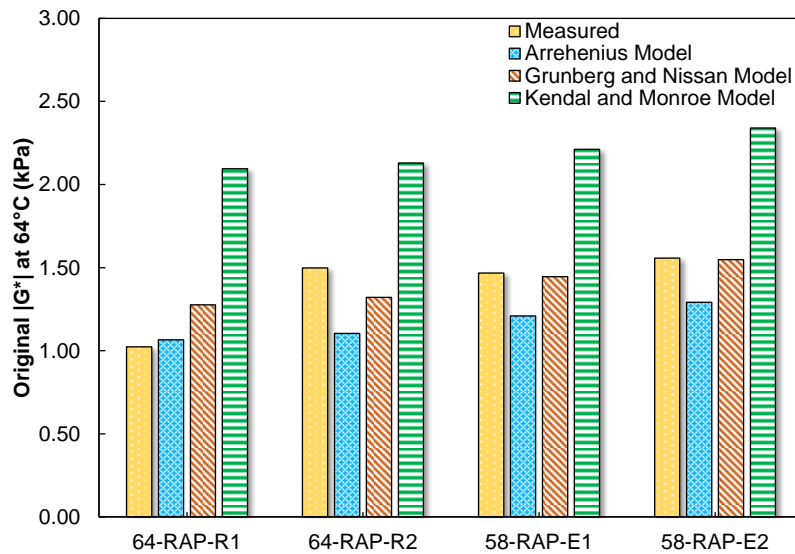


Figure 52. Comparison of model predictions for original $|G^*|$ at 64°C ($d=0.35$)

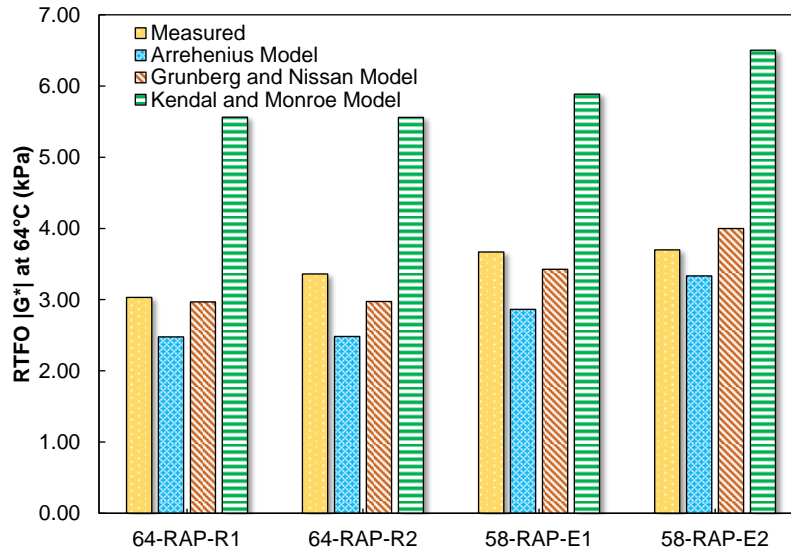


Figure 53. Comparison of model predictions for RTFO $|G^*|$ at 64°C ($d=0.35$)

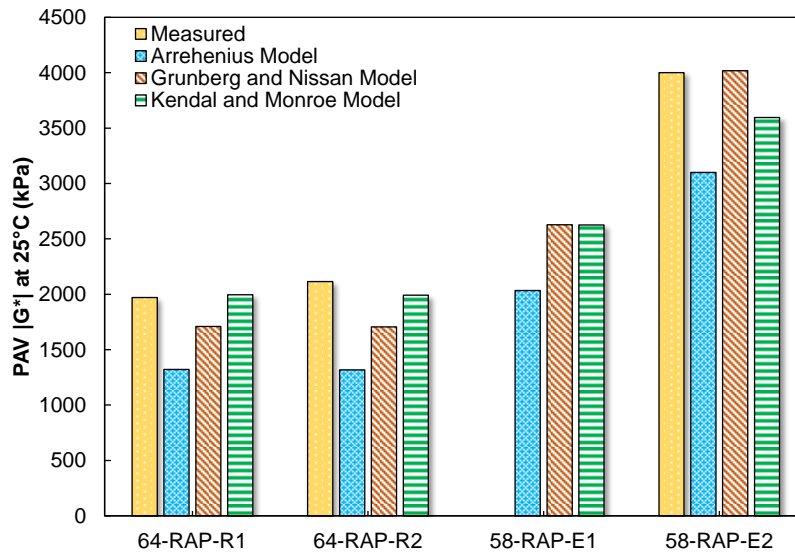


Figure 54. Comparison of model predictions for PAV $|G^*|$ at 25°C ($d=0.5$)

Model predictions for AASHTO M 320 specification parameters

Phase angle carries very important information about the viscoelastic response of asphalt binders indicating the degree or extent of elastic or viscous behavior in the overall response. The phase angle data is usually very sensitive to the experimental testing and can be challenging to model. To incorporate phase angle in the mixing model predictions and replicate its use in practice, it was considered as part of Superpave parameters at high and intermediate temperatures for different aging conditions. The Superpave performance grading assigns certain limits on these parameters for grading purposes. For example, $|G^*|/\sin \delta$ has a pass/fail criterion of 1kPa and 2.2kPa for unaged and RTFO aged conditions. Further, these parameters, $|G^*|/\sin \delta$ and $|G^*|\times \sin \delta$ are used to get an idea overall rutting and fatigue performance of the asphalt binders at high and

intermediate temperatures respectively. Figure 55, Figure 56, and Figure 57 show the model predictions of the respective parameters at unaged, RTFO-aged, and PAV-aged conditions respectively. It can be seen that Grunberg and Nissan model is able to predict these parameters very well, with an under prediction of around 10% in the worst case for $|G^*|/\sin \delta$ at high temperature RTFO-aged condition and of around 15% in the worst case for $|G^*|\times\sin \delta$ at intermediate temperature PAV-aged condition. Arrhenius model under predicts by over 25% for high temperature Unaged and RTFO-aged and over 35% for intermediate temperature PAV-aged condition. Kendal and Monroe model over predicts to around 100% for high temperature Unaged and RTFO-aged conditions and under predicts by a little over 10% for intermediate temperature PAV-aged condition for the worst cases.

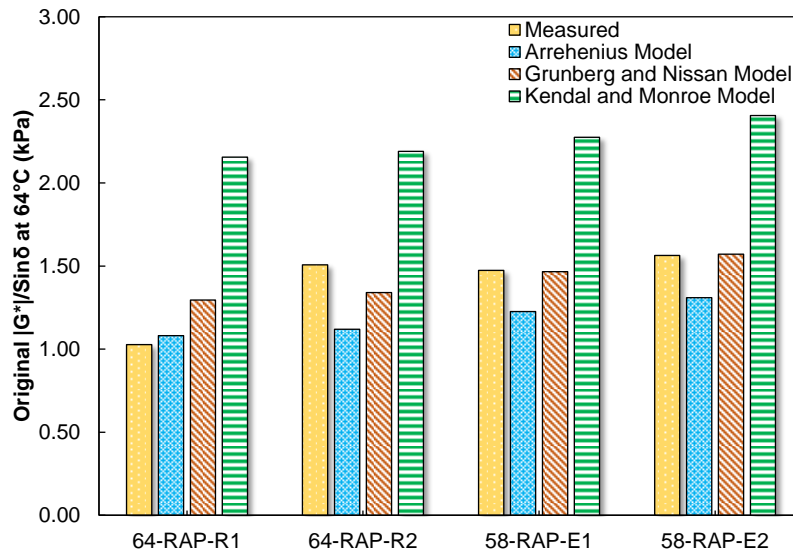


Figure 55 Comparison of model predictions for original $|G^*|/\sin \delta$ at 64°C ($d=0.35$)

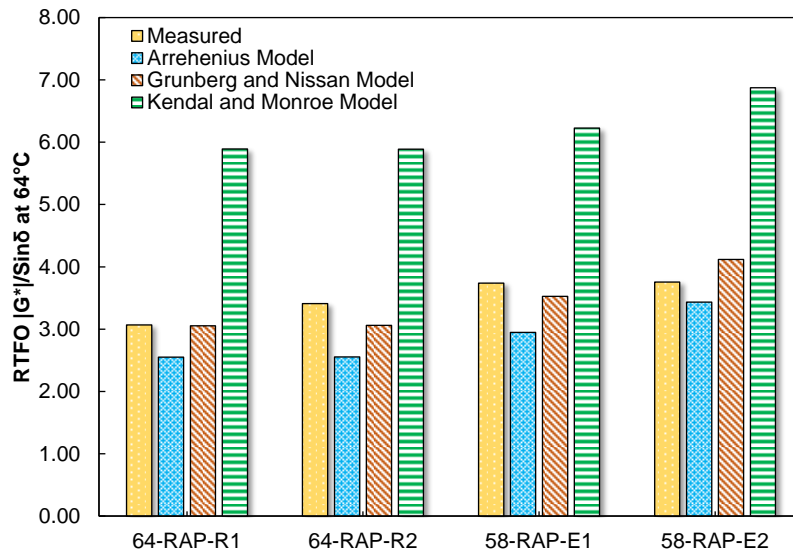


Figure 56 Comparison of model predictions for RTFO $|G^*|/\sin \delta$ at 64°C ($d=0.35$)

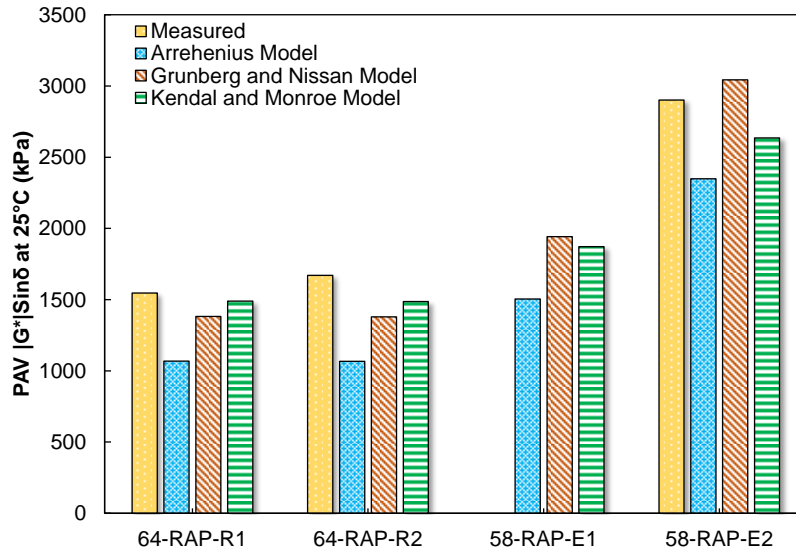


Figure 57 Comparison of model predictions for PAV $|G^*|\sin\delta$ at 25°C ($d=0.5$)

One blend with MRAS was prepared and tested for evaluating mixing rules. The Arrhenius model and Grunberg and Nissan model were used for this one blend for RTFO and PAV conditions. Initially, the interaction parameter values used for the RAP blends were tried but resulted in substantial under predictions so the interaction parameter was increased to its maximum possible value of one. Figure 58 shows the results for the two aging conditions and it can be seen that the Grunberg and Nissan model yields closer results to the measured values. These results suggest that while the Gunberg and Nissan model may be able to yield accurate predictions, the interaction parameter is likely dependent on the binders contained within the blend, thus limiting its widespread applicability.

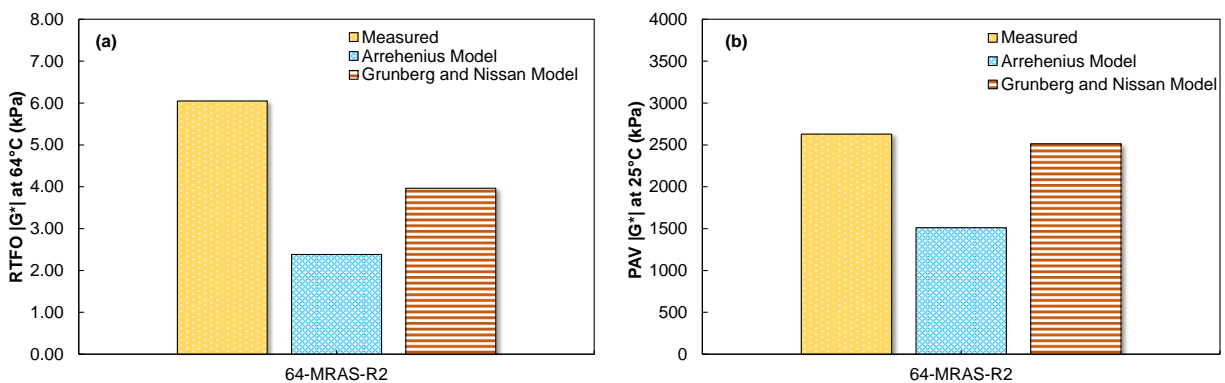


Figure 58 Model predicts for 64-MRAS-R2 blends for (a) RTFO and (b) PAV aging conditions ($d=1$)

SUMMARY OF FINDINGS

The Grunberg and Nissan model can yield fairly accurate predictions of Superpave high- and intermediate-temperature specification properties of a blend of recycled binder, virgin binder, and additive from testing of a blend of virgin binder and an additive and testing of the recycled binder.

However, the model requires an interaction parameter that appears to depend on age level and the properties of the virgin and recycled binders, thus limiting its viability for use in practice. The alternative mixing and micromechanical models that did not require an interaction parameter generally yielded inferior prediction to the Grunberg and Nissan model.

REFERENCES

1. Arrhenius, S. On the Internal Friction of Dilute Aqueous Solutions. *Journal of Physical Chemistry*, 1887, pp. 285-298.
2. Centeno, G., J. Sanchez-Reyna, J. Ancheyta, N. Munoz, and N. Cardona. Testing Various Mixing Rules for Calculation of Viscosity of Petroleum Blends. *Fuel*, Vol. 90, 2011, pp. 3561-3570.
3. Grunberg, L., and A. H. Nissan. Mixture Law for Viscosity. *Nature*, Vol. 138, 1932, pp. 41-48.
4. Kendall, J., and K. P. Monroe. The Viscosity of Liquids. II. The Viscosity-Composition Curve for Ideal Liquid Mixtures. *Journal of American Chemical Society*, Vol. 39, 1917, pp. 1787-1802.
5. Savarnya, A., N. Saboo, A. Das, M. Makowska, and T. Pellinen. Development of Ternary Binder Mixing Formulation for Asphalt Pavement Recycling. *International Journal of Pavement Engineering*, Vol. 23, No. 13, 2022, pp. 4739-4747.
6. Sharma, A., G. D. Ransinchung, and P. Kumar. Applicability of Various Mixing Rules for Hot Asphalt Recycled Binders. *Road Materials and Pavement Design*, Vol. 23, No. 11, 2022, pp. 2547-2566.
7. Taylor, G. T. The Viscosity of a Fluid Containing Small Drops of Another Fluid. *Proceedings of the Royal Society of London. Series A*, Vol 138, 1932, pp. 41-48.

APPENDIX E: SUPPLEMENTARY STATISTICAL ANALYSIS RESULTS

Table 39. Tukey HSD Results for $|G^*| \times \sin \delta$ @25°C, 10 rad/s (kPa) at the P20 Age Level

Level	Group					Mean
58.MRAS PAV	A					4432.5
64 PAV	A					3990.7
58.RAP PAV		B				3047
58.RAP.E2 PAV		B				2894.2
58.RAP.E1 PAV		B	C			2486.3
64.MRAS.R2 PAV			C	D		1979.6
58.RAP.E3 PAV			C	D		1978.1
64.RAP.R2 PAV				D	E	1669.1
64.RAP.R1 PAV				D	E	1533.6
64.MRAS.R1 PAV					E	1261.8
58 PAV					E	1248.7

Table 40. Tukey HSD Results for $|G^*| \times \sin \delta$ @25°C, 10 rad/s (kPa) at the P40 Age Level

Level	Group					Mean
58.RAP PAV 40	A					5588
64 PAV 40	A					5324
58.MRAS PAV 40	A					5258
58.RAP.E1 PAV 40		B				3068
64.MRAS.R2 PAV 40		B	C			2849
58.RAP.E2 PAV 40		B	C	D		2797
58.RAP.E3 PAV 40			C	D		2510
64.RAP.R2 PAV 40			C	D		2508
58 PAV 40			C	D	E	2487
64.RAP.R1 PAV 40				D	E	2316
64.MRAS.R1 PAV 40					E	1985

Table 41. Tukey HSD Results for G-R @ 25°C, 10 rad/s (kPa) at the P20 Age Level

Level	Group					Mean
58.MRAS PAV	A					5544.638
64 PAV		B				2955.633
58.RAP.E2 PAV		B				2620.546
58.RAP PAV		B				2402.775
58.RAP.E1 PAV		B				2384.566
64.MRAS.R2 PAV			C			1533.084
58.RAP.E3 PAV			C	D		1368.014
64.RAP.R2 PAV			C	D	E	1004.61
64.RAP.R1 PAV			C	D	E	980.7821
64.MRAS.R1 PAV				D	E	839.4683
58 PAV					E	625.9934

Table 42. Tukey HSD Results for G-R @ 25°C, 10 rad/s (kPa) at the P40 Age Level

Level	Group						Mean
58.MRAS PAV 40	A						8432.794
58.RAP PAV 40		B					7447.48
64 PAV 40			C				5870.716
58.RAP.E1 PAV 40				D			3947.87
58.RAP.E2 PAV 40				D	E		3389.979
64.MRAS.R2 PAV 40					E	F	3097.786
58.RAP.E3 PAV 40						F	2398.713
64.RAP.R2 PAV 40						G	2211.505
58 PAV 40						G	1933.235
64.RAP.R1 PAV 40						G	1815.722
64.MRAS.R1 PAV 40						G	1811.465

Table 43. Tukey HSD Results for G-R @ 15°C, 0.005 rad/s (kPa) at the P20 Age Level

Level	Group							Mean
58.MRAS PAV	A							339
58.RAP.E1 PAV		B						96.5
58.RAP PAV			C					81.5
64 PAV				D				63.5
58.RAP.E2 PAV					E			49
58.RAP.E3 PAV						F		30.5
64.RAP.R2 PAV						F	G	25.5
64.RAP.R1 PAV							G H	18
64.MRAS.R2 PAV							G H	16.5
58 PAV							H	12
64.MRAS.R1 PAV							H	10.5

Table 44. Tukey HSD Results for G-R @ 15°C, 0.005 rad/s (kPa) at the P40 Age Level

Level	Group							Mean
58.MRAS PAV 40	A							578
58.RAP PAV 40		B						345
58.RAP.E2 PAV 40			C					222
64 PAV 40			C	D				178.5
64.MRAS.R2 PAV 40				D	E			158.5
58.RAP.E1 PAV 40					E	F		118
64.RAP.R2 PAV 40						F	G	81.5
58.RAP.E3 PAV 40						F	G	68.5
58 PAV 40						F	G	64
64.MRAS.R1 PAV 40							G	60
64.RAP.R1 PAV 40							G	59.5

Table 45. Tukey HSD Results for ω_c (Hz) at the P20 Age Level

Level	Group							Mean	
58 PAV	A							6.248	
64.MRAS.R1 PAV		B						4.546	
64.RAP.R1 PAV			C					3.023	
64.MRAS.R2 PAV			C	D				2.815	
64.RAP.R2 PAV				D	E			2.483	
58.RAP.E3 PAV					E			2.159	
64 PAV						F		1.258	
58.RAP.E2 PAV						F		1.106	
58.RAP PAV						F	G	0.829	
58.RAP.E1 PAV							G	H	0.339
58.MRAS PAV								H	0.070

Table 46. Tukey HSD Results for ω_c (Hz) at the P40 Age Level

Level	Group							Mean
58 PAV 40	A							0.903
64.RAP.R1 PAV 40		B						0.688
64.RAP.R2 PAV 40			C					0.538
58.RAP.E3 PAV 40			C	D				0.481
64.MRAS.R1 PAV 40				D				0.449
64 PAV 40					E			0.227
64.MRAS.R2 PAV 40						F		0.132
58.RAP.E2 PAV 40						F		0.1102
58.RAP PAV 40						F	G	0.0934
58.RAP.E1 PAV 40						F	G	0.0726
58.MRAS PAV 40							G	0.0233

Table 47. Tukey HSD Results for T_c (°C) at the P20 Age Level

Level	Group								Mean
58.MRAS PAV	A								42.5
58.RAP.E1 PAV		B							36.25
58.RAP PAV			C						32.4
58.RAP.E2 PAV				D					31.7
64 PAV					E				30.6
64.MRAS.R2 PAV						F			29.1
58.RAP.E3 PAV						F			29.05
64.RAP.R2 PAV						F			29
64.RAP.R1 PAV							G		28.3
64.MRAS.R1 PAV								H	27.25
58 PAV								I	24.8

Table 48. Tukey HSD Results for T_c (°C) at the P40 Age Level

Level	Group						Mean
58.MRAS PAV 40	A						46.6
58.RAP.E1 PAV 40		B					42.5
64.MRAS.R2 PAV 40		B	C				41.3
58.RAP PAV 40			C				40.9
58.RAP.E2 PAV 40			C				40.3
64 PAV 40				D			37.0
64.MRAS.R1 PAV 40				D			36.65
64.RAP.R2 PAV 40					E		35.00
58.RAP.E3 PAV 40					E		34.75
64.RAP.R1 PAV 40					E		33.95
58 PAV 40						F	32.0

Table 49. Tukey HSD Results for Master Curve R at the P20 Age Level

Level	Group					Mean
58.RAP.E1 PAV	A					2.423
58.MRAS PAV	A					2.421
64.MRAS.R1 PAV		B				2.352
64.MRAS.R2 PAV		B				2.341
64.RAP.R1 PAV			C			2.262
58.RAP.E2 PAV			C			2.236
58.RAP.E3 PAV				D		2.150
64.RAP.R2 PAV				D		2.143
58.RAP PAV					E	2.091
58 PAV					E	2.084
64 PAV					F	2.010

Table 50. Tukey HSD Results for Master Curve R at the P40 Age Level

Level	Group					Mean
58.RAP.E1 PAV 40	A					2.909
58.MRAS PAV 40		B				2.553
64.MRAS.R2 PAV 40		B	C			2.536
64.MRAS.R1 PAV 40		B	C			2.518
58.RAP.E2 PAV 40			C			2.459
58.RAP.E3 PAV 40			C			2.457
64.RAP.R1 PAV 40				D		2.352
58.RAP PAV 40				D		2.313
64 PAV 40				D		2.294
64.RAP.R2 PAV 40				D		2.289
58 PAV 40					E	2.194

Table 51. Tukey HSD Results for NCHRP 09-59 R at the P20 Age Level

Level	Group						Mean
64.MRAS.R1 PAV	A						2.344
58.RAP.E1 PAV	A						2.287
64.MRAS.R2 PAV		B					2.182
58.RAP.E2 PAV		B	C				2.127
64.RAP.R1 PAV			C				2.076
58.RAP.E3 PAV			C				2.066
58.MRAS PAV			C	D			2.063
64.RAP.R2 PAV			C	D	E		2.045
58.RAP PAV				D	E	F	1.97
64 PAV					E	F	1.955
58 PAV						F	1.931

Table 52. Tukey HSD Results for NCHRP 09-59 R at the P40 Age Level

Level	Group				Mean
58.RAP.E2 PAV 40	A				2.42698
58.RAP.E1 PAV 40	A	B			2.41212
58 PAV 40	A	B	C		2.35622
64.MRAS.R2 PAV 40	A	B	C	D	2.24921
58.MRAS PAV 40		B	C	D	2.19086
64.MRAS.R1 PAV 40			C	D	2.16791
64.RAP.R1 PAV 40			C	D	2.15459
58.RAP.E3 PAV 40			C	D	2.13783
64.RAP.R2 PAV 40				D	2.1224
58.RAP PAV 40				D	2.03434
64 PAV 40				D	2.03126

Table 53. Tukey HSD Results for S(60) @ -18°C (MPa) at the P20 Age Level

Level	Group							Mean
64 PAV	A							383.5
58.MRAS PAV		B						323.5
58.RAP PAV			C					303
58 PAV				D				220
58.RAP.E2 PAV				D				207
58.RAP.E1 PAV					E			187
58.RAP.E3 PAV					E	F		181.5
64.RAP.R1 PAV					E	F		175.5
64.RAP.R2 PAV						F		172
64.MRAS.R2 PAV							G	139
64.MRAS.R1 PAV							H	93.5

Table 54. Tukey HSD Results for S(60) @ -18°C (MPa) at the P40 Age Level

Level	Group							Mean
64 PAV 40	A							408
58.RAP PAV 40		B						349.5
58.MRAS PAV 40			C					330.5
58.RAP.E2 PAV 40				D				240
64.MRAS.R1 PAV 40				D	E			230
58 PAV 40				D	E			229
64.RAP.R1 PAV 40					E	F		218.5
64.RAP.R2 PAV 40						F	G	203
58.RAP.E1 PAV 40							G	194
58.RAP.E3 PAV 40							G	194
64.MRAS.R2 PAV 40							G	185.5

Table 55. Tukey HSD Results for m(60) @ -18°C at the P20 Age Level

Level	Group						Mean
64.MRAS.R1 PAV	A						0.36
64.MRAS.R2 PAV		B					0.346
64.RAP.R2 PAV		B	C				0.344
64.RAP.R1 PAV		B	C				0.338
58.RAP.E3 PAV		B	C				0.336
58 PAV			C				0.335
58.RAP.E2 PAV				D			0.315
58.RAP.E1 PAV				D	E		0.306
58.RAP PAV					E		0.296
58.MRAS PAV						F	0.278
64 PAV						F	0.272

Table 56. Tukey HSD Results for m(60) @ -18°C at the P40 Age Level

Level	Group						Mean
58.RAP.E3 PAV 40	A						0.32
64.RAP.R2 PAV 40	A	B					0.3175
64.MRAS.R2 PAV 40	A	B					0.311
64.RAP.R1 PAV 40	A	B	C				0.3065
64.MRAS.R1 PAV 40		B	C				0.300
58.RAP.E1 PAV 40			C	D			0.2895
58 PAV 40				D	E		0.2805
58.RAP PAV 40				D	E	F	0.2725
58.RAP.E2 PAV 40					E	F	0.269
58.MRAS PAV 40						F	0.2615
64 PAV 40						F	0.256

Table 57. Tukey HSD Results for ΔT_c ($^{\circ}\text{C}$) at the P20 Age Level

Level	Group						Mean
64.RAP.R1 PAV	A						3.17
58.RAP.E3 PAV		B					0.58
64.RAP.R2 PAV		B	C				-0.215
58.RAP PAV		B	C				-0.350
64 PAV		B	C	D			-0.415
58.RAP.E2 PAV			C	D	E		-1.695
58.MRAS PAV				D	E		-2.270
58.RAP.E1 PAV					E	F	-3.265
58 PAV						F	-4.470

Table 58. Tukey HSD Results for ΔT_c ($^{\circ}\text{C}$) at the P40 Age Level

Level	Group			Mean
58.RAP.E3 PAV 40	A			-0.89
64.RAP.R2 PAV 40	A			-1.20
64 PAV 40	A			-1.81
58.RAP PAV 40	A	B		-1.93
64.RAP.R1 PAV 40	A	B		-2.02
58.MRAS PAV 40	A	B	C	-3.73
58 PAV 40		B	C	-4.71
58.RAP.E1 PAV 40			C	-5.01
58.RAP.E2 PAV 40			C	-5.05

Table 59. Pearson's Correlation Coefficients at the P20 Age Level

Parameter	$ G^* \times \sin \delta$ (kPa)	GR _{25°C} (kPa)	GR _{15°C} (kPa)	R ₀₉₋₅₉	R _{MC}	ω_c (Hz)	T _c (°C)	S(60) (MPa)	m(60)	ΔT_c (°C)	N _f @5%
$ G^* \times \sin \delta$ (kPa)											
GR _{25°C} (kPa)	0.94										
GR _{15°C} (kPa)	0.77	0.93									
R ₀₉₋₅₉	-0.29	-0.13	-0.09								
R _{MC}	0.01	0.29	0.42	0.79							
ω_c (Hz)	-0.79	-0.76	-0.61	-0.03	-0.23						
T _c (°C)	0.79	0.92	0.92	0.10	0.52	-0.82					
S(60) (MPa)	0.85	0.69	0.55	-0.69	-0.43	-0.50	0.47				
m(60)	-0.94	-0.83	-0.68	0.42	0.14	0.72	-0.70	-0.93			
ΔT_c (°C)	-0.55	-0.63	-0.55	-0.50	-0.49	0.61	-0.72	-0.23	0.54		
N _f @5%	-0.05	0.13	0.21	0.78	0.84	-0.27	0.42	0.84	0.10	-0.56	
N _f @15%	-0.41	-0.28	-0.18	0.75	0.65	0.25	-0.13	-0.67	0.56	0.14	0.69

Table 60. Pearson's Correlation Coefficients at the P40 Age Level

Parameter	$ G^* \times \sin \delta$ (kPa)	GR _{25°C} (kPa)	GR _{15°C} (kPa)	R ₀₉₋₅₉	R _{MC}	ω_c (Hz)	T _c (°C)	S(60) (MPa)	m(60)	ΔT_c (°C)	N _f @5%
$ G^* \times \sin \delta$ (kPa)											
GR _{25°C} (kPa)	0.96										
GR _{15°C} (kPa)	0.79	0.91									
R ₀₉₋₅₉	-0.45	-0.32	-0.14								
R _{MC}	-0.08	0.10	0.13	0.45							
ω_c (Hz)	-0.60	-0.71	-0.67	-0.02	-0.58						
T _c (°C)	0.57	0.74	0.81	0.14	0.62	-0.91					
S(60) (MPa)	0.89	0.79	0.60	-0.54	-0.31	-0.37	0.29				
m(60)	-0.74	-0.72	-0.64	-0.05	0.07	0.43	-0.44	-0.81			
ΔT_c (°C)	0.00	-0.18	-0.35	-0.83	-0.49	0.30	-0.51	0.08	0.53		
N _f @5%	-0.05	0.07	-0.02	0.41	0.87	-0.40	0.45	-0.31	0.10	-0.41	
N _f @15%	-0.22	-0.11	-0.11	0.14	0.69	-0.28	0.35	-0.39	0.37	-0.23	0.93